Aggregation and elastic properties of poly(ethylene oxide)-block-poly(butylene oxide) polymersomes

By Obed Andres Solis-Gonzalez

University of Sheffield

Faculty of Science

Department of Chemistry

October 2014

Thesis submitted to the University of Sheffield for the Degree of Doctor in Philosophy

In Memory of my granddad, Teodoro, and my grandma, Guadalupe.

Acknowledgments

It has been a long way since I first arrived to Sheffield and, finally, the thesis is finished. There have been moments of success and many others of experiencing technical difficulties. In these situations, many people helped me throughout my stay in Sheffield. This part is just to let them know how much I appreciated their help and support. Without their help, it would not be possible to finish this research work.

Firs at all, I would like to thanks to Professor Tony Ryan for accepting me in his research group and for guiding me in part of experiments. Thanks to Tony I could study in the University of Sheffield. Also, I would like to thanks to Professor Patrick Fairclough for supervising the present research work and for his very valuable support in experimental difficulties and interpretation of results. Also, thanks go to the National Council of Science and Technology of Mexico (CONACYT) and to the State Council of Science and Technology of Michoacan in Mexico for their economical support. Tanks to: Dr Patrick Smith for being interested in collaborated in the present project, to PhD student Mr Christopher Tse for his incredible help to prepare the inkjet printing samples, to Dr Stuart Johnson to teach me how to use the pipette puller equipment, to Dr. Svetomir Tzokov in helping me in experiments related with the transmission electron microscope and to Mr Garry Turner for making the pressure system and micropipette aspiration accessories. Also, special thanks to Dr Christine M. Fernyhough in teaching me how to use the dynamic light scattering equipment and for her incredible kindness in helping me to review part of this thesis. Thanks also to Professor Peter Winlove and Dr Peter Petrov in the University of Exeter for let me use the pipette aspiration equipment of the university and for their incredible kindness and support in my short stay in Exeter. Special thanks to my examiners Dr Ahmed Iraqui and Dr Alberto Saiani for reading the thesis and their valuable comments and corrections in the present research work.

Finally, very special thanks to my family: my dad, Norberto, and my mom, Hilda, my brother, Ismet, and my sister, Lisbeth, for always being with me. Thanks to all my friends in Sheffield and in the polymer scattering group.

Abstract

In this research work, the effect of salts and the membrane toughness of polymersomes made with the block copolymer poly(ethylene oxide)$_{16}$-poly(butylene oxide)$_{22}$ ($E_{16}B_{22}$) were studied, where the subscript correspond to the average degree of polymerisation. Also, a new methodology to form vesicles was implemented in order to be used in conjunction with a micropipette aspiration (MPA) equipment.

The effect of salts on nano- and giant vesicles was analysed using dynamic light scattering (DLS), transmission electron microscopy (TEM) and light microscopy. Aggregation was observed only for NaH_2PO_4 at high molar concentrations (3 M), which agrees with the Hofmeister series. Halide and sulphate sodium salts, at relative high (~1 M) and low concentrations (0.3 M), did not affect nanovesicles. Similarly, the presence of 0.2 M K_2SO_4 in a giant vesicle solution was determined not to induce aggregation.

In addition, polymersomes were made by hydrating micro-size polymer droplets, on a glass surface, created using an inkjet printer. Modifying the contact angle by surface treatment; the addition of different substances such as sugars and salt on the hydration process was studied. Polymersome unbinding from the polymer substrate can be obtained by doping the polymer substrate with sugar or salts in a molar ratio of at least 1:10 (polymer/additive). Addition of 0.1 M or 0.01 M salt solutions to doped polymer layers prevents vesicle formation. However, samples pre-hydrated with water, allowing vesicles to grow, and then additionally hydrating with a salt solution can permit vesicles to grow in a salt environment however only at low salt concentrations ($\geq$ 10 mM).

The area expansion modulus (K_A) was measured using the MPA technique and the inkjet printing technique. A modulus of 61.4 (±23.1) mN/m was found. The relative low value of $E_{16}B_{22}$ polymersomes compared with other polymer vesicles is attributable to a liquid-crystal like behaviour of EB block copolymers and the apparently longer times to reach equilibrium in the projection length.

Chapter 1: Introduction

This chapter is divided in the following way: section 1.1 provides a brief description of natural and synthetic amphiphilic molecules and the self-assembly of amphiphilics in a number of different morphologies. The general characteristics that govern the self-assembly and the parameters which are used to describe it are the subjects of section 1.2. Then, in section 1.3, a brief review of the literature on vesicles will be introduced including the advantages of polymersomes over liposomes, the different mechanisms of vesicle formation, the diverse techniques of vesicle preparation and various polymersome applications. Section 1.4 describes the different theories that attempt to explain the Hofmeister series and the aggregation of biological and synthetic macromolecules in solution as well as nanostructures. Finally, in section 1.5, the basic forms of deformations on membranes are explained and the mechanical properties, i.e. area stretching modulus and bending modulus, of polymersomes and liposomes are compared. Also, in this section, the effect of salt on the bilayer structure of vesicles will be explained.

1.1 Amphiphilic structures

An amphiphilic molecule is a structure which comprises two or more chemically dissimilar segments in the same molecule, e.g. a hydrophilic and a hydrophobic part, which are joined by a covalent bond. The hydrophilic part has a high solubility in water and can be anionic, cationic, zwitterionic, or an uncharged polar molecule, (e.g. polyethylene oxide) whereas the hydrophobic segment has a low solubility in water and can be a polycyclic molecule, an aromatic group or a long non-polar hydrocarbon chain[1]. Because of these ambivalent segments, when amphiphilic molecules are dissolved in a suitable solvent, they form nanostructures driven by the hydrophobic effect. For example, when naturally occurring phospholipids are dissolved in water, they can form micelles, or bilayers or vesicles (Figure 1). The common feature in these structures is that the head group is in contact with water (outward facing) and the tail is aggregated inwards, for the purpose of minimizing energetically unfavourable hydrophobe-water interactions[2]. This arrangement is primarily driven by entropic forces[3], the main function of which is to minimize the tension among chemically dissimilar molecules and, as a consequence, these molecules form spontaneous clusters as described above.

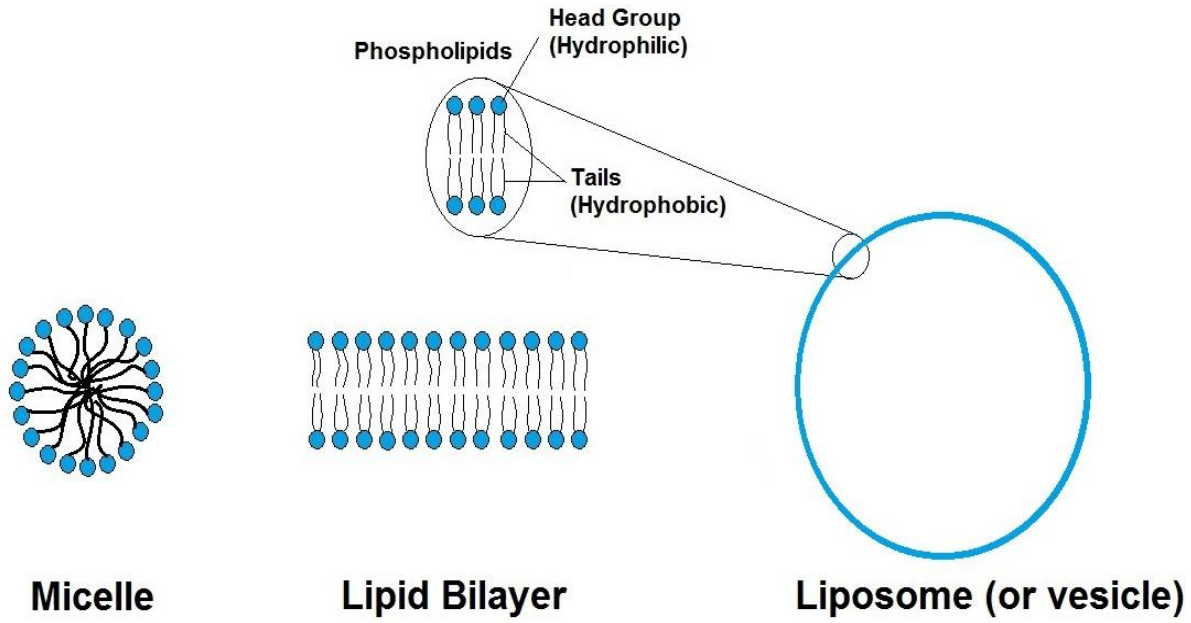

Figure 1. Examples of some nanostructures made with phospholipids which consist of a hydrophilic, and a hydrophobic segment. These molecules self-assemble in water and produce: micelles, lipid bilayers and liposomes.

Amphiphilic compounds can be "natural" with important biological functions, e.g. cholesterol[4], phospholipids[5] and proteins[1], or "synthetic", such as block copolymers. Block copolymers (BCs) consist of two or more monomers which form a series of blocks that are joined by a covalent bond. BCs can exist in different morphologies including diblock, triblock, pentablock, star block, miktoarm and graft block copolymers (Figure 2). One way to synthesise an amphiphilic molecule, for example BCs, is to create a diblock copolymer with one hydrophilic and one hydrophobic domain. Similar to its natural counterparts, this difference in chemical domains in synthetic amphiphilic macromolecules can result in self-assembled nanostructures if block copolymers are dissolved in water, or others selective solvent systems. These nanostructures include spherical micelles, cylindrical micelles, polymersomes and polymer membranes[6], among others. The self-assembly and, as a result, the morphology of aggregates depend on multiple factors. Some of them will be described in the next section.

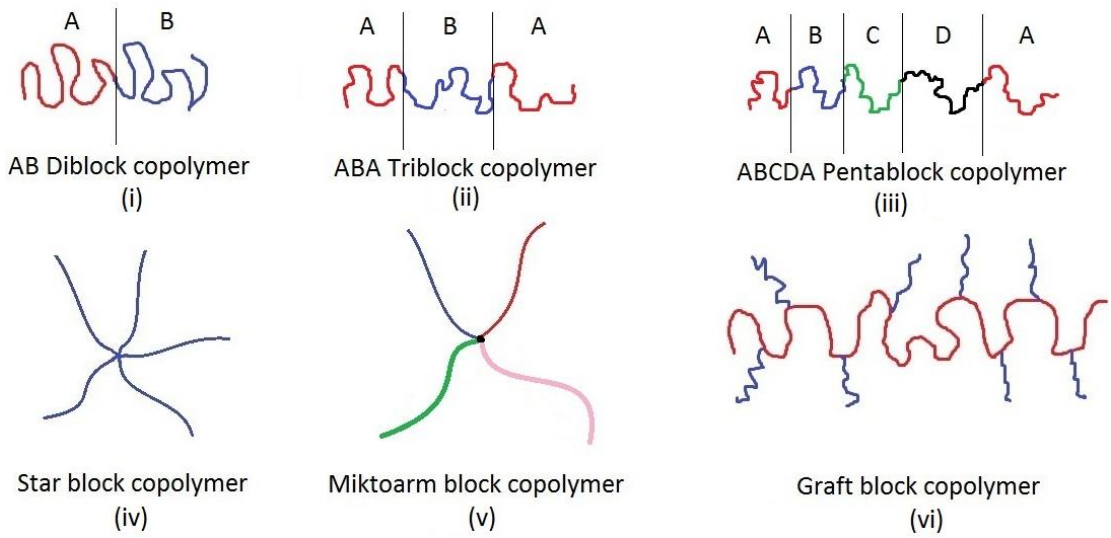

Figure 2. A selection of common block copolymer structures: diblock (i), triblock (ii), pentablock (iii), star (iv), miktoarm (v), and graft copolymer (vi).

1.2 Self-assembly of amphiphilic block copolymers

1.2.1 The hydrophobic effect in amphiphilic molecules

The hydrophobic effect is one of the key elements required to understand the aqueous self-assembly phenomenon of block copolymers. This spontaneous phenomenon is related to the thermodynamic interactions of hydrophobic molecules with water. Such interactions can be described in a qualitative and quantitative way. First, qualitatively, polar water molecules form hydrogen bonds. When a hydrophobic or non-polar molecule interacts with a polar molecule, the former disrupts the hydrogen bonding network and forces the water to form a cage around the hydrophobic compound. This is the "hydrophobic effect"[7]. As a consequence, there is a decrease in entropy and thus the free energy is not favourable. The decrease on entropy can be minimised if the hydrophobic molecules are aggregated into the aqueous solution. This minimizes the surface area of interactions between the hydrocarbon and water molecules. Quantitatively, the hydrophobic effect can be calculated within the Gibbs energy, or free energy, of the system, which indicates if a process occurs "spontaneously" into the system at both constant pressure (P) and temperature (T). The equation of the free energy is as follow:

$$\Delta G(P,T) = \Delta H - T\Delta S$$

Where ΔG is the change in free energy, T is the temperature and ΔH and ΔS are the change on enthalpy and entropy of the system, respectively. A negative value in ΔG means the process is thermodynamically spontaneous. This can be achieved either if enthalpy (ΔH) is negative or entropy

(ΔS) is positive. In the case of the hydrophobic effect, the self-assembly of long chain hydrocarbons in water is enthalpically unfavourable because it has a positive value. Therefore, the enthalpy of the system does not contribute to the "spontaneity" of the process. The entropy dominates since there is less order when water molecules surround hydrophobe aggregates, compared to when water molecules surround each individual hydrophobe in the solution, i.e. entropy increases for the latter case. For this reason, it is said that the hydrophobic effect is driven by entropic forces[8] and is the accepted explanation of the mechanism which governs the self-assembly in amphiphilics. However, this concept does not explain some different nanostructure morphologies found in experiments. In this case, another concept needs to be considered.

1.2.2 The packing parameter

The diversity of microstructures of amphiphilic molecules in solution can be understood if it is considered the amphiphile's molecular geometry[9]. This geometry can be characterised by the dimensionless packing parameter (p). Basically, this concept is based on the equilibrium of forces which exist in an aggregated system of amphiphilic lipid molecules. For example, the hydrophobic part represents the attraction forces which is responsible for the aggregation of molecules while the hydrophilic part represents repulsive forces that avoid further growth of the nanostructure[7,10]. Both forces can be described in terms of the geometry of the molecule. If two hydrophilic head groups are too close, they will repel each other, increasing the free energy of the system. On the other hand, if they are too far apart, hydrophobic molecules will come in contact with water which is an unfavourable interaction[11]. The balance between hydrophilic and hydrophobic forces leads us to an optimal free energy, i.e. minimal free energy, where the amphiphile is in equilibrium[10]. Thus, the optimal head group area (a_o) is where this minimum energy is found (Figure 3).

The packing parameter (p) suggests how an amphiphilic molecule is packed according to its geometry. We can write down the packing parameter in the following way:

$$p = \frac{v_o}{a_o \, l_o}$$

In the above expression, v_o is the volume of the hydrophobic chain, a_o is the optimal head-group area, and l_o is the length of the hydrophobic tail. As a general rule, when $p \leq 1/3$, spherical micelles are observed; when $1/3 \leq p \leq 1/2$, cylindrical micelles form and when $1/2 \leq p \leq 1$, polymersomes or vesicles form[2,10], when $p \approx 1$, bilayers and when $p > 1$, we have inverse micelles[9]. The packing parameter was initially used to describe low molecular weight amphiphilic molecules such as phospholipids, but it can be applied to some extent to block copolymers[12], e.g. for non-ionic surfactants with polyethylene oxide as the head group[13] (Figure 4).

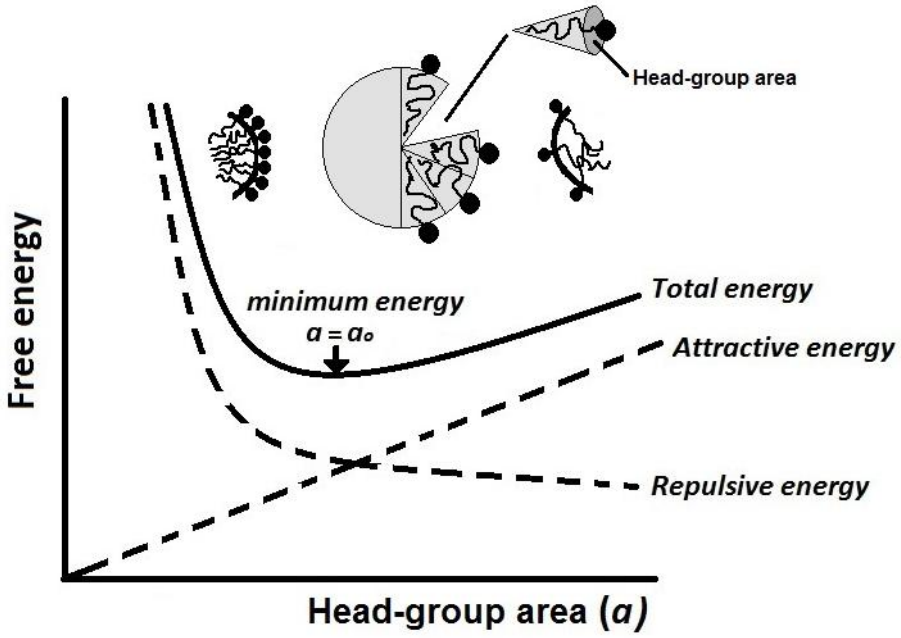

Figure 3. Schematic representation of the head-group area (a) of phospholipids in a micelle aggregation system. The balance between attractive (hydrophobic molecules) and repulsive (charge head groups) forces determinate the optimal minimum area (a_o) of the amphiphilic head group [11].

In literature, the packing parameter has been most associated to a_o since the ratio v_o/l_o keeps almost constant for typical phospholipids. However, a_o is not entirely based on geometrical characteristics of the amphiphilic head group but on thermodynamic conditions of the system[13]. This implies that a_o can have a series of values in different thermodynamic conditions. The optimal head group for a spherical micelle can be calculated in the following way (derived from Tanford's model of free energy and the Debye-Huckel theory for modelling electrostatic head-groups[13]):

$$a_0 = \left[\frac{2\pi e^2 d}{\epsilon\sigma}\frac{1}{1+\kappa l_o}\right]^{1/2}$$

Where e is the electric charge of the head-group, d is the capacitor thickness in the double layer model, ϵ is the dielectric constant of the solvent, σ is the interfacial free energy per unit length and κ is the inverse Debye length.

The self-assembly of copolymers in a solvent does not just depend of geometrical factors such as the length of individual polymer chains but solution parameters (e.g. concentration, pH, temperature, type of solvent, etc)[14] and, also, the method of preparation is important. For instance, modifying the method of preparation, different structures can be obtained such as micelles, polymersomes, nanospheres and nanocapsules[15]. Thus, the self-assembly is defined by the physical-chemical characteristics and also the kinetic history of the system. Among the great diversity of

nanostructures, the scientific community has been focused mostly on micelles and vesicles, using diblock[2] or triblock copolymers, because these have a wide variety of applications.

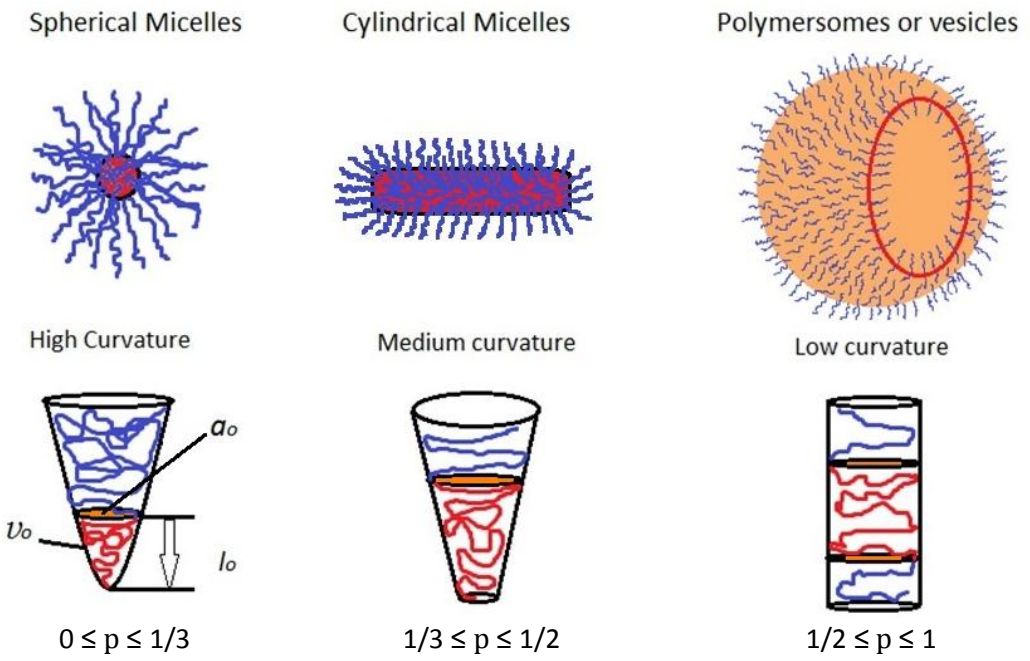

Figure 4. The packing parameter predicts different morphologies in block copolymers[2]. The morphologies can be spherical micelles ($0 \leq p \leq 1/3$), cylindrical micelles ($1/3 \leq p \leq 1/2$) or polymersomes ($1/2 \leq p \leq 1$).

1.2.3 The hydrophilic volume fraction

Another empirical way to predict the type of synthetic macromolecule morphologies, which is efficient for many B.C. systems[12], is with the use of the so-called "hydrophilic volume fraction". This hydrophilic fraction (f) is the ratio of hydrophilic to total volume. For example, increasing "f", for a given hydrophobic length, leads to the formation of spherical micelles rather than vesicles while further increasing causes the formation of cylindrical micelles[16].

The block copolymer ethylene oxide (*E*)/butylene oxide (*B*) (E_xB_y) is a well-known system, where *x* and *y* represent the average number of repetitive units in backbone chain. In such a case, literature[17] shows the effect of *E* lengths, i.e. the hydrophilic fraction, on polymer nanostructure formations with the following results. Block copolymers such as $E_{11}B_{11}$ (f= 34.6%), $E_{14}B_{10}$ (f= 42.5%) and $E_{16}B_{22}$ (f= 0.27%) readily formed vesicles whereas larger hydrophilic chains such as $E_{24}B_{10}$ (f= 55.9%) tend to form micelles[17]. As a general rule, if f≈ 35 ±10%, polymersomes would be favourable; if f > 45%, spherical micelles are usually formed[18]; and if f≈ 50%, cylindrical or worm-like micelles can be favored[12]. Furthermore, if f < 25%, inverted structures can form[19]. This is generally true when

disregarding the polydispersity index (PDI) of the polymer because *x* and *y* are average values of each block. Commonly in polymer solutions, there is a mix of different nanostructures. This is partly due to the small energetic differences between each phase and therefore the slow kinetics driving the conversion, as the system is hydrated.

1.3 Vesicles

Vesicles, also called bilayers or closed-spherical membranes, are structures compose of a flexible thin wall that can enclose a small amount of water, or other solvents. The bilayer, or wall, forms a partial barrier to the exterior and is made up of amphiphilic molecules, where the hydrophobic parts assemble in the middle of the membrane, and the hydrophilic segments cover the interior and exterior of the bilayer which are in contact with the solvent. There exist different ways to classify vesicles: (i) according to the size of the structure (e.g. small unilamellar vesicles (SUV), large unilamellar vesicles (LUV) and giant unilamellar vesicles (GUV)), (ii) according to the number of bilayers (e.g. multilamellar vesicles (MLV) and oligovesicular vesicles (OVV)[20] (Figure 5)), and (iii) according to the chemical nature of the amphiphilic building block (e.g. liposomes made of natural occurring phospholipids, polymersomes made of synthetic block copolymers, and niosomes made of non-ionic surfactants with a mixture of cholesterol and anionic lipids). Apart of these commonly-used amphiphilic molecules, it is also possible to form bilayers using more exotic synthetic amphiphiles such as functionalised fullerenes[21], i.e. C_{60} or "buckyballs", and dendrimers[22].

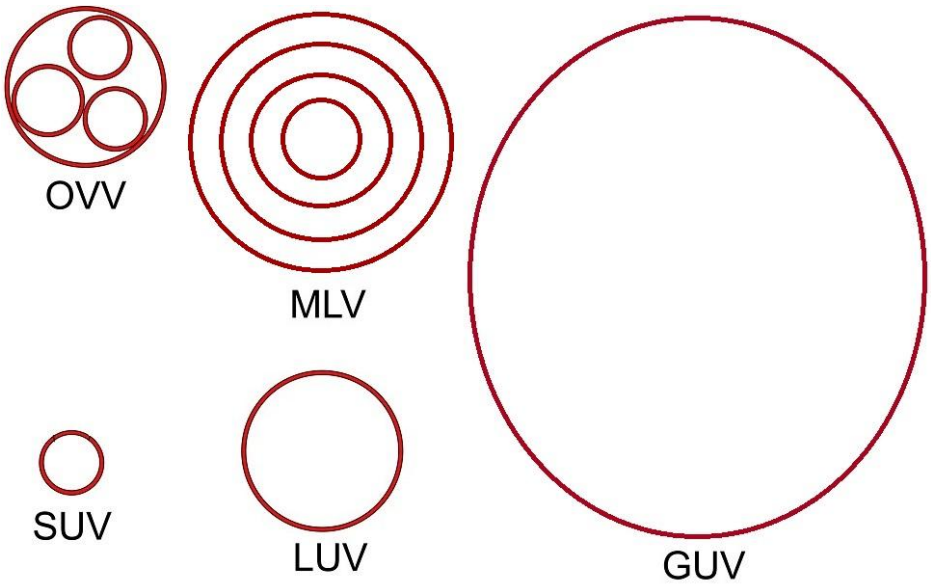

Figure 5. Different sort of vesicles according to their size and number of layers: small unilamellar vesicles (SUV), large unilamellar vesicles (LUV), multilamellar vesicles (MLV), oligovesicular vesicles (OVV) and giant unilamellar vesicles (GUV)[20].

The first reports of vesicles date back to 1965 when Bangham et al.[23] described for the first time aqueous-spherical membranes made of phospholipids, later termed "liposomes", in 1967, in order to generalise these type of lipid bilayer structures[24]. Then, in the 1970's, niosomes were first employed in drug delivery applications[25], opening the possibility of a new era of medicine. It was not until 1995 when block polymer vesicles were discovered by Zhang and Eisenberg[26] and later, in 1999, Discher and co-workers[27] studied for the first time the mechanical properties of giant vesicles and coined the term polymersomes[28]. This helped to expand the analysis of vesicles into the study of membrane mechanics.

1.3.1 Advantages of polymersomes versus liposomes

One important characteristic of amphiphilic BCs is their high molecular weight (MW) compared with phospholipids. For example, the range of MW in polymers is between 2-20 KDa[19], and in some cases MW is up to 100 KDa[12], whereas common phospholipids have a MW less than 1 KDa[19]. This factor has an impact on vesicle formation because the MW provides thermodynamic and kinetically stability to the self-assembled structure[29]. In terms of stability of polymersomes made of high MW copolymers, there is scarce interchange of monomers between the vesicle and the bulk solution, i.e. non-ergodic behaviour[30]. The vesicle structure is kinetically stabilised by the non-ergodicity due to the lack of mobility and chain entanglement of block copolymers[31]. This has been exploited in the pharmacology industry as the high stability of polymersomes can provide higher retention times of drugs into the lumen[32]. However, in some cases, polymersomes are highly permeable to small solutes, e.g. polyoxyethylene-polyoxypropylene-polyoxyethylene[33] or poly(ethylene oxide)-co-poly(butylene oxide)[34], compared to liposomes. This can prevent the use of certain polymer vesicles in some drug delivery applications, although they can still be useful to encapsulate large biomolecules. Since permeability depends on membrane thickness, chain entanglement[31] and the polarity of membrane[2], block copolymers can be tailored to enhance this property in vesicles. For example, the membrane thickness of natural phospholipids is commonly about 3-4 nm, whereas some block copolymers (e.g the polystyrene-block-poly(phenylquinoline)[31], can be up to 200 nm, which provide less membranes permeable. Also, using polyethylethylene-block-poly(ethylene oxide) in the creation of vesicles can reduce permeability to water by up to 10 times when compared to phospholiposomes[31].

In addition, another application is in the field of biology. Giant vesicles can serve as a model for studying basic biological phenomena. For example, fusion in biological membranes is extremely rapid, of the order of milliseconds, and in liposomes, it is a little slower, on the time scale of seconds. However, the fusion event studied in polymersomes has the advantage of occurring over a time

scale of minutes[16]. This longer time helps researches to identify and analyse the several stages that are involved in this process.

The use of polymers instead of phospholipids can improve the vesicle properties in a number of ways, tailoring them for different applications[35,36]. In drug delivery, for instance, polymer vesicles can be synthesised with pH-responsive block polymers. These BCs are generally either polyacids or polybases or a combination of both[37]. This provides pH-responsive characteristics. For example, as the pH of the vesicle solution is modified[38], hollow spheres can change to micelles. Nanostructures capable of a pH-response have been designed to fight cancer. In this respect, one possible strategy is the development of nanostructures capable of releasing a drug in acidic conditions since most tumours have a pH around 5.8-7.2. In this way, the release efficiency can be maximized and the side effects of highly toxic drugs are minimised[37].

Therefore, block copolymers can enhance the overall membrane properties. The great advantage of vesicles made of BCs is that can be synthetically tailored with diverse amphiphilic macromolecules of different properties to create polymersomes for selective permeability, mechanical toughness, pH-sensitivity and biodegradability[2,16].

1.3.2 Mechanism of vesicle formation

The elucidation of the vesicle mechanism is important for technological and scientific reasons. A better understanding of how vesicles form can provide a major improvement in drug encapsulation processes and better vesicle yields. Until now, there have been several proposed mechanisms using common surfactants and amphiphilic block copolymer. Although vesicle genesis can vary between phospholipids and macromolecules, the results show that they are very similar in their pathways[39]. Some studies have been carried out theoretically[39,40], which allows the determination of short lived transition intermediates, and experimentally[41], with good agreement between both. However, these results need to be interpreted with caution because the specific pathway depends on the properties of the system (e.g. block copolymer lengths, solvent, temperature, etc.) and, also, multiple pathways can coexist.

The lamellar hydration pathway

In the first mechanism, unilamellar and multilamellar giant vesicles can be explained in terms of lamellar hydration (Figure 6). Here, vesicle formation originates from a thin, dry layer deposited over a surface. In this layer, there are many phospholipid bilayers with a certain space between each other, i.e. thickness between plane-parallel bilayers. In the case of unilamellar vesicle formation (Figure 6(A-C))[42], dried lipid layers can have defects or holes along the layers and when they are hydrated, water goes through these defects, beginning the process of swelling. This provokes the

formation of a small bulge or blister which commences to grow because of both the hydration and osmotic forces. Then, the lamella starts to close since defects in bilayers expose hydrophobic domains creating a bending instability that is reduced when the bilayer edges bind. In the case of multilamellar vesicles[43] (Figure 6(D-F)), the process is similar to unilamellars. When water is added to phospholipid layers, the outermost bilayers are hydrated more than the other bilayers, creating a series of bumps. The hydration helps to increase the surface area of phospholipid heads and, as a result, lamellar structures grow and separate between them. Then, after agitation, bilayer structures detached and exposed the hydrophobic segments to water, forcing the lamellars to close and form multilamellar vesicles.

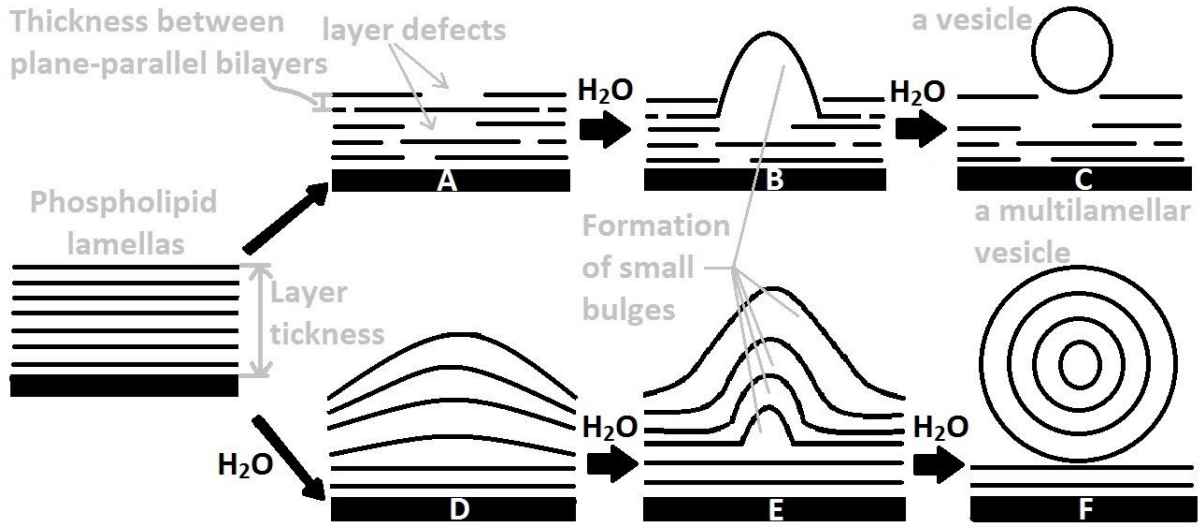

Figure 6. Mechanism of formation of unilamellar[42] and multilamellar[43] vesicles. From a lamellar structure, when a bilayer with defects is hydrated (A), water solution begins to inflate the bilayers (B) until finally the lamellar form a spherical vesicle. Other pathway is the hydratation of several layers (D) that start to grow because of the increment in the surface area of the polar head groups. Then, after agitation, bilayers detached and closed, forming a multilamellar vesicle.

The flat disk formation

In a second proposed mechanism (Figure 7), amphiphilic block copolymers (Figure 7(A)) self-assemble into aqueous solution in small micelle structures[39] (Figure 7(B)). Then, these spherical micelles fuse among them and, as a result, micelles grow into a disk-like or open-cylindrical structure (Figure 7(C)). Finally, the flat disk closes forming a closed bilayer structure or polymersome[39,40] (Figure 7(D)). This pathway, which was developed using molecular simulation, can also be applied to phospholipids. For example, according with experiments using the detergent depletion method[43], which consists of a mix of phospholipid and detergent micelles and the removing of detergent by dialysis, large unilamellar vesicles (LUVs) can be formed[41]. So, in short, the general pathway is as

follows[43]: mixed micelles formation → disk-like micelles fusion→ bending of bilayered phospholipid fragments (BPF) → LUVs. BPFs are just bigger disk-like micelles that grow by fusion. The overall pathway can be understood in terms of the system for achieving a minimal total free energy. Accordingly, disk-like structures have exposed hydrophobic edges that have unfavourable interaction with water; nonetheless there are some detergent surfactant shielded the edges[44]. The energy of this boundary is determined by the following equation[44]:

$$E_b = \gamma S$$

Where γ is the boundary interaction energy per unit length and S is the circumference of the polar/non-polar interface. Thus, to reduce the adverse interactions of hydrophobes with water, and as a result minimise E_b, the total circumference of the system is decreased by fusion of disk-like micelles[43,44]. The total circumference of the micellar system decreases at a constant phospholipid surface area. After a while, when there is a depletion of detergent, the system will require a further minimisation of E_b that can be achieved by bending BPF structures[43] and, consequently, there is an increase of the elastic curvature energy:

$$E_c = \frac{1}{2}\left(\frac{kA}{R^2}\right)$$

In the above equation[44], k is the elastic module, A is the surface area of a lamella and R is the mean radius of curvature. Therefore, there is a balance between the curvature energy and boundary energy that stabilises the creation of vesicles. As a consequence, these parameters are the forces that drive vesicle formation in order to reduce unfavourable interactions between hydrophes and water[45].

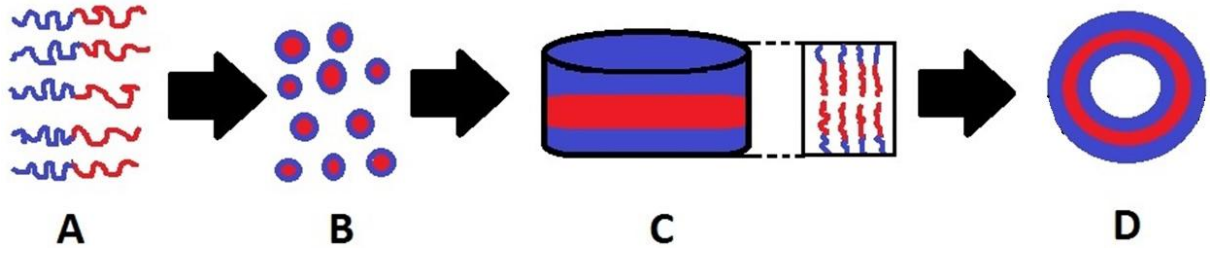

Figure 7. Mechanism of polymersome formation as described by molecular simulation[39]. Amphiphilic block copolymers (A) self-assemble into spherical micelles (B). Then, these small micelles merge with each other and form a bigger disk-like structure (C). Finally, the flat disk closes forming a closed bilayer structure or vesicle.

Experimental evidence of theoretical mechanism of vesicle formation

Also, there is experimental evidence that some block copolymer systems follow a very similar pathway of the mechanism described above. For instance, poly(ethylene oxide)-b-poly(caprolactone) (PEO-b-PCL)[46], when dissolved in tetrahydrofurane and then in water, have the following aggregation behaviour: spherical micelles → worm-like micelles → lamellar structures→ vesicles. The only difference with relation to the phospholipid vesicle mechanism is the formation of a lamellar intermediate before the creation of vesicles. Polymersomes formed when two bilayers, one above the other, have a small space of separation. This facilitates the closing of the edges in a "zipper-up fashion" and minimises the curvature and interfacial energies. After complete vesicle closure, water diffuses through the membrane interior and vesicles begin to adopt a spherical form, i.e. a minimal energy structure. However, these morphological transitions for polymersome formation was observed in samples prepared for dynamic-cryo TEM, i.e. a modified environment, and were not observed *in situ* from bulk sample solutions using the same copolymer.

However, with the introduction of more versatile polymerisation techniques, amphiphilic block copolymers can be synthesised "in situ" from a bulk aqueous solution by the use of the polymerisation induced self-assembly method[47]. The general principle of this technique is the generation of a hydrophilic living polymer precursor using controlled/living free radical polymerisation and conducting a reaction of this polymer with hydrophobic monomers in solution, in order to form amphiphilic block copolymer[47]. Basically, the hydrophobicity of the amphiphile will evolve through time, i.e. the hydrophobic part will be constantly growing. For example, in a experiment[48], a poly(glycerol monomethacrylate)$_{65}$ macro-chain transfer agent (G_{47}), which was used as the hydrophilic polymer, reacted with 2-hydroxylpropyl methacrylate monomers (H_X), which was the water-miscible monomers. The resulting diblock copolymers (G_{47}-H_X, where the subscripts indicate the monomer average number) were used to study the aggregation structures in aqueous solution at different percent of conversion of "H", up to G_{47}-H_{200}. These samples were examined revealing vesicles. According with their results, they found a rich diversity in nanostructures. For example, depending of the reaction conversion, they found spherical micelles → worm micelles → "Y-junction" micelles → highly branched micelles→ bilayer octopi structures→ jellyfish structures → vesicles. Apparently, "jellyfish" are the precursors of vesicles and its "tentacles" merge to give a closed polymersomes.

1.3.3 Techniques to prepare vesicles

There are many methods for vesicle preparation. All the methods described in this section can form giant vesicles (GV) with sizes in a range of 1-100 μm or SUV with sizes < 50 nm, depending on the variation of initial conditions in the specific technique. Some of the most representative techniques

to make vesicles are: the film hydration, with or without the use of an electric field, the switching solvent methodology, the water/oil (w/o) emulsion and vesicle preparation using microtechnology, e.g. a microfluidic device or an inkjet printing[35,49].

Hydration techniques

An example of a hydration method is the film hydration technique[49,50]. This method requires the dissolution of a block copolymer into a volatile solvent and the formation of a polymer film on a solid surface, commonly glass, after solvent evaporation. Then, the dry bilayer film is hydrated and giant vesicles are formed after a certain time of addition of an aqueous solution. The advantages of this method are the simplicity and relative rapidity of vesicle formations[51]. However, the disadvantages are a large size distribution of vesicles and some solvent can remain after drying the polymer film[52]. Other names given to this technique are: spontaneous swelling, natural swelling, gentle hydration[49] or film swelling via an organic solvent free technique[50,53]. However, strictly speaking, this method is not completely organic solvent free because one step of the procedure uses an organic solvent. A really solvent free technique is the bulk swelling[50,53] in which pure water is added to a bulk polymer. Then, a vigorous agitation for a long time of the polymer solution perfectly hydrates the sample and forms a wide distribution size of vesicles. A procedure usually used to narrow vesicle dispersion is extrusion[51]. This technique consists of passing vesicles through a pore membrane several times in order to fragment and monodisperse the vesicle sample[54]. In addition, the extrusion technique can be used for obtaining narrow sizes of either SUV (50-100 nm) or GUV (5 μm)[54].

An interesting variation of the film hydration technique, which can control giant vesicle sizes, was proposed by Howse and co-workers[55]. In their research, they used a soft-lithography technique in order to make hydrophilic islands surround by hydrophobic fluorocarbon surfaces. Then, the spin-casting of a polymer solution of poly(ethylene oxide)$_{16}$-b-(butylene oxide)$_{22}$/water provided ultra-thin polymer films (several hundreds of thickness) in each hydrophilic island by spontaneous dewetting of the film these hydrophilic surfaces. Finally, after addition of pure water, lamellar phases into the polymer film grew and formed vesicle structures, which spontaneously detached from the hydrophilic surfaces. Howse et al. achieved a control size distribution of polymersomes by modifying the island enclosed space.

Another method of vesicle production is the electroformation technique[49]. Similar to the film hydration method in that a polymer layer must be first created on a surface with an organic solvent, except this time, the polymer solution is deposited on palladium wires or a conductive glass surface, e.g. a glass coated with indium tin oxide (ITO). In the electroformation technique, water addition and an alternating electric current are applied on palladium wires or ITO glass. The electric current

promotes the formation of giant unilamellar vesicles which can be seen after about 90 minutes. The main advantages[51] of this method is a relative good control on the size distribution of vesicles and the production of only giant unilamellar vesicles (GUVs). However, this technique is time consuming and only a few vesicles are obtained each time.

The switching solvent technique

This method is based on dissolving the copolymer in an organic solvent before amphiphilic bilayer aggregation[50]. A suitable organic solvent is used to dissolve the copolymer macromolecules and then the solution is brought in contact with water in order to induce vesicle formation[50,53]. This can be done in two ways; either adding water dropwise to the organic polymer solution or injecting the organic solution into pure water[35]. This method is also termed the phase inversion technique[35] and affords the formation of both SUV and GUV[56]. For instance, when graft copolymer chitooligosaccharides-g-polycaprolactones is dissolved in 1,4-dioxane and water is added dropwise, under a vigorous stirring, this copolymer can form vesicles from 400 nm to several microns of diameter, depending on the water content into the organic solution[56] (up to 50 %w). In this technique, the organic solvent can be removed using a suitable procedure, e.g. dialysis[53]

The water/oil (w/o) emulsion technique

A third method of preparation of vesicles is derived from the formation of an amphiphilic copolymer monolayer at the interface of a w/o system (Figure 8). This method[49] begins with the preparation of a copolymer oil-phase in equilibrium, i.e. phase separated, in a water phase. Then, this w/o system is incubated in order to promote the migration of amphiphilics to the w/o interface and create a monolayer. After that, with the copolymer dissolved in the emulsion, a w/o emulsion is added to the previous formed two-phase equilibrium system and create small droplets of water coated with amphiphilics. Then, water droplets begin to migrate from the upper oil phase to the lower aqueous phase because of difference in densities. At some point of the migration, the droplets crossed the w/o interface and form a enclosed-bilayer membrane, i.e. a vesicle. An example of this technique is the elaboration of polymersomes made of polyethyleneoxide-b-polybutadiene (PEO-b-PBD)[57]. So, in order to form the w/o two-phase equilibrium system, the upper-oil phase is composed of PEO-b-PBD/toluene and the lower-aqueous phase is referred as internal buffer composed of sucrose-based buffer. Also, an emulsion is prepared using the same components as the other oil phase, i.e. copolymer/toluene, but with glucose solution as the aqueous phase. This emulsion is added to the w/o system and centrifugation is applied to the system in order to promote migration of water droplets to the aqueous phase and, as a result, vesicle formation, according with the above description. The typical polymersome sizes are around 50 μm.

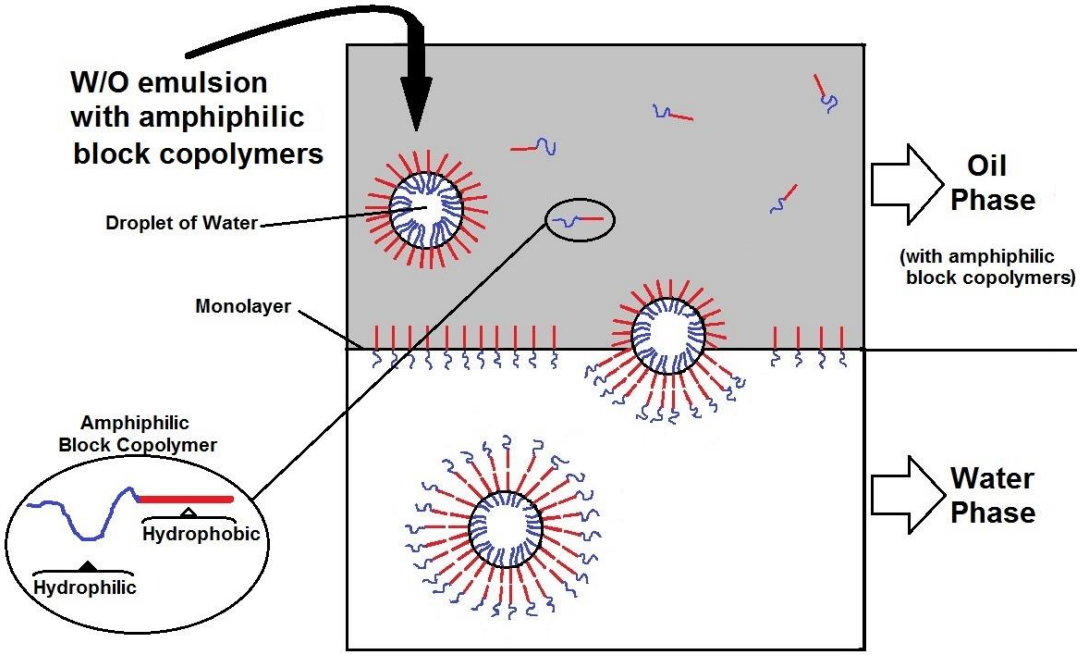

Figure 8. W/O method for GV formation[49]*. An oil and water phase-separated systems is prepared with a low concentration of amphiphilic block copolymer in the oil phase. After a time, amphiphiles migrate at the interface and create a monolayer. Then, a W/O emulsion is prepared with the same amphiphilic used to create the monolayer. In this emulsion, the water droplets are stabilised in the oil phase with amphiphilic molecules. Addition of this emulsion to the oil phase and centrifugation made the droplets to migrate to the interface and, when cross the interface, create an enclosed bilayers or vesicles.*

Inkjet printing technique

In literature, there are few articles about the use of inkjet printing on vesicle preparation. For example, in one experiment[58], unilamellar vesicles with sizes between 50-200 nm were created by jetting droplets of lipid or polymer solution into water. The inkjet cartridge was loaded with approximately 1-1.5 ml of a solution of phosphatidylcholines or poly(2-vynil-pyridine-b-ethyleneglycol)/ethanol and then the solution was ejected into a 10 ml stirring water recipient. According to the DLS and crio-TEM results, nanovesicles were produced with a narrow size distribution (standard deviation less than 0.1). In addition, encapsulation experiments were conducted using two slightly different procedures. In the first method, fluorescein was encapsulated by ejecting a fluorescein/ethanol/copolymer solution from the cartridge into pure water. In the second method, fluorescein was dissolved into water and an ethanol/copolymer solution was thrown out from the cartridge. In both cases, nanovesicles with fluorescein enclosed into the nanostructures were obtained even though the encapsulation efficiency was different. In the first

case, i.e. fluorescein/ethanol/ copolymer “printed” into the aqueous solution, the encapsulation efficiency was three times higher than the second case.

In another experiment, giant vesicles were detached from a planar lipid membrane by applying a pulse with an inkjet printing nozzle, which can contain a potential encapsulated compound (Figure 9(A-B))[59]. In this way, the material ejected from the nozzle can automatically be enclosed into the vesicle. The planar membrane can be formed[60] by first dissolving amphiphiles in a droplet of organic solvent in a suitable humidification chamber. Then, the injection of two water droplets at each side of the solvent, in such a way that the organic phase touches the water phase, allows the formation of a water/oil/water system. The bilayer is created at the water/oil interfaces. Vesicles can be produced[59] by introducing an inkjet printing nozzle into one water droplet and generating a small liquid pulse close enough to the lipid membrane. This small perturbation blew out the membrane and created a small sack which separated from the membrane and formed a vesicle. The interior of the liposome contained water and the compound ejected from the nozzle. Due to the vesicle sizes, i.e. 300-600 µm, it was feasible to enclose cells and chromosomes. However, the main disadvantages of this technique were vesicle sizes and trace of organic solvent within the membrane.

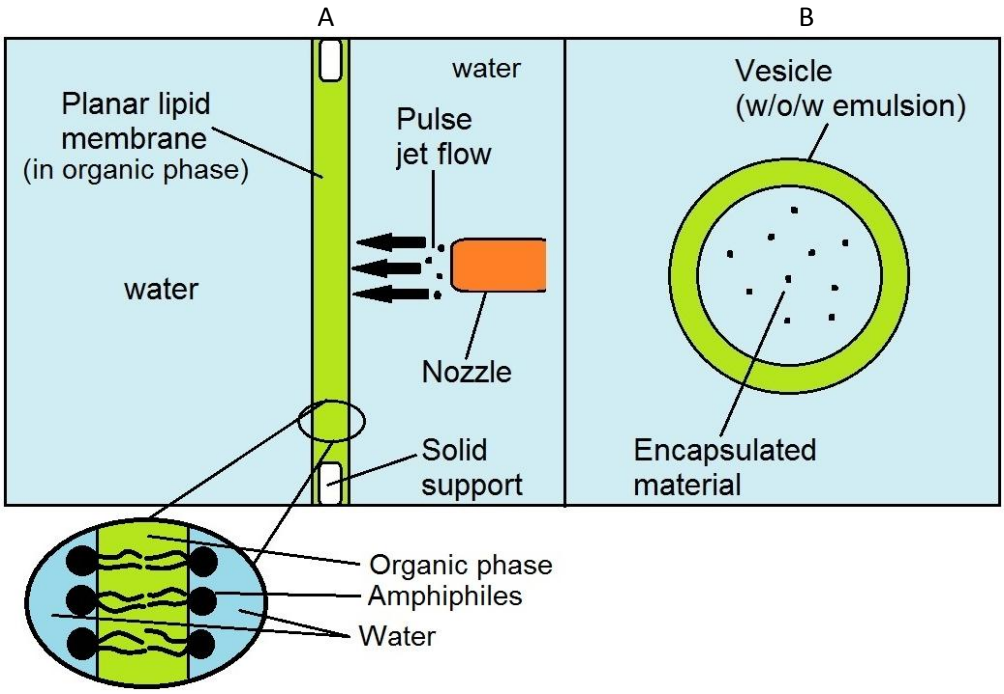

Figure 9. Vesicle formation using an inkjet printing nozzle and a planar lipid bilayer[59]. The GUVs were formed by applying a small “pulse” close to the membrane (A). The main advantage of this method is the automatically encapsulation of a compound by loading the inkjet printing reservoir with the desired reagent (B).

Using the same principle of formation of planar lipid membranes and the use of a nozzle to form vesicles, another study controlled the vesicle sizes in the range of 10-400 μm by modifying the inkjet printing parameters and the lipid solution viscosity[61]. So, a high-throughput in vesicle formation can be achieved because one nozzle pulse can generate one vesicle, leaving the bilayer membrane unaltered after many pulses. Indeed, thousands of GUVs per minute can be generated since the typical time of vesicle formation is 5 ms[62]. Also, using the inkjet printing technique is possible to create smaller liposomes of about 4 μm[63] with asymmetric lipid membrane since different lipids can be dissolved in each droplet of water. The asymmetric membrane was confirmed using a specific selective dye which just binds to one of the lipid monolayers that make up the asymmetric membrane.

1.3.4 Polymersome applications

The main application of polymersomes is drug delivery[66]. A polymersome can entrap a drug in two ways: into its volume-water cavity surround by a polymeric membrane or into the hydrophobic membrane. This structural feature in vesicles provides them versatility in drug encapsulation and the possibility of store both hydrophobic and hydrophilic drugs in the same structure. For example, nanovesicles made of a mixture of PEG-poly(lactic acid) (PEG-PLA) and PEG-polybutadiene (PEG-PBD) can encapsulate doxorubicin (a hydrophilic drug) into the aqueous lumen and placlitaxel (a highly hydrophobic drug) within the membrane[67]. The result of this study reflects an increment in the toxicity and accumulation of the medication in the tumour cell which means a more efficient drug delivery[66]. Such effectiveness is due in part to the sizes of polymersomes, in the range of 80-150 nm, which promote high retention times in the body since excretion organs have pore sizes between 40-60 nm, and nanovesicles cannot be trapped within these pores. As a consequence, nanovesicles can endure relative long times in the body without been expelled and have the opportunity of “find” and accumulate in tumours’ pores with are commonly larger than liposomes[12].

Polymersomes can also be used as bioreactors. An interesting example is the generation of adenosine triphosphate (ATP) by means of a reaction between adenosine diphosphate and inorganic phosphate, and using ATP synthase as catalyst[68]. The ATP synthase is embedded in the polymersome membrane and works like a motor which fabricates ATP. Another example[69] is to carry out a reaction with an encapsulated enzyme into the lumen and reagents outside the vesicle that can pass the membrane via membrane pores. Thus, reagents can react with the enzyme. These researches proved the possibility of complex reactions using polymersomes as bioreactors.

1.4 The Hofmeister series

It is well known, since the last century, that salts can cause certain effects in natural[70,71] and synthetic macromolecules[72]. For example, they can affect biological phenomenons such as protein-stability, protein-protein interactions, protein folding, enzyme activity and micelle formation[73,72], among others[74]. The first systematic study about the effect of salts on protein colloidal behaviour was conducted by Frank Hofmeister[75]. Basically, Hofmeister noticed that certain ions have a greater influence on the solubility of proteins in aqueous solution, than others salts. This is termed the salting effect or Hofmeister effect. Since then, a large number of articles tried to explain and elucidate the mechanism of interactions between ions-water-macromolecules in the salt effect process. In most of these studies, the common trend is the order of the ions which is basically the same, as in Figure 10, in different biological and synthetic macromolecules. There is not a complete and definitive explanation about this specific order of ions in the Hofmeister series; however, it can be partially related with the size of the ion and its charge density and how these parameters affect the water structure in solution[76]. For example, in the following ion series: F^-, Cl^-, Br^- and I^-, the surface density (i.e. electric charge per unit volume) of the ion decreases and as well as the power of hydration, which agrees with the Hofmeister effect. Therefore, high surface densities ions (i.e. small ions and high charges) have stronger interactions with water. This can be explained if ions are considered as spheres with a point charge in the center. In such a case, water molecule close to the center of the ion will interact stronger than water-water molecules in the bulk, i.e. ions have stronger hydration power than big ions. However, when the salt effect is applied to other related phenomena[77], as described at the beginning of this paragraph, and depended on experimental conditions[78], others arrangements in the series are possible. The series can be reversed or some ions can be in a different order, for instance.

1.4.1 The effect of salts on biological macromolecules

Figure 10 is a representation of the Hofmeister series, specifically the effect of anions for molecular aggregation. Generally, anions have greater efficacy in salting-effect than cations[73,77,79]. However, in some cases, such as the study of the hydrodynamic radius of DNA[80], cations have a strong interaction with biological macromolecules. Commonly, chloride is considered the anion which divides the series. The species to the left side of chloride have higher hydration strength and, as a consequence are more capable of stabilising and aggregating proteins[73]. These anions are used to promote the salting-out effect in macromolecules and are known as “kosmotropes”. Conversely, anions to the right side of chloride give rise to solubilisation and destabilisation of macromolecule solutions and, as a result, promote the salting-in effect and are known as “chaotropes”[73].

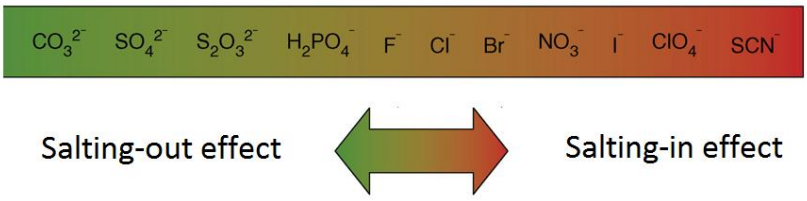

Figure 10. The strength of anions in the Hofmeister series[73]

In addition, kosmotropes are "water structure makers" because they promote hydrogen bonding around the co-solvent molecules, increasing the water order[81]. In contrast, chaotropes are "water structure breakers" because they destabilise the hydrogen bonding networking around the co-solvent, decreasing water order[81]. The water order can be seen in the perspective of hydrogen bonding networking and the effect of ions with these bonds (Figure 11)[81].

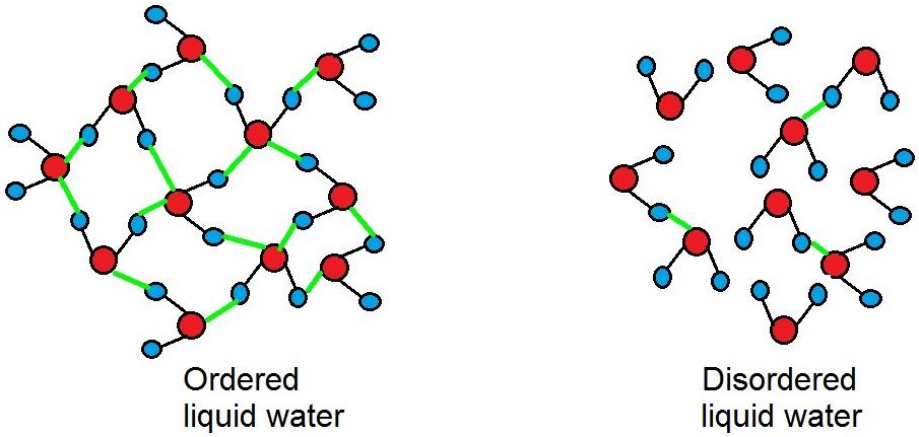

Figure 11. Order of water relative to hydrogen bonding[81].

With respect to ion-water interactions, the water structure in a salt solution is the result of the equilibrium between the electric charge on the ion with water molecule's dipole, on the one hand, and interactions between bulk water on the other[82]. The consequence of salt addition to water will be a rearrangement of water molecules into a well defined shell, or shells, depending of the strength of the ionic charge density around the electrolyte[77]. In the case of chaotropes, where these types of species are considered weakly hydrated, i.e. low solvation power, the bonding force between the ion and water molecules in the first layer is considered less strong than the hydrogen bonding force between water-water molecules in the bulk. Consequently, water molecules are more "available" to hydrate a macromolecule and dissolve it (salting-in effect)[83]. A similar argument can be applied to kosmotropes in order to explain the salting-out effect. However, recently, the interpretation around salt solutions that can change the water structure has been challenged. New evidence indicates that kosmotropes and chaotropes do not have a great influence in the dynamic properties of bulk

water[73,84]. Thus, the conception of long-range ion forces that can orient water molecules throughout a long distance was finally dismissed.

Definitions of kosmotrope and chaotrope were given based on the first interpretations of the Hofmeister series which were focused more on the effect of salts over the structure of water. However, in order to have a better understanding of this phenomena on aggregation, it is important to know the effect of ions on macromolecule structures[73,83]. In this case, cations and anions can bind to the solute molecular surface and affect its colloidal properties. In order to understand this type of electrostatic force, it is necessary to introduce the "law of matching water affinities". This concept says that oppositely charged ions with equal affinities are more able to form ion pairs than opposite charge ions with different water affinities. This means that chaotropes have affinities with chaotropes and kosmotropes have affinities with kosmotropes[77,85], i.e. "like likes like". When a chaotropic salt is dissolved in an aqueous protein solution, the positively charged regions in the macromolecule will attract anionic-salt chaotropes. For example, in a protein comprised of Lysine aminoacids, the positive charge surface comes from ammonium groups[86] which can be considered chaotropes[87], i.e. they can contribute to protein solubility. So, electrostatic attractions of anion salts to the positive-charged fragments of the protein surface will have a consequently decreased in protein solubility[88], which can be related with the salting-out effect. Such a case, the Hofmeister series is reversed.

1.4.2 The effect of salts on block copolymers and their nanostructures

In the case of synthetic non-ionic block copolymers in solution, salts have different effects on the physical behaviour of the polymer solution. One of the first investigations compared the amphiphilic block copolymer poly(vinyl alcohol-*co*-vinyl acetate) (PVA-PAc) with poly(vinyl alcohol) (PVA) in aqueous solution using different inorganic salts[89]. According to the results, PVA-PAc system follows the Homeister series regarding solubility in salt and the effect of anions is stronger than cations, i.e. the type of cation does not affect the order of anions in the Hofmeister series. Moreover, it was determined that anionic chaotropes interact more strongly with the hydrophobic segments (acetate groups in PAc) than with the hydrophilic parts (hydroxyl groups in PVA) in the block copolymer.

There are several theories that explain the effect of salts over hydrophobic molecules. One first theory, the internal pressure concept, focuses problem in terms on ion/water interactions rather than ion/non-polar bindings. The general idea is that the addition of salt to water causes a volume change in the solvent medium which can induce salting-in or salting-out phenomena in hydrophobic solutes, depending if the change in volume is positive (i.e. water expansion) or negative (i.e. water contraction), respectively[90]. Another model takes into account the small charge of the ion and its

effects on the system. So, an ion generates an electric field that attracts molecules with higher dielectric constants and does not interact with molecules with lower dielectric constants. In aqueous solution, most hydrophobic molecules posses a lower dielectric constant than that of water, therefore non-polar molecules are segregated from the network of hydrated ions[91]. This situation is related to the salting-out effect since there is a reduction of the salt concentration close to the solute surface. Another hypothesis, is that the salting effect can be explained in terms of the binding or exclusion of ions relative to the hydrophobic material. For example, the salting-in effect can be depicted as low-charge density ions which bind to hydrophophic surfaces and, as a consequence, reduce the interactions between these surfaces and water[91].

In literature, there are reports on the effect of salts on poly(oxyalkylenes), both polymers and block copolymers, because of the technological implications represented by these types of macromolecules. One of the most common system studied is poly(ethylene oxide) (PEO). It is well known that this macromolecule is fully soluble in water; according to the model of a tetrahedral water network, the PEO structure, (i.e. the ether oxygen and the methylene group) fits into the intricate molecular cluster of liquid water, completely stabilising hydrogen bonding structures[92]. In addition, a thermodynamic study on the process of mixing PEO and water determinates that the negative entropy of solution indicates an increase in water structuring around the PEO, with the corresponding hydration shell[92].

In the system PEO + salt + water, the salting effect needs to be interpreted in terms of the interactions of the proximity of ions in the hydration shell of the PEO rather than the salt-polymer interaction, due to the uncharged nature of PEO[93]. For example, the addition of alkali and halide salts to a PEO solution caused phase separation preceded by a cloud point. The authors concluded, after a thermodynamic analysis of a slightly increment of the salt concentration in the polymer-poor phase, that the PEO surface contains a region of low salt concentration in comparison with the bulk[93]. This finding agrees with the entropic origin of the salting-out effect[91] since an asymmetric hydration due to salt distribution into the solution can produce a disturbance in molecular configuration into the system, i.e. ions form hydrated structures away from the PEO which diminish the volume occupied of all species into the solution, and PEO macromolecules are more available to agglomerate.

Another important poly(oxyalkylene) is the triblock copolymer poly(ethylene oxide)-poly(propylene oxide)-poly(ethylene oxide) (PEO-PPO-PEO) which behaves differently upon the addition of salts, i.e. micelle aggregation[72], a lyotropic phase transition (e.g. from sphere-to-cylinder[94]) or macromolecular aggregation (e.g. formation of micelles[95]). Specifically, PEO-PPO-PEO has two different phases in

solution: they can form micelles and micelle aggregates. This can be observed by thermoresponsivity measurements on the polymer, principally critical micelle temperature and cloud point temperature. Normally two step phase transitions are observed, however with the addition of chaotropic anions one step transition can be seen[72].

In the case of aggregation in nanovesicles, allyl dodecyl dimethylammonium bromide (ADDB)/ sodium dodecyl sulfonate (SDS) spontaneously form liposomes of about 80 nm in aqueous solution[96]. Addition of 250 mM NaBr to the vesicle solution makes them flocculates, increasing the hydrodynamic radius to 250 nm. According to the Derjaguin-Landau-Verwey-Overbeek (DVLO) theory of colloid stability[97], vesicle aggregation is due to van der Waals attractions. However, the DVLO theory does not take into account water interaction around the hydrophilic part, i.e. short rage interactions, important to explain the salting-out effect[98]. In the above case, the aggregation behaviour of the liposome solution was attributed by the screening effect of counterions to the head groups of bilayer[96]. Another feature is that salt addition can induce fusion in vesicles. For instance, vesicles made of poly(ethylene oxide)-b-poly(butadiene) under agitation and low salt concentration[99], i.e. 10 mM NaCl, induce fusion of large vesicles (about 200 nm) into giant vesicles (above 1 μm). In order to promote membrane fusion, both vesicle aggregation and defect creation in the adjacent membranes must occur[100]. In the polymersome case, sample stirring allowed vesicle contact and salt introduced a stress in the bilayer, collapsing PEO chains, which in turn affect the hydrophobic part and destabilised the membrane causing fusion.

With respect with the block copolymer poly(ethylene oxide)-poly(butylene oxide) (E_XB_Y, where *x* and *y* indicate the average number of monomer), there is some research on the effect of salts on E_XB_Y systems. For example, experimental results[101] on the hydrodynamic radius (R_h) of $E_{90}B_{10}$ micelles in aqueous solution, determinate that addition of K_2SO_4 does not affect the R_h at relative low concentration (0.2 mol/dm^3). Also, this system is not affected by changes in temperature. Moreover, it was concluded that K_2SO_4 (0.2 mol/dm^3) is a poor solvent for the copolymer if it is compared to water, since the second virial coefficient, which in this case illustrates the interactions among the copolymer and solvent, is lower in ionic solution than in the solvent[101]. Similar results were obtained for the block copolymer $E_{86}B_{10}$[102]. However, the salt effect at high salt concentrations in this system is unknown.

1.5 Elastic properties of membranes

Membranes are ubiquitous in biological systems since they can be found in all types of cells, enveloped viruses, and organelles[103]. One important characteristic in biological membranes is their

softness and, as a consequence, their unusual elastic behaviour. For example, some forms of cells posses extremely soft structures but at the same time they are tough. This is the case of red blood cells which need to be very flexible to pass through narrow arteries but at the same time tough in order to endure for about 120 days in the circulatory system[104]. Also, the mechanical behaviour of a membrane plays a vital role in the proper functioning of the cell (stability and permeability) affecting several biological processes (e.g. endocytosis and exocytosis) and is related to the influence, at least in part, to disease (e.g. virus infection)[105]. Therefore, one important factor in order to fully characterise the membrane is to take into account its mechanical properties.

A membrane can be modelled as a thin 2D-sheet forming a 3D cavity because the difference between the thickness (2D) and vesicle diameter (3D) is several orders of magnitude[106]. The membrane curvature in any surface point can be defined if a bilayer is cross-sectioned by two normal planes to the surface[107] (Figure 12). The curvature in each plane will be the best fit circle along the surface and the radii that generates will be the principal radii of curvature, i.e. R_1 and R_2. The principal curvatures are defined as: $C_1=1/R_1$ and $C_2=1/R_2$. Therefore, when C_1 and C_2 are zero, the membrane is flat and when both have positive values and $C_1 = C_2$, a sphere is formed. Others close-related parameters that can be defined using the principal curvatures is the Gaussian curvature: $K_G = C_1 C_2$ and mean curvature: $H=1/2 (C_1 C_2)$.

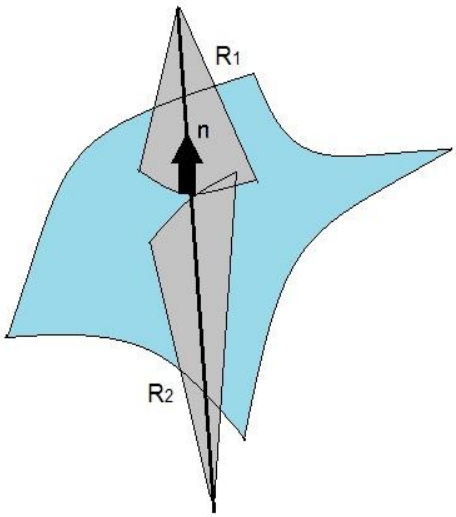

Figure 12. A curved surface that represents the membrane. The membrane surface is cut by two planes with an angle of 90^0 to the surface. In each plane, a circle just touches the surface and the inverse radii in these circles are known as the principal curvatures C_1 and C_2. The principal curvature can be positive or negative depending of the bend towards the normal of way from it[106].

1.5.1 Basic modes of deformations in bilayers

There exist three conventional types of deformations which can be used to characterise the physical properties of membranes. These parameters are dilation, bending, and sheering forces[108]. However, also possible is the movement of the inner and outer membrane leaflets resulting in monolayer slipping[109].

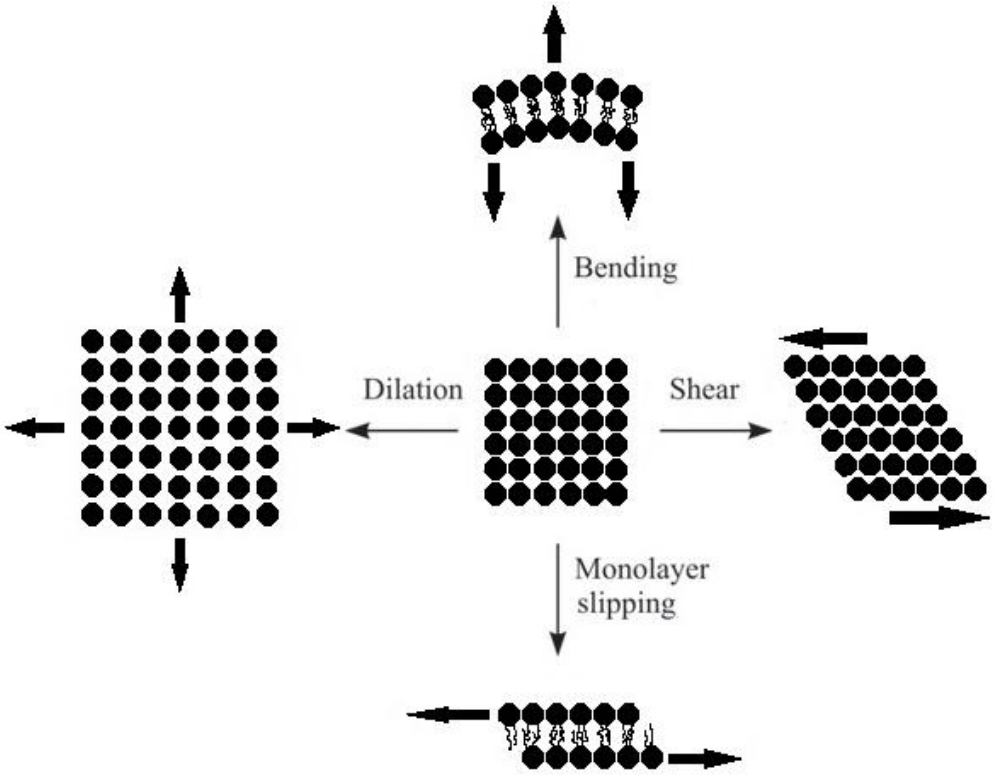

Figure 13. Basic modes of deformation in a lipid bilayer membrane: dilation, bending, shear and monolayer slipping[109].

Dilation, also known as stretching, is characterised by a force that pulls the sides of a membrane and is opposed by the internal stress of the bilayer from its equilibrium state, causing a change in membrane area[110]. The energetic cost of this change is represented in the following equation[111]:

$$E_{stretch} = \frac{1}{2} K_A[mN/m] \frac{(A - A_o)^2[m^4]}{A_o[m^2]} [=] [mN\ m]$$

K_A is usually called either the area stretching modulus or area compressibility (or expansion) modulus and the variables A_o and A are the membrane area at the beginning and after external-lateral tension, respectively. This lateral tension (τ) applied to the membrane is defined in terms of partial derivatives of the energy of stretching with respect to the membrane area and can be seen as

the consequence of Hook's Law that relates stress with strain, i.e. force versus elongation (or compression), using a constant of proportionality which in this case is the stretch modulus K_A[111].

$$\tau \equiv \frac{\partial E_{stretch}}{\partial A} = K_A \frac{A - A_o}{A_o} = K_A[mN/m] \frac{\Delta A[m^2]}{A_o[m^2]} [=] [mN/m]$$

In a membrane stretching event in liposomes, the change in membrane area (ΔA) usually does not surpass a value of 5% before rupture[112]. This is probably because at such related tensions the bilayer begins to form small pores, which affect the stability of the membrane, finally bursting it[113]. However, lysis or vesicle break is strongly dependent on the tension rate (force/m/s) applied to the membrane. In some cases, the area change can be as much as 13% which indicates a phenomenon of kinetic origin[114] because there is a dependence of the tension-loading rate and membrane rupture. In such case, the rate of tension will dictate the formation and evolution of micropores until vesicle rupture[115].

Membrane bending can be characterized based on a membrane curvature model using the bending energy as mathematical tool to describe this type of elasticity. The bending energy can be defined as the work necessary to bend a bilayer sheet away from its basic form towards a new shape[116] and is described by the following equation[117]:

$$E_{bend} = \frac{1}{2} k_c \, (2H - c_0)^2 + \bar{\kappa} K_G$$

Where k_c is the bending modulus, H is the mean curvature, c_0 is the spontaneous curvature of the basic form, $\bar{\kappa}$ is the saddle splay modulus and K_G is the Gaussian curvature. The concepts of H and K_G are as defined previously. c_0 is related to the typical curvature of a bilayer based on an amphiphilic's specific chemical characteristics[107]. The bending modulus can be seen as a parameter which indicates the rigidity of a membrane. High values of k_c denotes that the membrane does not easily bend while low values indicate flexible membranes.

Finally, membrane shearing is the force which is exerted in opposed directions lateral to the membrane (Figure 13). According to the mosaic model, membranes can be approached as fluids and, as such, they are unable to resist shear forces, unless the membrane is part of a cytoskeleton. Shear forces are important in more complex membranes, such as red blood cells[110], which contain a cytoskeletal network membrane. For example, red blood cells can adopt different shapes and they

can be explained when the shear forces is taken into account in the overall picture of the model, a part of considering bending and stretching forces.

1.5.2 The mechanical properties of vesicles

There have been several studies published about the elastic behaviour of vesicles using the micropipette aspiration technique (MPA). These studies relate the effects of molecular weight (Mn), hydrophilic core thickness (d), and chemical characteristics of the amphiphile with respect to the elastic parameters of the bilayer, specifically k_c and K_A, with the differences between liposome and polymersome elastic properties being compared.

The typical block copolymers cited in literature are polyethyleneoxide-b-polyethylethylene (PEO-PEE) and polyethyleneoxide-b-polybutadiene (PEO-PBD). In one experiment, four different molecular weight of copolymers (PEO_{26}-PBD_{46}, PEO_{50}-PBD_{55}, PEO_{80}-PBD_{125}, PEO_{150}-PBD_{250} with a range of M_n= 3.6-20 kg/mol and d= 9.6-21 nm) were used to study the effect of amphiphilic sizes on the stretching modulus of polymersomes[118]. According to their results, K_A did not fluctuate too much between block copolymers and can be considered unaffected by M_n and *d* (average= 102 ±10mN/m). The stretching modulus has been found to be related to the chemical composition of the bilayer rather than the thickness[118]. Based on this, K_A can be described via the interfacial tension (γ), which depends on the chemical composition, at each interface of the bilayer (i.e. K_A= 4 γ). As an approximation, it has been suggested that hydrocarbon/water tensions can provide a good estimation to K_A in polymersomes. Since typical values of γ are between 20-30 mN/m[119], the values of K_A are expected to be in the region of 80-120 mN/m in accordance with the above equation. This range mostly agrees with values published in literature, e.g. PEO_{40}-PEE_{37} with K_A= 120 ±20mN/m[27] and PEO_{26}-PBD_{46} with K_A= 107 ±14mN/m[120]. K_A is also associated with the number of bilayers which comprise the vesicle[121]. This means that lowest values of K_A will indicate fragile membranes, as a consequence of having unilamellar structures, whereas higher values will suggest the presence of multillamellar vesicles.

Membrane thickness for liposomes are typically 3-5 nm[122]; however**,** the stretching modulus of different types of liposomes cover a wide range of values. For example, some lecithin vesicles have magnitudes between 135-190mN/m[123] and phosphatidylcholine (PC) liposomes (twelve different PC's) range from 229 to 265 mN/m[124]. Also, the addition of an extra component to a pure phospholipid can greatly affect K_A. This is the case of a lipid mixture of 1-stearoyl-2-oleoylphosphatidylcholine (SOPC)/cholesterol (63 % mol) which can achieve magnitudes up to six times higher than that of the pure SOPC liposomes, i.e. from ~193 to ~1251 mN/m[125]. Apparently cholesterol molecules enhance and reinforce bilayer cohesion into the structure. These results

support the idea of the dependence of K_A on the type of amphiphiplic molecule that form the bilayer. Comparing the results of the stretching moduli cited above, in general, polymersomes have lower magnitudes of K_A than liposomes.

In the case of the bending elasticity parameter, experiments have shown that such modulus has a strong dependence to bilayer membrane thickness (d), contrary to K_A. For instance, typical values of k_c are between 14-30 k_BT for liposomes[124] (d= 3.4-4.4 nm) and 33-465 k_BT for polymersomes (d= 8-14.8 nm)[126]. In general, the membrane rigidity of vesicles increases as the membrane thickness increases[126]. In the case of liposomes, according with a theoretical study, the bending properties of phospholipid bilayers come from the decrease of conformational entropy of the tails[127].

The relation of k_c and d can be expressed in the next equation (according with a simple model of uniform plates since a bilayer is comprised of two elastic sheets)[128]:

$$k_c = \frac{K_A d^2}{\alpha}$$

Where α is a constant which depends on the feasibility of monolayers to slip among each other and, as a result, affect the membrane bending by making the bilayer more rigid in the case that the monolayers are coupled. In this way, α can have values of 12 or 48 if monolayers are coupled or uncoupled, respectively. Experimental results agreed with this model. For example, a series of different amphiphilic molecules[126] such as DMPC, SOPC, PEO_{40}-PEE_{37}, PEO_{26}-PBD_{46} and PEO_{80}-PBD_{125} presented a nearly linear fit when data of the ratio of k_c/K_A was plotted against d. In another experiment[124], but this time employing the bending modulus of different PC's, k_c was determined to scale with membrane thickness according with the polymer brush model, i.e. $k_c = K_A d^2/24$.

Much of the research on the mechanical properties in polymersomes has been focused on PEO-PEE and PEO-PBD block copolymers amphiphilics. The common features of these two copolymers is that have low glass transition temperatures (T_g), i.e. exhibit fluid phases, and are characterized by a coil-coil structure. So, there was no data about the effect of rod-coil amphiphilic copolymers with gel-like behaviour on the stretching parameter. Examples of such types of block copolymer[57] are PEO-b-PA444 and PEO-b-PA6ester1 (see Figure 14) which behave as liquid crystals at room temperature, i.e. the hydrophobic part of the amphiphilic is in the glassy state. Contrary to what one might expected, the results showed a stretching modulus slightly below than fluid polymersomes, i.e. PEO-b-PA6ester1 with a K_A= 81 ±10 mN/m, and a much lower value, i.e. PEO-b-PA444 with a K_A= 30 ±15

mN/m. In this last case, a possible explanation is that the Flory-Huggins parameter (χ), which is related to γ and depend on the chemical structure of the macromolecule, is small.

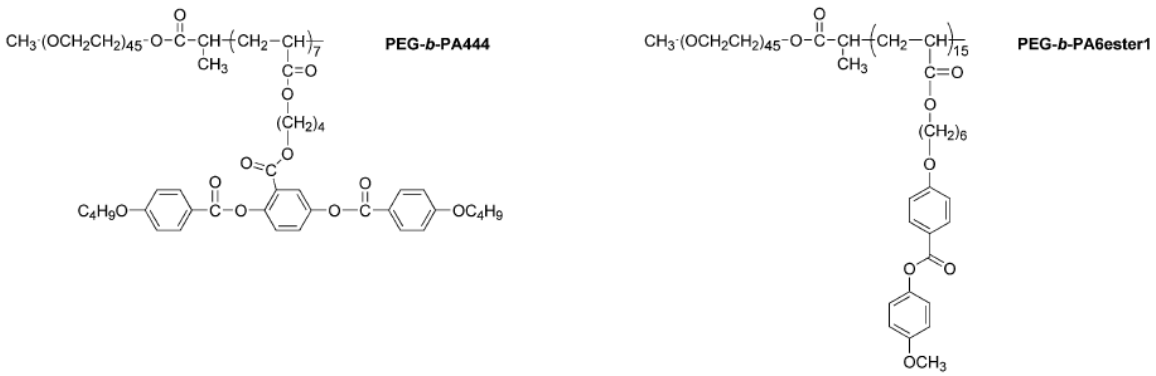

Figure 14. Block copolymers with a hydrophobic part glassy phase. These macromolecules were labelled as PEO-b-PA444 and PEO-b-PA6ester1[129].

1.5.3 The salt effect on membranes

In the case of liposomes, one parameter that greatly influences the elastic behaviour is the electric charges of natural amphiphilics. For example, the phospholipid membrane of a cell have a negative surface and, as a result, are able to attract cations forming a diffusive electric double layer[130]. In a similar way, ions can bind to either negative[131] or positive or neutral[132] phospholipid vesicles and form the same type of layer. This double layer and the charge surface are largely responsible for the elastic behaviour in phospholipids membranes.

It is feasible to have an analytical expression which illustrates how the electrostatic forces of a charged membrane affect the bending moduli (k_c)[133]. This can be achieved by solving the equations for the electrical free energy of the double layer, using the linearized Poisson-Boltzmann equation, which provides the electric potential and the surface charge distribution. Then, the curvature elastic free energy of a spherical-closed membrane, can be obtained, which provides the bending rigidity[133]**.** Then, combining the electrical and bending free energy equations, the contribution of the electric double layer to the bending moduli (k_c^{el}) is obtained:

$$k_c^{el} = \frac{\sigma^2(1+\delta^2)}{\varepsilon_w\,\kappa}\frac{3}{4\kappa^2} \quad (1)$$

Where σ is the total surface charge density, δ is the gradient of the surface charges of the inner and outer monolayers, ε_w is the dielectric constant of the aqueous medium and κ is the inverse Debye length, i.e. $\kappa = \left(\frac{2n_o e^2}{\varepsilon_w k_B T}\right)^{1/2}$. The Debye length ($\kappa^{-1}$) can be seen as the radius of the electrostatic charge density of an ion[134]. In this last equation, n_o is the density of ions of one sign in the electrolyte far from the membrane, e is the elementary charge, k_B is the Boltzmann's constant and T is the absolute temperature. Equation (1) is based on the Debye–Hückel theory and provides a first insight of the effect of salts on the elasticity of phospholipids membranes. Though, there exist intrinsic limitations to the theoretical framework used to deduce this equation (i.e. the Debye–Hückel approximation considers monovalent ions in the system, low surface potentials and low electrolytes concentrations[130]) which should be considered in order to interpret data.

According with equation (1), the phenomenological dependence to the bending energy will be dictated mainly by σ and κ. Analysing these two terms, the surface charge originates either from the remaining charge of ionic dissociation of phospholipid groups or from "external"-ion adsorptions of membrane surface[130] and the Debye distance is influenced largely of the aqueous electrolyte solution. The above implies that part of the deformation behaviour in charged membranes depends on the ionic strength, i.e. salt concentration[135], and the type of salt where the vesicles are immersed. When hydrated ions are attached to the bilayer, they dehydrate the membrane surface and modify the electric double layer and the surface charge density, hence their material properties. For example, for negatively charge membranes of dioleoylphosphatidylglycerol (DOPG), k_c is affected by the hydration strength of anions ($Cl^- > Br^- > I^-$)[136] and both the biding and hydration forces of cations ($Li^+ > Na^+ > K^+ > Rb^+ > Cs^+$) because the binding properties of cations in these sort of membranes is more relevant than those of anions[137]. For DOPG bilayers, the binding and hydration phenomena have the same tendency[136, 137], i.e. the bending energy decreases as the ionic hydration forces also decrease. In the case of multilamellar vesicles (MLVs) made of neutral zwitterionic phosphatidylcholines (PC) [138], the bending rigidity is unaffected by the addition of either 1 M of KCl or KBr since salts do not modify the bilayer fluctuations. However, higher salt concentrations such as 3 M and 5 M, $CaCl_2$, decreases the elasticity of neutral lipids[139]. Apparently, the additions of either 3 or 5 M salt concentrations increased the main phase transition of temperature (T_m) of the phospholipid, making rigid the membrane, and, as a result, affected the bending rigidity.

General Aims

The ability of block copolymers to self-assemble into polymersomes provides them with intrinsic advantages over liposomes due to their synthetic nature. Of particular interest to this research

group is the diblock poly(ethylene oxide)$_{16}$-poly(butylene oxide)$_{22}$ ($E_{16}B_{22}$, Figure 15) which has been proven to spontaneously form [140] both nanovesicles and giant vesicles in aqueous solution. This copolymer has been extensively studied[55,140,141,142,143,144,145] because of its potential applications mainly in biomedicine e.g. as a drug and gene delivery agent since ethoxylated groups can provide intrinsic biocompatibility and mechanical stability to the structure[17]. It is also important to know the polymersome behaviour under a salt environment since there is little research looking into the effects of salts into solution for EB systems[146,147,148]. In addition, the study of salts on nanovesicles may provide insight into the impact of ions on possible fusion events, since aggregation is a requirement to induce fusion in vesicles[149].

One aim of this project was to study the effect of salt on $E_{16}B_{22}$ vesicles. It was expected that the aggregation behaviour of this system would be dependent on the salt used and on the ionic strength. The concentration where these nanostructures can be found is in the range of 0.001-10 %(w/w)[150] in water, therefore, concentrations of 0.1 %(w/w) were used in experiments.

A further property which has not been characterized for $E_{16}B_{22}$ polymersomes is the membrane toughness, which is another important parameter for biomedical applications. A method widely use to measure this parameter is the micropipette aspiration technique (MPA). It is advantageous to develop a methodology of vesicle production allowing for the easy collection of giant vesicles for analysis. Therefore, a new methodology of vesicle production was implemented using an inkjet printing technique and its scopes were tested in preparing neutral charge polymersomes of $E_{16}B_{22}$ in different salt environments. In the final stage of this project, experiments were conducted using the MPA equipment, holding individual giant vesicles so that the stretching modulus of $E_{16}B_{22}$ polymersomes could be measured and this result can be compared with other values of block copolymer vesicles in literature.

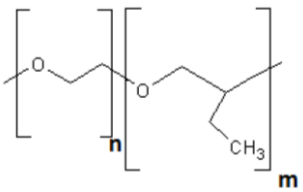

Figure 15. The chemical structure of the diblock copolymer of ethylene oxide-1,2-butylene oxide.

References

1. D. Lichtenberg, R. J. Robson, and E. A. Dennis, *Biochim. Biophys. Acta*, 1983, **737**, 285–304.

2. A. Blanazs, S. P. Armes, and A. J. Ryan, *Macromol. Rapid Commun.*, 2009, **30**, 267–277.

3. W. Blokzijl and J. B. F. N. Engberts, *Angew. Chem. Int. Ed. Engl.*, 1993, **32**, 1545–1579.

4. H. Ohvo-Rekilä, B. Ramstedt, P. Leppimäki, and J. P. Slotte, *Prog. Lipid Res.*, 2002, **41**, 66–97.

5. W. Dowhan, *Annu. Rev. Biochem.*, 1997, **66**, 199–232.

6. T. Smart, H. Lomas, M. Massignani, M. V. Flores-Merino, L. Ruiz-Perez, and G. Battaglia, *nanotoday*, 2008, **3**, 38–46.

7. C. Tanford, *The Hydrophobic Effect: Formation of Micelles and Biological Membranes*, John Wiley & Sons, Inc., London, 1973.

8. N. T. Southall, K. A. Dill, and A. D. J. Haymet, *J. Phys. Chem. B*, 2002, **106**, 521–533.

9. J. N. Israelachvili, *Intermolecular and Surface Forces*, Elsevier, London, Third edit., 2011.

10. J. N. Israelachvili, D. J. Mitchell, and B. W. Ninham, *J. Chem. Soc., Faraday Trans. 2*, 1976, **72**, 1525–1568.

11. R. A. J. Jones, *Soft Condensed Matter*, Oxford University Press, New York, First edit., 2002.

12. R. P. Brinkhuis, F. P. J. T. Rutjes, and J. C. M. van Hest, *Polym. Chem.*, 2011, **2**, 1449–1462.

13. R. Nagarajan, *Langmuir*, 2002, **18**, 31–38.

14. K. Kitatokarczyk, J. Grumelard, T. Haefele, and W. Meier, *Polymer (Guildf).*, 2005, **46**, 3540–3563.

15. K. Letchford and H. Burt, *Eur. J. Pharm. Biopharm.*, 2007, **65**, 259–69.

16. G. Battaglia, C. LoPresti, H. Lomas, M. Massignani, and T. Smart, *J. Mater. Chem.*, 2009, **19**, 3576–3590.

17. J. K. Harris, G. D. Rose, and M. L. Bruening, *Langmuir*, 2002, **18**, 5337–5342.

18. V. K. Mourya, N. Inamdar, R. B. Nawale, and S. S. Kulthe, *Indian J. Pharm. Educ. Res.*, 2011, **45**, 128–138.

19. D. E. Discher and F. Ahmed, *Annu. Rev. Biomed. Eng.*, 2006, **8**, 323–341.

20. G. Tresset, *PMC Biophys.*, 2009, **2**, 1–25.

21. S. Zhou, C. Burger, B. Chu, M. Sawamura, N. Nagahama, M. Toganoh, U. E. Hackler, H. Isobe, and E. Nakamura, *Science (80-.).*, 2001, **291**, 1944–1947.

22. J. C. M. van Hest, D. A. P. Delnoye, M. W. P. L. Baars, M. H. P. van Genderen, and E. W. Meijer, *Science (80-.).*, 1995, **268**, 1592–1595.

23. A. D. Bangham, M. M. Standish, and J. C. Watkins, *J. Mol. Biol.*, 1965, **13**, 238–252.

24. *milestone in liposme history in http://www.liposomesociety.org*, .

25. D. E. Discher and A. Eisenberg, *Science (80-.).*, 2002, **297**, 967–973.

26. L. Zhang and a Eisenberg, *Science*, 1995, **268**, 1728–31.

27. B. M. Discher, Y.-Y. Won, D. S. Ege, J. C.-M. Lee, F. S. Bates, D. E. Discher, and D. A. Hammer, *Science (80-.).*, 1999, **284**, 1143–1146.

28. M. Antonietti and S. Förster, *Adv. Mater.*, 2003, **15**, 1323–1333.

29. G. Battaglia and A. J. Ryan, *Nat. Mater.*, 2005, **4**, 869–876.

30. M. Massignani, H. Lomas, and G. Battaglia, in *Modern Techniques for Nano- and Microreactors/-reactions*, ed. F. Caruso, Springer, 2010.

31. J. A. Opsteen, J. J. L. M. Cornelissen, and J. C. M. van Hest, *Pure Appl. Chem.*, 2004, **76**, 1309–1319.

32. T. Smart, H. Lomas, M. Massignani, M. V Flores-Merino, L. R. Perez, and G. Battaglia, *Nanotoday*, 2008, **3**, 38–46.

33. R. Rodríguez-García, M. Mell, I. López-Montero, J. Netzel, T. Hellweg, and F. Monroy, *Soft Matter*, 2011, **7**, 1532–1542.

34. G. Battaglia, A. J. Ryan, and S. Tomas, *Langmuir*, 2006, **22**, 4910–4913.

35. J. S. Lee and J. Feijen, *J. Control. Release*, 2012, **161**, 473–483.

36. K. Daoulas and M. Muller, *Adv Polym Sci*, 2010, **224**, 197–233.

37. S. Dai, P. Ravi, and K. C. Tam, *Soft Matter*, 2008, **4**, 435–449.

38. J. Rodriguez-Hernandez, F. Checot, Y. Gnanou, and S. Lecommandoux, *Prog. Polym. Sci.*, 2005, **30**, 691–724.

39. T. Uneyama, *J. Chem. Phys.*, 2007, **126**, 114902.

40. X. He and F. Schmid, *Macromolecules*, 2006, **39**, 2654–2662.

41. A. Akbarzadeh, R. Rezaei-Sadabady, S. Davaran, S. W. Joo, N. Zarghami, Y. Hanifehpour, M. Samiei, M. Kouhi, and K. Nejati-Koshki, *Nanoscale Res. Lett.*, 2013, **8**, 102.

42. M. I. Angelova and D. S. Dimitrov, *Faraday Discuss. Chem. Soc.*, 1986, **81**, 303–311.

43. D. D. Lasic, *Biochem. J.*, 1988, **256**, 1–11.

44. D. D. Lasic, *Biochim. Biophys. Acta*, 1982, **692**, 501–502.

45. S. A. Safran, P. Pincus, and D. Andelman, *Science (80-.).*, 2013, **248**, 354–356.

46. D. J. Adams, C. Kitchen, S. Adams, S. Furzeland, D. Atkins, P. Schuetz, C. M. Fernyhough, N. Tzokova, A. J. Ryan, and M. F. Butler, *Soft Matter*, 2009, **5**, 3086–3096.

47. B. Charleux, G. Delaittre, J. Rieger, and F. D'Agosto, *Macromolecules*, 2012, **45**, 6753–6765.

48. A. Blanazs, J. Madsen, G. Battaglia, A. J. Ryan, and S. P. Armes, *J. Am. Chem. Soc.*, 2011, **133**, 16581–16587.

49. P. Walde, K. Cosentino, H. Engel, and P. Stano, *Chembiochem*, 2010, **11**, 848–865.

50. J. Du and R. K. O'Reilly, *Soft Matter*, 2009, **5**, 3544–3561.

51. *http://mit.edu/sjiang2/www/Resources/Prepare%20Lipid%20Vesicles.pdf*, Retrieved on Sep.17, 2012.

52. M. Riaz, *Pak. J. Pharm. Sci.*, 1996, **19**, 65–77.

53. K. Kita-Tokarczyk, J. Grumelard, T. Haefele, and W. Meier, *Polymer (Guildf).*, 2005, **46**, 3540–3563.

54. T. F. Zhu and J. W. Szostak, *PLoS One*, 2009, **4**, e5009.

55. J. R. Howse, R. A. L. Jones, G. Battaglia, R. E. Ducker, G. J. Leggett, and A. J. Ryan, *Nat. Mater.*, 2009, **8**, 507–511.

56. K.-J. Gao, G. Li, X. Lu, Y. G. Wu, B.-Q. Xu, and J.-H. Fuhrhop, *Chem. Commun.*, 2008, 1449–1451.

57. E. Mabrouk, D. Cuvelier, L.-L. Pontani, B. Xu, D. Lévy, P. Keller, F. Brochard-Wyart, P. Nassoy, and M.-H. Li, *Soft Matter*, 2009, **5**, 1870–1878.

58. S. Hauschild, U. Lipprandt, A. Rumplecker, U. Borchert, A. Rank, R. Schubert, and S. Förster, *Small*, 2005, **1**, 1177–1180.

59. K. Funakoshi, H. Suzuki, and S. Takeuchi, *J. Am. Chem. Soc.*, 2007, **129**, 12608–12609.

60. K. Funakoshi, H. Suzuki, and S. Takeuchi, *Anal. Chem.*, 2006, **78**, 8169–8174.

61. J. C. Stachowiak, D. L. Richmond, T. H. Li, F. Brochard-Wyart, and D. a Fletcher, *Lab Chip*, 2009, **9**, 2003–2009.

62. J. C. Stachowiak, D. L. Richmond, T. H. Li, A. P. Liu, S. H. Parekh, and D. a Fletcher, *Proc. Natl. Acad. Sci. U. S. A.*, 2008, **105**, 4697–4702.

63. K. Kamiya, R. Kawano, T. Osaki, and S. Takeuchi, *16th Int. Conf. Miniaturized Syst. Chem. Life Sci.*, 2012, 1597–1599.

64. E. Tekin, P. J. Smith, and U. S. Schubert, *Soft Matter*, 2008, **4**, 703–713.

65. B.-J. de Gans, P. C. Duineveld, and U. S. Schubert, *Adv. Mater.*, 2004, **16**, 203–213.

66. O. Onaca, R. Enea, D. W. Hughes, and W. Meier, *Macromol. Biosci.*, 2009, **9**, 129–39.

67. F. Ahmed, R. I. Pakunlu, A. Brannan, F. Bates, T. Minko, and D. E. Discher, *J. Control. release*, 2006, **116**, 150–158.

68. H.-J. Choi and C. D. Montemagno, *Nano Lett.*, 2005, **5**, 2538–2542.

69. K. T. Kim, J. J. L. M. Cornelissen, R. J. M. Nolte, and J. C. M. van Hest, *Adv. Mater.*, 2009, **21**, 2787–2791.

70. R. A. Curtis, J. Ulrich, A. Montaser, J. M. Prausnitz, and H. W. Blanch, *Biotechnol. Bioeng.*, 2002, **79**, 367–380.

71. M. Boström, D. R. M. Williams, and B. W. Ninham, *Curr. Opin. Colloid Interface Sci.*, 2004, **9**, 48–52.

72. B. A. Deyerle and Y. Zhang, *Langmuir*, 2011, **27**, 9203–9210.

73. Y. Zhang and P. S. Cremer, *Curr. Opin. Chem. Biol.*, 2006, **10**, 658–663.

74. K. D. Collins and M. W. Washabaugh, *Q. Rev. Biophys.*, 1985, **18**, 323–422.

75. W. Kunz, J. Henle, and B. W. Ninham, *Curr. Opin. Colloid Interface Sci.*, 2004, **9**, 19–37.

76. K. D. Collins, *Methods*, 2004, **34**, 300–311.

77. Y. Marcus, *Chem. Rev.*, 2009, **109**, 1346–1370.

78. J. Lyklema, *Chem. Phys. Lett.*, 2009, **467**, 217–222.

79. M. G. Cacace, E. M. Landau, and J. J. Ramsden, *Q. Rev. Biophys.*, 1997, **30**, 241–277.

80. B. S. Fujimoto, J. M. Miller, N. S. Ribeiro, and J. M. Schurr, *Biophys. J.*, 1994, **67**, 304–308.

81. S. Moelbert, B. Normand, and P. De Los Rios, *Biophys. Chem.*, 2004, **112**, 45–57.

82. B. Hribar, N. T. Southall, V. Vlachy, and K. a Dill, *J. Am. Chem. Soc.*, 2002, **124**, 12302–12311.

83. M. G. Cacace, E. M. Landau, and J. J. Ramsden, *Q. Rev. Biophys.*, 1997, **30**, 241–277.

84. A. W. Omta, M. F. Kropman, S. Woutersen, and H. J. Bakker, *Science (80-.).*, 2003, **301**, 347–349.

85. K. D. Collins, *Biophys. J.*, 1997, **72**, 65–76.

86. I. Gitlin, J. D. Carbeck, and G. M. Whitesides, *Angew. Chemie - Int. Ed.*, 2006, **45**, 3022–3060.

87. K. D. Collins, *Biophys. Chem.*, 2006, **119**, 271–281.

88. M. M. Ries-Kautt and A. F. Ducruix, *J. Cryst. Growth*, 1991, **110**, 20–25.

89. S. Saito, *J. Polym. Sci. Part A-1 Polym. Chem.*, 1969, **7**, 1789–1802.

90. F. A. Long and W. F. MacDevit, *Chem. Rev.*, 1952, **51**, 119–169.

91. R. Zangi, M. Hagen, and B. J. Berne, *J. Am. Chem. Soc.*, 2007, **129**, 4678–4686.

92. R. Kjellander and E. Florin, *Chem. Phys.*, 1981, **77**, 2053–2077.

93. E. Florin, R. Kjellander, and J. C. Eriksson, *J. Chem. Soc. Faraday Trans. 1*, 1984, **80**, 2889–2910.

94. C. Booth and D. Attwood, *Macromol. Rapid Commun.*, 2000, **21**, 501–527.

95. O. V Elisseeva, N. A. M. Besseling, L. K. Koopal, and M. A. Cohen Stuart, *Langmuir*, 2005, **21**, 4954–4963.

96. X.-Y. Wang, G.-M. Zeng, Y.-L. Wang, J.-B. Wang, X.-H. Xu, T.-T. Zhou, and H.-K. Yan, *Chinese J. Chem.*, 2008, **26**, 439–444.

97. G. Cevc and D. Marsh, *Phospholipid Bilayers: Physical Principles and Models*, Wiley-Interscience, New York, 1987.

98. A. M. Carmona-Ribeiro and H. Chaimovich, *Biophys. J.*, 1986, **50**, 621–628.

99. I. M. Henderson and W. F. Paxton, *Angew. Chem. Int. Ed. Engl.*, 2014, **53**, 3372–3376.

100. G. Cevc and H. Richardsen, *Adv. Drug Deliv. Rev.*, 1999, **38**, 207–232.

101. L. Derici, S. Ledger, S. Mai, C. Booth, W. Hamley, and J. S. Pedersen, *Phys. Chem. Chem. Phys.*, 1999, **1**, 2773–2785.

102. I. W. Hamley, J. A. Pople, C. Booth, L. Derici, M. Imperor-Clerc, and P. Davidson, *Phys. Rev. E*, 1998, **58**, 7620–7628.

103. P. Yeagle, *The Membrane of Cells*, Academic Press, Inc., London, 1987.

104. D. Needham and D. Zhelev, in *Perspectives in Supramolecular Chemistry: Giant Vesicles*, eds. P. J. Luisi, P. Walde, D. Needham, and D. Zhelev, John Wiley & Sons, 2000, pp. 103–147.

105. M. L. Longo and V. L. Hung, in *Methods in Membrane Lipids*, 2007.

106. U. Seifert, *Adv. Phys.*, 1997, **46**, 13–137.

107. Http://en.wikipedia.org/wiki/Membrane_curvature, Retrieved on June 10, 2014.

108. E. Sackmann, in *Handbook of Biological Physics*, eds. R. Lipowsky and E. Sackmann, Vol.1 edn., 1995, vol. 1, pp. 213–303.

109. R. Dimova, S. Aranda, N. Bezlyepkina, V. Nikolov, K. a Riske, and R. Lipowsky, *J. Phys. Condens. matter*, 2006, **18**, S1151–S1176.

110. C. A. Haselwandter, *Introduction to the Physics of Membranes*, 2010.

111. M. Deserno, *Fluid lipid membranes – a primer*, Germany.

112. D. Needham and D. V Zhelev, in *Vesicles*, ed. M. Rosoff, Marcel Dekker, New York, 1996, pp. 373–439.

113. F. R. Hallett, J. Marsh, B. G. Nickel, and J. M. Wood, *Biophys. J.*, 1993, **64**, 435–442.

114. V. Heinrich and W. Rawicz, *Langmuir*, 2005, **21**, 1962–1971.

115. E. Evans, V. Heinrich, F. Ludwig, and W. Rawicz, *Biophys. J.*, 2003, **85**, 2342–2350.

116. J. Zimmerberg, *Curr. Biol.*, 2006, **16**, R272–R276.

117. W. Helfrich, *Zeitschrift für Naturforsch. C-A J. Biosci.*, 1973, **C28**, 693–703.

118. H. Bermudez, A. K. Brannan, D. A. Hammer, F. S. Bates, and D. E. Discher, *Macromolecules*, 2002, **35**, 8203–8208.

119. S. Wu, *J. Polym. Sci. Part C Polym. Symp.*, 1971, **34**, 19–30.

120. J. C.-M. Lee, H. Bermudez, B. M. Discher, M. A. Sheehan, Y.-Y. Won, F. S. Bates, and D. E. Discher, *Biotechnol. Bioeng.*, 2001, **73**, 135–145.

121. R. Kwok and E. Evans, *Biophys. J.*, 1981, **35**, 637–652.

122. D. Marsh, *Handbook of Lipid Bilayers*, CRC Press, 2nd. edit., 2013.

123. E. Evans and W. Rawicz, *Phys. Rev. Lett.*, 1990, **64**, 2094–2097.

124. W. Rawicz, K. C. Olbrich, T. McIntosh, D. Needham, and E. Evans, *Biophys. J.*, 2000, **79**, 328–339.

125. D. Needham and R. S. Nunn, *Biophys. J.*, 1990, **58**, 997–1009.

126. H. Bermúdez, D. A. Hammer, and D. E. Discher, *Langmuir*, 2004, **20**, 540–543.

127. I. Szleifer, D. Kramer, A. Ben-Shaul, D. Roux, and W. M. Gelbart, *Phys. Rev. Lett.*, 1988, **60**, 1966–1969.

128. D. Boal, *Mechanics of the cell*, Cambridge University Press, 2nd ed., 2002.

129. R. Dimova, U. Seifert, and B. Pouligny, *Eurupean Phys. J. E*, 2002, **7**, 241–250.

130. D. Andelman, in *Handbook of Biological Physics*, eds. R. Lipowsky and E. Sackmann, Elsevier Science B.V., 1995, vol. 1, pp. 603–641.

131. S. McLaughlin, N. Mulrine, T. Gresalfi, G. Vaio, and A. McLaughlin, *J. Gen. Physiol.*, 1981, **77**, 445–473.

132. P. M. Macdonald and J. Seeling, *Biochemistry*, 1988, **27**, 6769–6775.

133. M. Winterhalter and W. Helfrich, *J. Phys. Chem.*, 1988, **92**, 6865–6867.

134. Http://en.wikipedia.org/wiki/Debye_length), Retrieved on June 10, 2014.

135. Http://www.epa.gov/caddis/ssr_ion_int.html, Retrieved on June 10, 2014.

136. M. M. a E. Claessens, B. F. van Oort, F. a M. Leermakers, F. a Hoekstra, and M. a Cohen Stuart, *Biophys. J.*, 2004, **87**, 3882–3893.

137. M. M. A. E. Claessens, F. A. M. Leermakers, F. A. Hoekstra, and M. A. Cohen Stuart, *J. Phys. Chem. B*, 2007, **111**, 7127–7132.

138. H. I. Petrache, S. Tristram-Nagle, D. Harries, N. Kucerka, J. F. Nagle, and V. A. Parsegian, *J. Lipid Res.*, 2006, **47**, 302–309.

139. G. Pabst, A. Hodzic, J. Strancar, S. Danner, M. Rappolt, and P. Laggner, *Biophys. J.*, 2007, **93**, 2688–2696.

140. G. Battaglia and A. J. Ryan, *J. Am. Chem. Soc.*, 2005, **127**, 8757–8764.

141. G. Battaglia and A. J. Ryan, *J. Phys. Chem. B*, 2006, **110**, 10272–10279.

142. J. R. Howse, R. a L. Jones, G. Battaglia, R. E. Ducker, G. J. Leggett, and A. J. Ryan, *Nat. Mater.*, 2009, **8**, 507–511.

143. T. P. Smart, A. J. Ryan, J. R. Howse, and G. Battaglia, *Langmuir*, 2010, **26**, 7425–7430.

144. T. P. Smart, C. Fernyhough, A. J. Ryan, and G. Battaglia, *Macromol. Rapid Commun.*, 2008, **29**, 1855–1860.

145. J. L. Martinez-Hurtado, *Nanomaterials*, 2011, **1**, 20–30.

146. C. Booth, D. Attwood, and C. Price, *Phys. Chem. Chem. Phys.*, 2006, **8**, 3612–3622.

147. L. Derici, S. Ledger, S.-M. Mai, C. Booth, I. W. Hamley, and J. S. Pedersen, *Phys. Chem. Chem. Phys.*, 1999, **1**, 2773–2785.

148. N.-J. Deng, Y.-Z. Luo, S. Tanodekaew, N. Bingham, D. Attwood, and C. Booth, *J. Polym. Sci. Part B Polym. Phys.*, 1995, **33**, 1085–1096.

149. M. Wong and T. E. Thompson, *Biochemistry*, 1982, **21**, 4133–4139.

150. G. Battaglia and A. J. Ryan, *Macromolecules*, 2006, **39**, 798–805.

Chapter 2: The effect of salts on $E_{16}B_{22}$ polymersomes

2.1 Introduction

The effect of salts has been shown to induce a number of phenomena such as protein precipitation[1,2], protein folding[3], enzyme activity[4], bacterial growth[5] and polymer aggregation[6,7,8], among others. Also, the effect of salts on the aggregation behaviour of colloidal systems can be seen as a mimic for the first steps in the fusion event of biological cells. As the cell must first come together and this is intimately related to the mechanism of agglomeration[9,10], prior to the fusion event. Fusion is defined as the event where two membranes approach each other and then emerge to form a single continuous structure. In order to promote membrane fusion, vesicle aggregation is necessary[11]. In the scientific community, this agglomeration is commonly termed the salting-out effect[6].

In literature there are studies on aggregation of poly(ethylene oxide)$_{16}$-poly(butylene oxide)$_{22}$ ($E_{16}B_{22}$) induced by addition of PEO to polymersomes, also know as vesicles, in solution[12,13] but there are no studies on how different salts impact the aggregation behaviour of $E_{16}B_{22}$ vesicles in water and how this can be related with the Hofmeister effect. This chapter will focus on this phenomenon hence the interest to know the Hofmeister series. For this purpose, the microstructured (i.e. giant unilamellar vesicles, GUVs) and nanostructured (i.e. nanovesicles) vesicles from the $E_{16}B_{22}$ block copolymer were employed. Two series of experiments were conducted. In the first series, the effect of K_2SO_4 on GUVs was analysed using optical microscopy. These vesicles were made using the electroformation method first introduce by Angelova[14]. In the second set of experiments, selected salts at low and high concentrations were used to study the salting-out effect on nanovesicles system by dynamic light scattering (DLS) and transmission electron microscopy (TEM). These two techniques were used with the purpose of characterizing the polymer nanostructures. Additionally, optical microscopy was employed to observe the presence of long aggregates at high salt concentrations.

2.2 Methodology

The block copolymer poly(ethylene oxide)$_{16}$-poly(butylene oxide)$_{22}$ ($E_{16}B_{22}$) was employed in all polymersome preparations. The $E_{16}B_{22}$ was synthesised initially by Dr. Shao-Min Mai[15] using sequential anionic polymerization. The number average molecular weight of $E_{16}B_{22}$ was 2300 g/mol as calculated by C^{13} *NMR* spectroscopy and a P.D.I. of 1.1.

2.2.1 GUVs preparation and salt addition

The experimental protocol of GUVs formation via the electroformation method is as follows[16,17]:

1.-A polymer-chloroform solution was prepared with a concentration of approximately 5 mg/ml. The solvent can be any highly volatile suitable solvent (e.g. chloroform, formaldehyde or methanol).

2.-With a Pasteur pipette two or three drops of the polymer-solvent solution was taken and used to coat the two palladium electrodes (20 x 5 x 2 mm) with a thin film of polymer.

3.-The two electrodes were placed in a small vial and left for 24 hrs in a vacuum oven to dry. Evaporation of the solvent left a thin polymer layer on the electrodes.

4.-The two palladium bars were attached to the electroformation device (Figure 1) by two small screws and connected to an alternating current (AC) function generator.

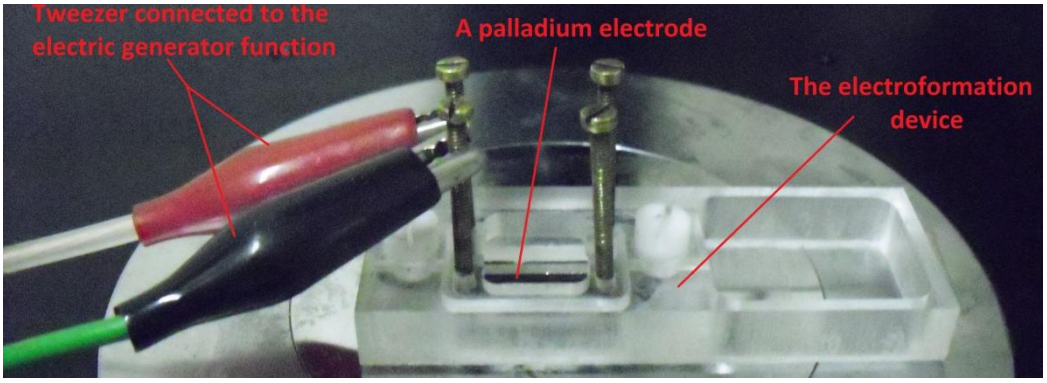

Figure 1. In the above picture, the electroformation device is shown with two palladium electrodes connected to an electrical field generator. This device was used to make giant unilamellar vesicles.

5.-The function generator creates an AC voltage which was tuned to a voltage of 10 volts and a frequency of 10 Hertz.

6.- After about 90 minutes giant vesicles were formed on the palladium electrodes which were observed using an optical light microscope.

Vesicles were visualised using the bright field microscopy technique. An improved setup would be to use confocal laser scanning microscopy which is based on fluorescence properties of materials. However, bright light microscopy was used because this technique does not require additional experimental equipment to be employed.

Methodology for GUVs salt addition

Salt addition experiments were first conducted by preparing a solution of 0.2 M of K_2SO_4/water and adding one or two droplets directly onto the GUVs system with a Pasteur pipette. Before addition of salt, the function generator was turned off in order to avoid influence of an electric field on vesicle aggregation. K_2SO_4 was employed because the sulphate ion is a strongly hydrated anion and has the capability to induce the salting-out effect, according to the Hofmeister series[18,19]. In these experiments, a slight modification to the above protocol was made for preparing GUVs. A special microscope slide was used, with a cavity on the surface, in order to reduce vesicle difussion when salt was added. The electrodes were placed between this concave cavity (Figure 2) and the electroformation device was placed over the electrodes. This experimental setup allowed better control over difussion compared to a flat microscope slide as the concave cavity creates a controlled water volume which encloses water and this reduced the perturbation by flow that the salt solution induces in the vesicles sytem.

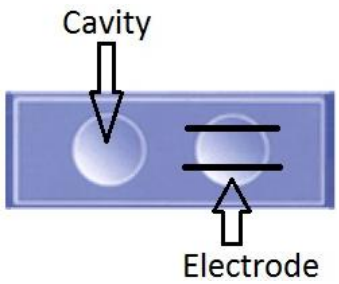

Figure 2. A microscope slide with a cavity where the electrodes were place over.

2.2.2 Nanovesicles preparation, salt addition and equipment used

In all nanovesicle sample preparations (i.e. polymer solutions and salt solutions), ultra high quality water (UHQW) and filters of 0.2 μm of PTFE polymer were used to prepare dust free solutions. Firstly, several polymer solutions of 0.1 %(w/w) were prepared in glass vials using a small amount of the polymer, i.e. 0.015 g of $E_{16}B_{22}$, in 15 g in water and stirred overnight. In our experiments, these solutions were used as stock solutions. In order to form a more uniform sample[20], with regards to the vesicle diameter, these solutions were ultrasonicated for 110 minutes. The effect of sample sonication is the reduction of polymersome sizes which creates smaller stable nanostructures[21]. Subsequently 3 ml of solution was transferred from the glass vial to a cuvette using the above mentioned PFTE filters, with the aim of decreasing dust contamination of the sample. Then, from the filtered solution, 1 ml was taken and extruded by a LiposoFast™ device.

The LiposoFast™ is a small extrusion device which consists of two glass gas-tight syringes, attached to either side of a metal chamber containing a polycarbonate membrane of 100 nm pore size (see

Figure 3). The method comprises the filling of a syringe with the sample which is subsequently passed repeatedly through the membrane by pushing the sample back and forth between the two syringes. The result of this process is the reduction of liposomes' (or polymersomes') size to that of the membrane dimension and the transformation of multillamellar vesicles into unilamellar structures[22].

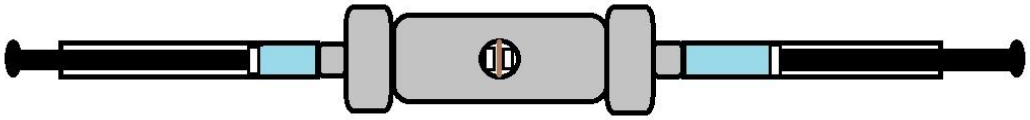

Figure 3. LiposoFast™ extrusion device consists of two glass gas-tight syringes that are attached to a metal chamber containing a polycarbonate membrane. A polymer aqueous solution is passed through the membrane several times in order to obtain more homogenous vesicle sizes[23].

After complete this process using the LiposoFast™, the resulted extruded solution was transferred in another cuvette and the weight of the sample was recorded in order to calculate the initial polymer concentration. Then, this cuvette was taken immediately to the DLS equipment where experiments were conducted.

Dynamic light scattering (DLS) was used to characterise the effect of salt solutions on the $E_{16}B_{22}$/water system. In all the experiments, a Zetasizer Nanoseries DLS-equipment from Malvern instruments was used with a 4 mW He-Ne solid-state laser operating at 633 nm and backscattering at 173^{o}. This instrument is straightforward to use and works with small volumes of sample, from 0.5 to 1.5 ml. All experiments were run at a temperature of 25^{o}C.

Dynamic light scattering technique is mainly used to determinate the hydrodynamic diameters of colloidal solutions. The principle of operation of this equipment is as follow. When a laser irradiates light and hits particles smaller than the laser wavelength, particles scatters light in all directions (Figure 4) according with Rayleigh scattering theory[24]. Subsequently, the photon detector device collects the scatter light intensity, i.e. a fluctuating intensity signal throughout time, and transforms it in an electrical signal. Then, this signal is supplied to a digital correlator which generates the autocorrelation function[25]. This signal, which fluctuates through time, is random at long periods (e.g. milliseconds or ten of milliseconds)[26,27]. However, there are strong correlations of the intensity with other signals at different very short time scales (e.g. nanoseconds or microseconds)[27]. A autocorrelation function is applied to the left-side graph of Figure 5 in order to remove "noise" and extract valuable information about colloidal particles. It can be observed in the right-side of Figure 5 that this curve is smooth and exponentially decaying which suggests that it is a non-random signal.

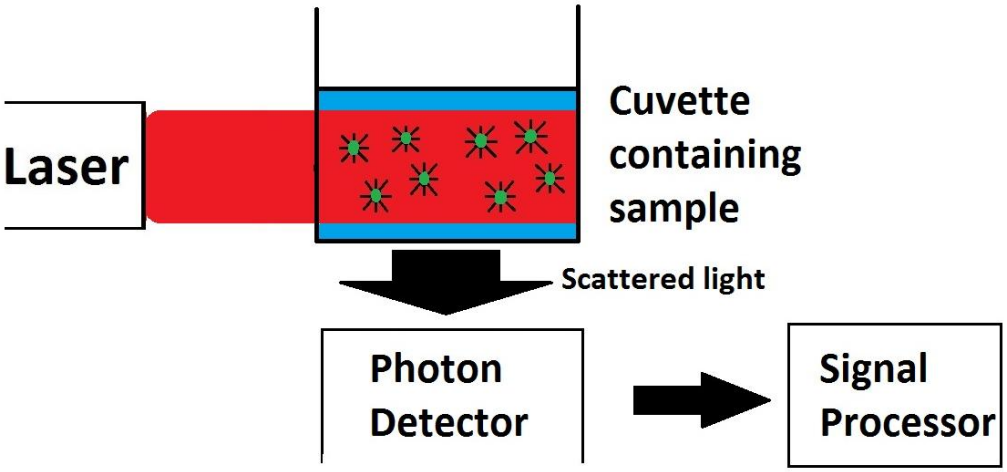

Figure 4. Scattering volume formed by the detector and laser when the first is at 90^o with respect to the second. In the illustration, the particles scatter the laser light in all directions and the detector senses the photon energy and transforms it to an electric signal. Then with a software, the diffusion coefficient and hydrodynamic diameter can be calculated using the Stoke-Einstein equation[24].

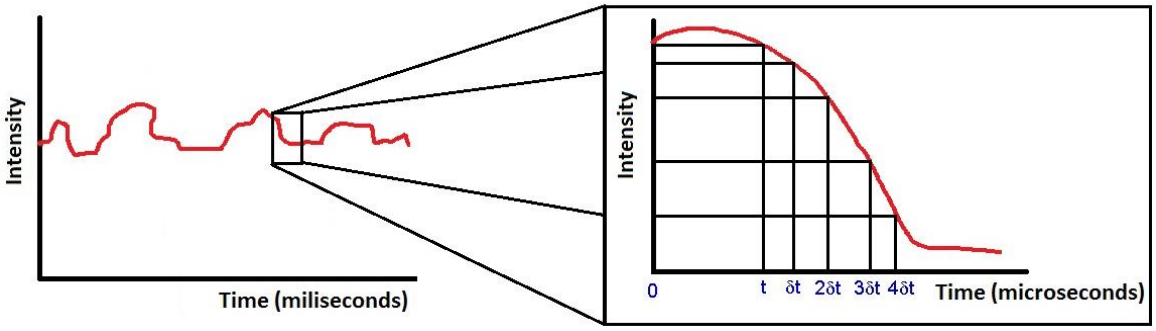

Figure 5. At long periods of time, the intensity fluctuation signal can be seen as random and without a special pattern (left-side graph). However, at short periods and using correlation statistics, it can be found that the signal has an exponential decay through time and important data can be extracted from this data, as the diffusion coefficient (right-side graph)[26,27].

Therefore, with correlation statistics, the correlation function of the particles is obtained allowing the degree of non-randomness (correlation) to be known in an apparent random signal. This correlation function is defined by the following equation[28]:

$$G(\tau) = \langle I(t)I(t+\tau)\rangle = \frac{1}{N}\sum_{i=1}^{N} I(t_i)I(t_i+\tau) \quad \text{Equation (1)}$$

Where, $G(\tau)$ is the correlation function, $I(t)$ is the initial scattering intensity, $I(t+\tau)$ is the scattering intensity at a certain delayed time τ, N is the number of sampling times, and the angle

brackets indicate average values. Equation 1 can be normalized for a long period of time since $G(\tau)$ is independent of the starting time. The new function will be as follow[28]:

$$G(\tau) = \frac{I\,(t)\,I(t+\tau)}{(I)^2} \quad \text{Equation (2)}$$

Where $(I)^2$ is for a τ tending to ∞. The decay of this coefficient versus time determinates the size of the particles. Large particles lose correlation over long periods of time and small particles in short periods of time.

Equation 2 can be transformed to the exponential form since there are a large number of particles in the colloidal system[27].

$$G(\tau) = A[1 + Be^{-2q^2D\tau}] \quad \text{Equation (3)}$$

Where *A* is the baseline of the correlation function*, B* is the intercept of the correlation function; *D* is the diffusion coefficient; and *q* is the scattering vector:

$$q = \left(\frac{4\pi n}{\lambda_o}\right) sin\left(\frac{\theta}{2}\right) \quad \text{Equation (4)}$$

In the above equation, n is the refractive index, λ_o is the laser wavelength and θ is the scattering angle. For a more sensitive function in analysing data, equation (3) can be written as[27]:

$$G(\tau) = A[1 + Bg_1(\tau)^2] \text{ Equation (5)}$$

In equation (5), g_1 represents all the exponential decay that exits in $G(\tau)$. The diffusion coefficient can be related to the particle size since the Stokes-Einstein equation provides a link between the velocity of the particle and the hydrodynamic radius[24]:

$$D = \frac{k\,T}{6\pi\eta R_h} \quad \text{Equation (6)}$$

In the above equation, k is the Boltzman constant at T temperature, R_h is the hydrodynamic radius, η and D are the viscosity and the diffusion coefficient of the particle, respectively.

From equation (6), it can be seen that the R_h is the result of considering a particle diffusing and has the same translational diffusion coefficient as a hard sphere particle[27], even though the real morphology can be non-spherical. If the particle were a perfect real hard-sphere, the radius would be the Stoke's radius[29] (R_s) (Figure 6). There is another radius, the radius of gyration (R_g), that can define as the average distance from the centre of gravity to the chain segment.

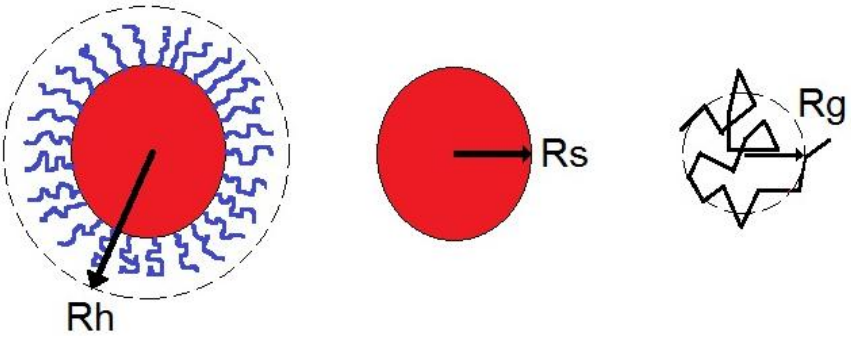

Figure 6. Representation of different radii that can be found in a particle-colloidal system. The radius of gyration (R_g) is defined as the average distance from the centre of gravity to the chain segment and this radius is shorter than the Stoke radius (R_s). R_s is the radius of a theoretical hard sphere and, the hydrodynamic radius (R_h) corresponds to the radius of a colloidal particle in constant motion[29].

From equation (3) the diffusion coefficient, and as a result the R_h, can be obtained by fitting the correlation function with a suitable algorithm. There are several methods used to calculate the R_h of particles from a correlogram. The most common methods are the Cumulants analysis and the CONTIN algorithm[27]. Equation (3) is an example of the Cumulants method which assumes a single exponential decay in order to calculate the z-average diameter, i.e. the harmonic intensity averaged particle diameter, and the polydisperse index of the sample[27]. The other method is the CONTIN algorithm which determinates the distribution of particle sizes according with the best fit of exponential decays in the correlation function curve[27], equation (5). In our analysis of data, we utilised the CONTIN algorithm in order to determine the hydrodynamic radius of the $E_{16}B_{22}$ nanostructures.

In the DLS experiments, the running-time for measurements to calculate R_h was 10 minutes. First at all, the hydrodynamic radius of the polymer solution was measured prior to salt addition. 0.1 ml of a specific salt solution to the cuvette was added via a Gilson pipette. After six minutes, a second run was performed in order to measure any change in hydrodynamic radius. The process was repeated four times, until a total of 0.4 ml of salt solution had been added to the sample, and each experiment was repeated between three to five times in order to ensure that consistent results were obtained and also to calculate the standard error in the experiments.

Electron microscopy was employed to analyse and to indentify nanostructures of unsalted and salted $E_{16}B_{22}$/water system. Samples for TEM examination were prepared using the negative staining technique of uranyl formate. Two samples were imaged, one salt-free and the other one with the effect of 0.1 M Na_2SO_4 salt addition to the polymer solution. This technique first required a carbon coated TEM grid to be treated by glow discharge to change the surface from hydrophobic to

hydrophilic. This allows the polymer solution to stick to the grid. A small amount of the polymer solution (e.g. 5 μL) was absorbed for 1 minute onto the carbon support film and was then blotted with filter paper. The grid was then washed with one droplet of water and dipped in uranyl formate. Then, for the second time, the grid was dipped onto the droplet of uranyl formate for a longer time, about 20 seconds. Finally, the sample was ready to be analysed by TEM.

Finally, optical light microscopy was employed to observe polymer aggregation at high salt concentration. The procedure was as follow. First of all, the samples which were cloudy to the naked eye were selected, as this would indicate large aggregates of the order of the wavelength of light. Several drops were placed on a glass slide using a Pasteur pipette and optical images were taken using magnifications of 4x and 60x with an inverted light microscope.

2.3 Results and discussion

2.3.1 GUV experiments

GUVs were produced by the electroformation method with typical diameters in the range of 20-80 microns. In Figure 7, one can see a GUV attached to the palladium electrode, with a diameter of around 50 μm, 90 minutes after the voltage was applied. These GUVs were observed using the 60x objective lens in the inverted light microscope.

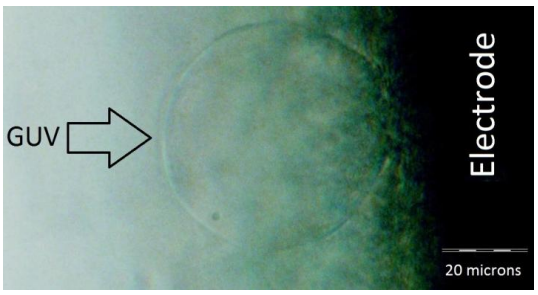

Figure 7. A visible GUV attached to the Pd electrode 90 minutes after the voltage was applied.

Interesting morphologies can be seen in Figure 8, which are polymersomes that have detached from the palladium electrode. Figure 8(A) and (B) depict the same vesicle which can be described as a long tube attached to a pear-like "head". This type of deformation is the result of the vesicle movement, may be because of Brownian motion, through water and, as a result, the generation of a small pressure gradient along the vesicle structure which originates the pear-shape morphology[30]. Also, the great flexibility of this soft material helps to deform the vesicle. The length of the polymersome in Figures 8(A-B) is about 75 μm. In Figure 8(C), a small vesicle is trapped inside a bigger one what is known as an oligovesicular vesicle. An possible explanation to this morphology can be elaborated if we take into account the process of vesicle evolution[31,32]. Firstly, lamellar structures were deposited

onto the surface of the electrodes after solvent had evaporated. When these lamellas are hydrated, one or more layers begin to swell and grow. In this case, it seems that two layers grew at different rates and detached from the surface of the electrode at different times to form the oligovesicular structure seen in Figure 5(C). This type of morphology can be a by-product of using the electroformation method[33]. Figure 5(D) is the evolution of the polymersome (C) through time.

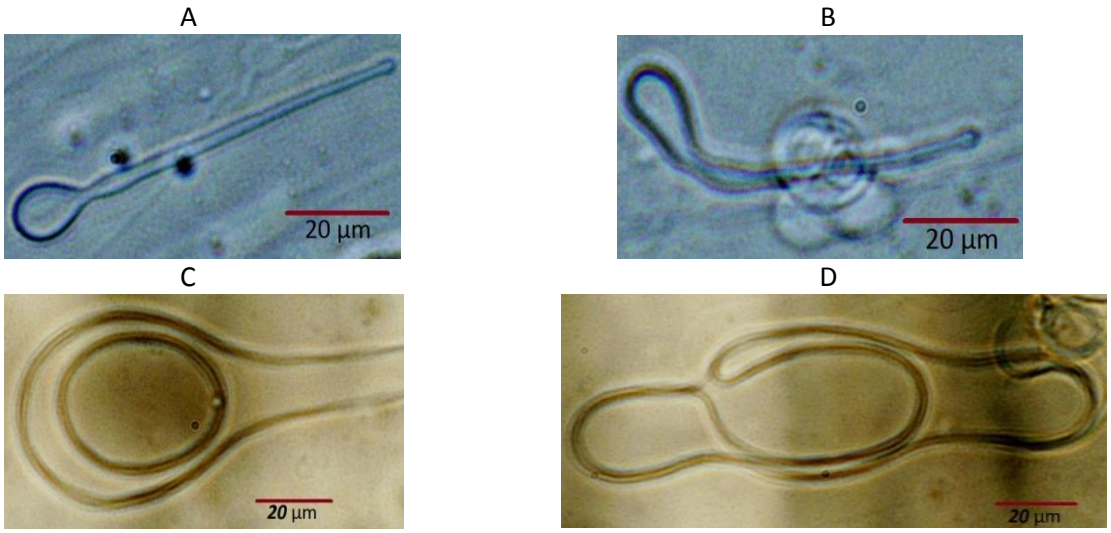

Figure 8. Morphologies of GUVs. (A) and (B) are pictures taken at different times of the same vesicle. In picture (C), it can be seen an oligovesicular structure, very similar in morphology to (A) and (B), but with a small vesicle entrapped in a bigger one. (D) is the evolution of (C) through time.

In Figure 9, one can see a sequence of images before and after salt addition. Prior to the addition of salt, the electrical device was turned off in order to avoid the effect of electric fields in the system. Figure 9(A) despictes some small vesicles, previous to salt addition, which are close to each other, and can be seen attached to the electrode (in black). After salt addition (Figure 9(B-H), 0 s to 5 min 15 s), aggregation was seen to evolve with time. In Figures 9(B) and (C), the semitransparent material, i.e. vesicles, remained over the electrodes just after addition of salt. In Figure 9D, some vesicles are aggregated which possibbly could be evidence of the saltiing-out effect in polymersomes. However, in the same microphotograph, there are thicker aggregates indentified by “black spots”, which also grew over time with the rate of agglomeration increasing within a relative short time, 2 min 36 s in Figure 9(E-H). These regions are likely to be polymer lumps derived from the polymer-coated palladium electrode which were peeled off when the salt solution was added. Hydration forces[34] could account for the initial short time scale aggregation (i.e. Figure 9B-D) but the agglomeration phenomena continued several minutes after salt addition. How this polymeric material was agglomerated is not clear. A possible explanation is that the addition of salt solution led to the detachment of the thin polymer layer coating the Pd electrode as a result of hydrodynamic

forces, driven by osmotic pressure. Small fragments of the detached polymer subsequently attached themselves to the vesicles present on the electrode. Polymer material attached to existing vesicles could have facilited accumulation of material, as can be seen in Figures 9(E-H). These combined factors probably produced the agglomeration found in these experiments. In addition, it is unlikely that this flocculation was induced by the salting-effect. The aggregation process took around 5 min 15 s. However, this time does not seem long enough to be attributed to the salting-effect. For example, Quemeneur *et al.* observed GUVs made of phospholipid/chitosan aggregates after 20 minutes when 10 mM of NaCl was added into the bulk solution[35]. The present study did not show reproducibility between experiments; it is therefore unlikely that the salting-out effect occurred in this system. In conclusion, the salting effect can be disregarded in our system as it is believed that our observations are due to aggregation at the palladium electrode (a consequence of the adhesion of the polymer in a fixed position) and no into the bullk solution.

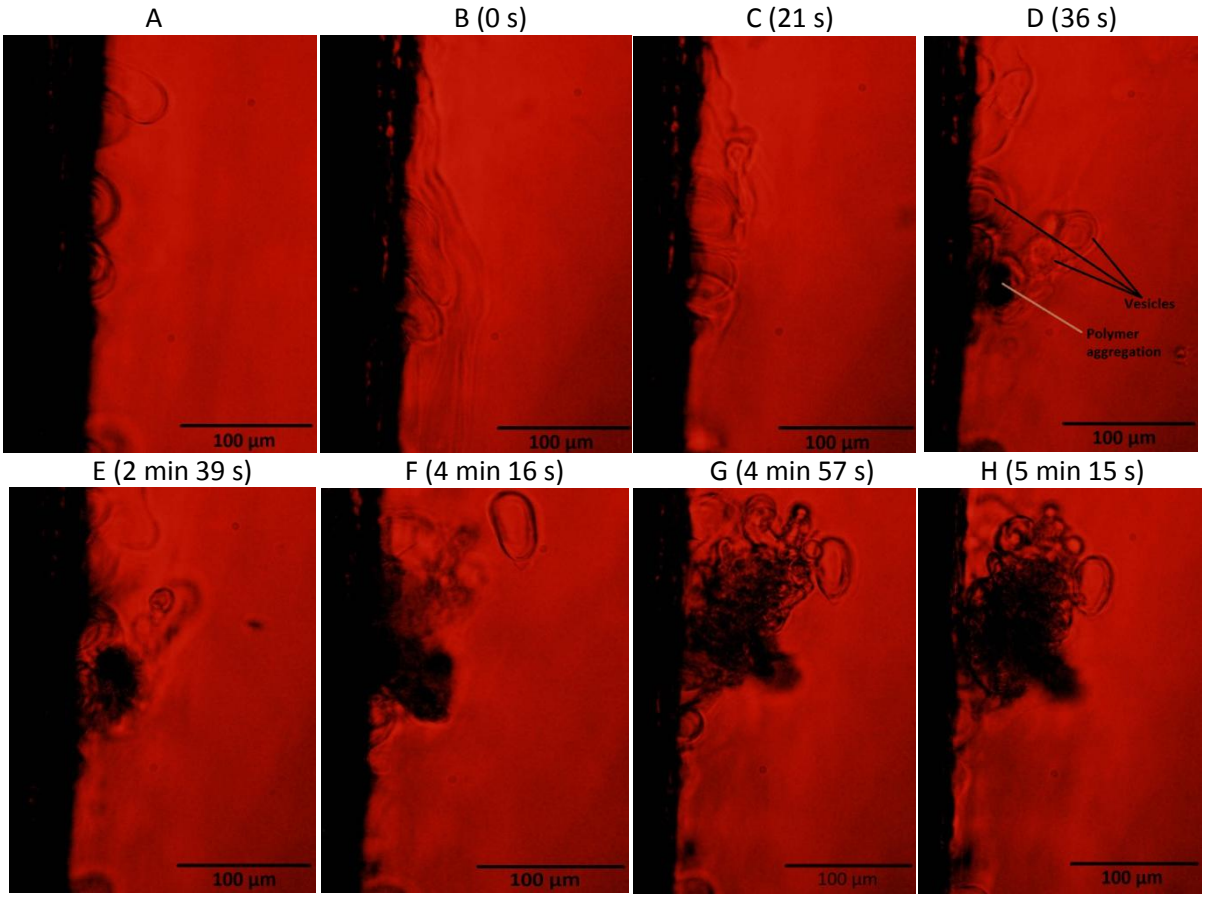

Figure 9. Several semitransparent vesicles are attached to the electrode (black) before salt addition, (A). Sequence of seven micropictures after the addition of 0.2 M K_2SO_4: 0 s (B), 21 s (C), 36 s (D), 2 min 39 s (E), 4 min 16 s (F), 4 min 57 s (G), 5 min 15 s (H). In these pictures, the aggregation behaviour was induced by the palladium electrode that helps to fix polymer material in a place and this in turn provided "adhesiveness" to concentrate more material in the same point .

2.3.2 Nanovesicle experiments

The salting-out effect was studied by analysing different anions but using the same cation because, according to the Hofmeister series, anions have more effect on salting-out solutions[36]. The following solutions were used: 0.3, 1 and 5 molality of NaI, NaH_2PO_4, and individual salt solutions of 1 molality of Na_2SO_4 and 5 molality of NaBr. It can be seen that the common cation in this series of salts was sodium. Then, the molality (m) concentration was converted to molarity (M) because it is the most common concentration unit in literature; however, there are some studies which used molality concentrations[37,38,39]. This conversion was carried out using the densities of both the salts and water. In first instance, molality was used to prepare the salt solutions because this greatly facilitated the experimental procedure and, also, weight measurements are more accurate than volume measurements. The above information is summarized in Table 1.

	Sample 1	**Sample 1**	**Sample 2**	**Sample 2**	**Sample 3**	**Sample 3**
Salt	m (mol/kg solv)	M (mol/dm^3soln)	m (mol/kg solv)	M (mol/dm^3soln)	m (mol/kg solv)	M (mol/dm^3soln)
NaI	5	4.14	1	0.96	0.3	0.29
NaH_2PO_4	5	3.05	1	0.88	0.3	0.29
Na_2SO_4			1	0.95		
NaBr	5	4.31				

Table 1. This table specified the salt solutions and concentrations prepared for the experiments with the DLS equipment.

According to literature, the copolymer $E_{16}B_{22}$ can form equilibrium phases of both small unilamellar vesicles and multilamellar vesicles in aqueous solution with diameters between ~30-300 nm and above 300 nm, respectively[40]. In our experiments, dynamic light scattering (DLS) suggests the present of nanostructures into the polymer solution because the average hydrodynamic radius measured by DLS was between 45-55 nm, indicative of nanovesicles. This narrow size distribution, together with production of small unilamellar vesicles (SUV), was expected since the sample was extruded. Experiments using transmission electron microscopy (TEM) confirmed the presence of nanovesicles and showed species with diameters ranging from 20 to 50 nm which may reflect the presence of more than one type of aggregate. Here, it should be noted that the sizes of the particles determinate the intensity of light scattered. So, larger particles will exponentially scatter more light than smaller particles by an exponent of six, i.e. $I \alpha d^6$ where I is the light intensity and d is the diameter of the particle. In these terms, the intensity size distribution graph, where it was obtained

the *Z*-average radius for the samples, provides a high degree of effectiveness to detect long particles and, as a result, aggregation behaviour.

The DLS results are summarised in Figures 10, 11 and 12. The hydrodynamic radius is stated as the normalised by the un-salted versus concentration of added salts. The error bars in the graphs were calculated using the following equation: $S.E. = \sigma/\sqrt{N}$. The bars represent two times the standard error (S.E.), sigma (σ) is the standard deviation and N is the number of conducted experiments. In this instance, three, four or, sometimes, five repetitions of the experiment took place under the same conditions.

Figure 10 shows the effect of addition of 0.29 M NaI and NaH_2PO_4 salt to 0.1 %(w/w) polymer solutions. In this graph, from 0 M to about 0.05 M the R_h is constant. At 0.07 M, there is a small increase for NaH_2PO_4 in the R_h but this increase is within the range of experimental error. Thus, at low concentrations, it seems that there is not salting-out effect on the sample.

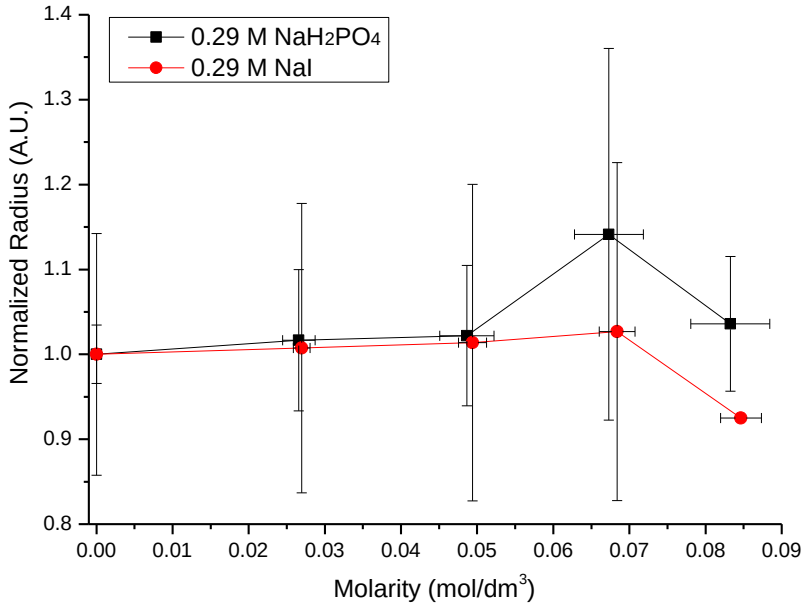

Figure 10. Addition of NaH_2PO_4 and NaI at 0.29 M and their effect on the normalized hydrodynamic diameter of polymer nanostructures made them with 0.1 %(w/w) $E_{16}B_{22}$ aqueous solution.

In Figure 11, the effect of NaH_2PO_4, NaI and Na_2SO_4 at salt concentrations of about 1 M are shown. With NaI, there is a fluctuation of hydrodynamic diameter, but this is within experimental error. In this salt solution, it cannot be indentified any discernible pattern on data. In contrast, the addition of NaH_2PO_4 and Na_2SO_4 salts to the polymer solution has a tendency to increase the hydrodynamic diameters as the molarity increases. Apparently, these two salts have very similar effects on the

vesicle diameter. If we compare phosphate and sulfate salts at similar absolute concentrations, i.e. about 0.085 M and 0.15 M, the polymersome sizes are around the same. At upper concentrations, the effect of Na_2SO_4 on vesicle sizes is slightly bigger than that of NaH_2PO_4. It appears that the small difference in hydrodynamic diameters is the result of dissolving a more concentrated salt solution, i.e. 0.95 M instead of 0.88 M at equal addition volumes, into the polymer sample. Thus, this difference is not due to an ion-sal specificity effect but to the predetermined experimental conditions. Additionally, when comparing NaI and Na_2SO_4 at an absolute concentration of about 0.275 M, there is a rise in the hydrodynamic radius of about 5 nm for Na_2SO_4. This increment is too tiny in order to be a vesicle aggregation but it is likely to be a morphological transition from spherical vesicle to cylindrical structure. According with literature, a relative big difference in the salt gradient between the inside (poorly salty) and outside (rich salty) of the small unilamellar liposome lumen can cause a deformation from spherical to cylindrical-like shape with an increasing diameter of some nanometers[41]. This defomation is maybe the increment in the vesicle size in the this experiment.

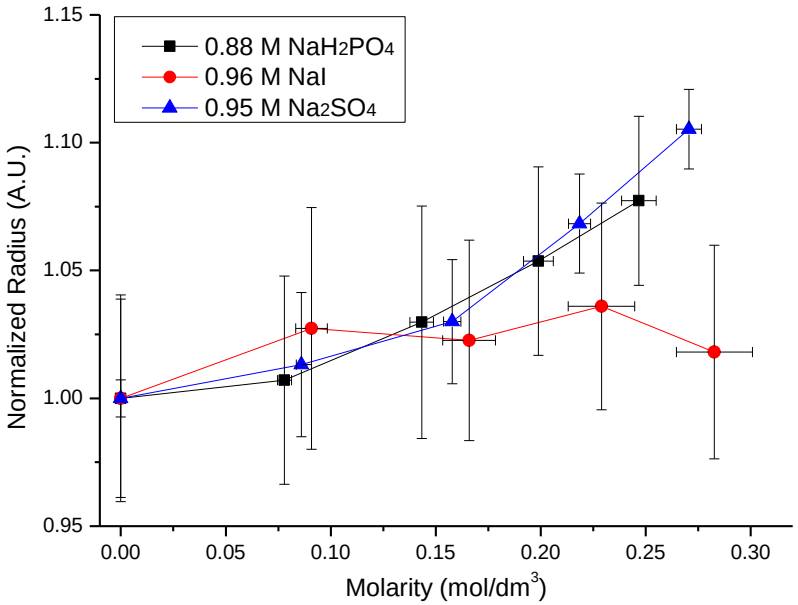

Figure 11. Addition of 0.96 M NaI, 0.95 M Na_2SO_4 and 0.88 M NaH_2PO_4 and their effect on the normalized hydrodynamic diameter of polymer nanostructures made them with 0.1 %(w/w) $E_{16}B_{22}$ aqueous solution.

Figures 12 show the addition of 3.0 M NaH_2PO_4, 4.3 M NaBr and 4.1 M NaI. However, the data related to the NaH_2PO_4 is limited due to the large increase in R_h on the addition of this salt to the polymersome solution. Figure 13 contains the whole range of concentrations for this salt. The purpose of plotting early data points for NaH_2PO_4 in these graphs was to show the dramatic effect of

its addition when compared to that of the NaBr and NaI salt solutions. For example, according to Figure 12 at 0.4 M, NaBr and NaI addition has no discernable effect on the sample. Further addition of NaBr slightly decreases the R_h and it then plateaus. For NaI, there is a stabilization of the effect of this salt at about the same concentrations. At about 0.6 M, one can observe that NaH_2PO_4 greatly affects R_h compared to the other salts, this is a clear indication of aggregation. To summarise, the strength of the anion in salting-out follows the Hofmeister series: $H_2PO_4^-$ > Br^- ≈ I^-.

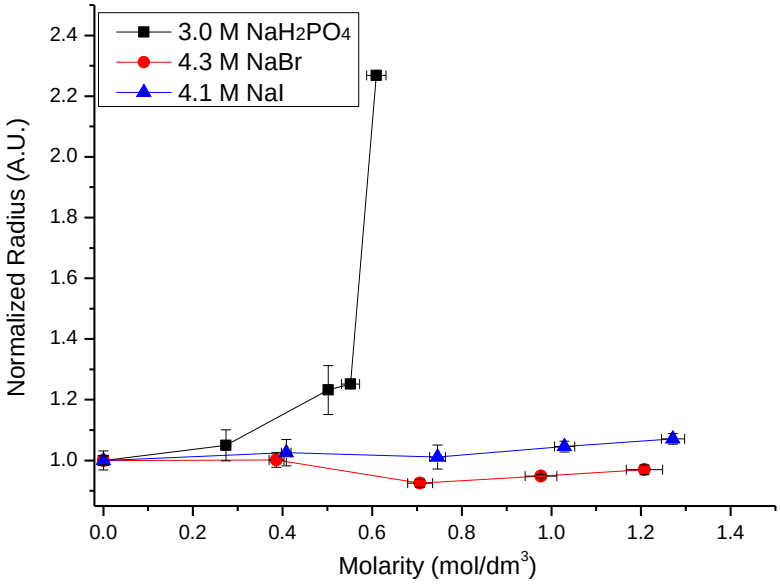

Figure 12. Addition of 3.0 M NaH_2PO_4, 4.3 M NaBr and 4.1 M NaI and their effect on the hydodynamic diameter of polymer nanostructures made with a 0.1 %(w/w) $E_{16}B_{22}$ aqueous solution.

A general view of all the experiments is depicted in the logarithmic graph of Figure 13, on which all salt concentrations were plotted. The highest and most significant increment in the R_h was for NaH_2PO_4. When the sample had a molarity of about 0.7, the increment of the R_h was about forty times higher with respect to NaI and NaBr at about the same concentration. For these two last salts, the experimental average R_h's were 50.89 and 48.5 nm, respectively, for NaH_2PO_4 was 1841.7 nm; therefore there was an increment in radius of about 1800 nm (i.e. 1.8 μm). Furthermore, at the end of the experiment, the physical appearance of the sample, which contained NaH_2PO_4, was observed to turn cloudy. Aggregates were possible to be examined with an optical microscope. The results are presented in Figure 14(A-C).

With a 4x objective, one can observe in Figure 14(A) many fragments disperse throughout the aqueous solution. At 60x, Figure 14(B) presents more visible aglomerations with sizes betwen 4-19

µm and a larger one in Figure 14(C) of about 56 µm. Results of DLS and optical microscopy provide evidence of $E_{16}B_{22}$ polymersome aggregations due to the salting-out effect of NaH_2PO_4.

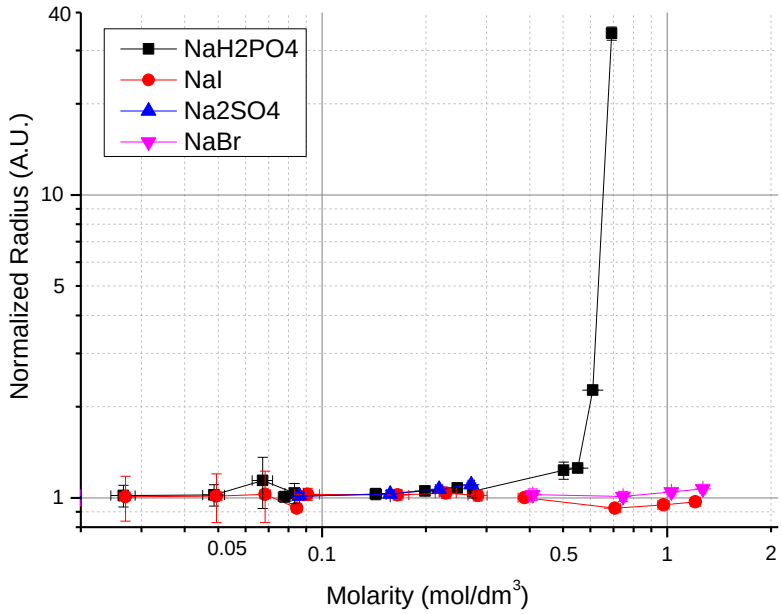

Figure 13. Addition of NaH_2PO_4, NaBr and NaI, Na_2SO_4 at different salt concentrations and their effect on the hydodynamic diameter of polymer nanostructures made with a 0.1 %(w/w) $E_{16}B_{22}$ aqueous solution.

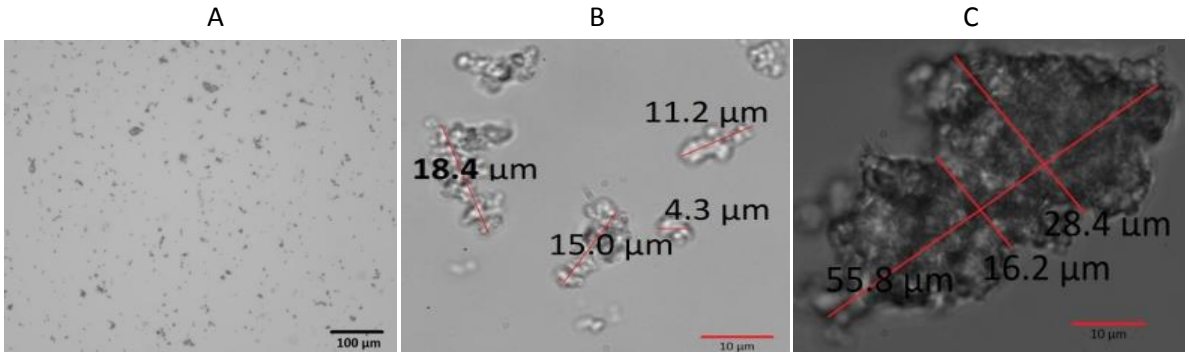

Figure 14. Some selected samples using 3 M of NaH_2PO_4. Picture (A) shows a sample at 4x magnification. (C) and (D) are the same sample at different zones, both images are taken at a magnification of 60x. Scale bars at the bottom-right corner indicate the length scale.

A possible mechanism of vesicle aggregation in the EB system can be related with ion-water molecules interactions and how this synergy affects the hydrophilic part, i.e. poly(ethylene oxide) (PEO), of the vesicle membrane. These type of interactions are expected since a neutral (uncharged) block copolymer was used to prepare the nanostructures. Thus, the introduction of a strong hydrated-ion such as ion phosphate can cause a competition for water molecules around the PEO[6],

reducing its solubility and collapsing PEO chains. Since PEO/PEO macromolecules can attract each other[39,42], when two vesicles are approaching, they can adhere and form large agglomeration fragments as was observed in the optical microscope. Attractive interactions between nanostructures probably comes from depletation forces[43] in which ions at high concentration exerted a osmotic pressure towards these structures, keeping them together.

In order to study the nanostructure behaviour of $E_{16}B_{22}$ with (Figure 15(E-G)) and without (Figure 15 (A-D)) the effect of a salt, TEM microphotographs were taken. Samples were prepared using the negative staining technique of uranyl formate. In the case of a free-salt polymer sample, Figure 15(A) shows a small unilamellar vesicle of about 100 nm with the hydrophobic membrane highly contrast from the rest of the structure. This TEM micropicture is very similar with another electron microscopy analysis using the same polymer[21]. In Figures 15(B-D), there are a wide range of morphologies and sizes. It seems that most of these structures are vesicles with sizes between 30 nm to about 1 μm. For example, Figures 15(B) depicts many small unilamellar vesicles with sizes of 20-60 nm and, also, in the centre of the picture, a relative big vesicle with a diameter of about 180 nm. Specifically, the membrane thickness can be clearly noticed in this polymersome because of contrast in colour, i.e. the membrane is lighter than the core. In addition, it can be found in the top right of Figure 15(B) two pear-shape vesicles with sizes of about 300 nm. Also, the same morphology can be observed at the top and at the bottom of Figure 15(C). Another morphology in Figure 15(B) and (C) that can be distinguished is of the type of tubular vesicles. The longest of the worm vesicles has a length of around 800 nm, Figure 15(B). The exact reason for all these type of aggregates is unknown but it may be related to the small difference in equilibrium energy between each structure or it may be an artefact of the sample preparation since the most common artefacts found using the staining technique are the flattening of spherical or cylindrical structures[44]. The effect of sample drying can be observed in Figure 15(D) since there is a different in population if it is compared the top-right zone with the rest of the picture. It seems that solvent evaporation aggregated the nanostructures to the left side of the picture.

Figures 15(E-G) show images with the effect of 0.1 M Na_2SO_4 to the polymer solution. In Figure 15(E), it can be seen some vesicles aggregates uniformly distributed in a part of the sample. Figures 15(F) and (G) are zooms-in of Figure 15(E). In these micropictures, one can observe smaller fragments of vesicles adjacent between each other. So, in generally, if it is compared salt-contained samples with free-salt samples, polymersomes are longer and, apparently, there is vesicle aggregation in the former case. However, results in TEM should be taken with caution because vesicle aggregation can

be a consequence of drying of the sample and also this can lead to major changes in the nanostructure, which may explain the bigger vesicle size in salt addition samples.

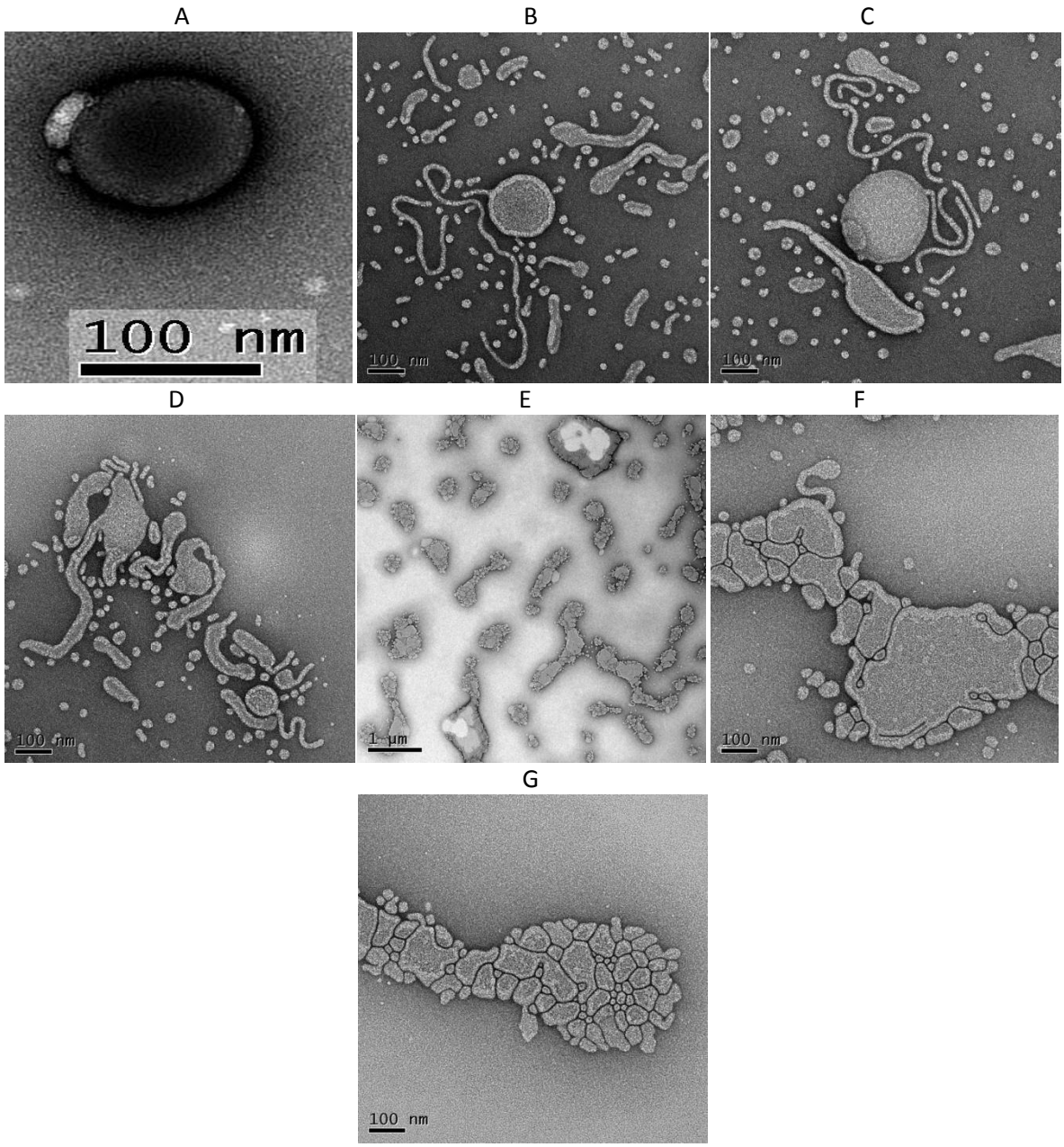

Figure 15. Micrographs taken by TEM. (A-D) are before 0.1 m Na_2SO_4 addition and (E-G) is after salt addition.

In summary, in the first set of experiments with GUVs, the addition of 0.1 M of Na_2SO_4 produced an agglomeration of vesicles; however, there is no clear evidence that this aggregation behaviour was directly correlated to the addition of the salt solution. This is partly due to the diffusion of the salt throughout the solution, which perturbed the vesicle static equilibrium and may have induced collisions and agglomeration, plus the "stickiness" of GUVs which also could promote agglomeration.

In the second set of experiments with nanovesicle nanostructures, the results can be divided in three parts: effect of salts at low (0.3 M), medium (0.88 - 0.96 M) and high (3-4.3 M) concentrations. If one considers the increment in the hydrodynamic radius (R_h) as a measurement of aggregation, we can assess the salting-out effect based on the increase in vesicle size. At low concentrations, the salting-out effect on polymer nanostructures of $E_{16}B_{22}$ was discarded because no variation in R_h could be seen, this is in accordance with literature[45,46]. At medium concentration, the R_h began to gradually increase for both Na_2SO_4 and NaH_2PO_4. These two salts have similar/the same salt effect on $E_{16}B_{22}$ vesicles since, after compared their results according with their relative concentration between each other, the R_h had a small variation. Also, at this concentration, there was a small increment of about 5 nm in the R_h when the sulphate sodium was added to polymer solution. Perhaps, this was due to a change in morphology from spherical to cylindrical vesicles. At high concentrations, the $E_{16}B_{22}$ polymer solution was greatly affected by the anion $H_2PO_4^-$ which produced an evident salting-out effect. At this concentration, the system followed the Hofmeister series in the following order $H_2PO_4^- > Br^- \approx I^-$.

References

1. Y. C. Shih, J. M. Prausnitz, and H. W. Blanch, *Biotechnol. Bioeng.*, 1992, **40**, 1155–1164.

2. M. M. Ries-Kautt and A. F. Ducruix, *J. Cryst. Growth*, 1991, **110**, 20–25.

3. L. M. Pegram, T. Wendorff, R. Erdmann, I. Shkel, D. Bellissimo, D. J. Felitsky, and M. T. Record, *Proc. Natl. Acad. Sci. U. S. A.*, 2010, **107**, 7716–7721.

4. L. Vrbka, P. Jungwirth, P. Bauduin, D. Touraud, and W. Kunz, *J. Phys. Chem. B*, 2006, **110**, 7036–7043.

5. P. Lo Nostro, B. W. Ninham, A. Lo Nostro, G. Pesavento, L. Fratoni, and P. Baglioni, *Phys. Biol.*, 2005, **2**, 1–7.

6. B. A. Deyerle and Y. Zhang, *Langmuir*, 2011, **27**, 9203–9210.

7. E. Thormann, *RSC Adv.*, 2012, **2**, 8297–8305.

8. P. Bahadur, K. Pandya, M. Almgren, P. Li, and P. Stilbs, *Colloid Polym. Sci.*, 1993, **271**, 657–667.

9. M. Wong and T. E. Thompson, *Biochemistry*, 1982, **21**, 4133–4139.

10. A. M. Carmona-Ribeiro and H. Chaimovich, *Biophys. J.*, 1986, **50**, 621–628.

11. G. Cevc and H. Richardsen, *Adv. Drug Deliv. Rev.*, 1999, **38**, 207–232.

12. T. P. Smart, A. J. Ryan, J. R. Howse, and G. Battaglia, *Langmuir*, 2010, **26**, 7425–7430.

13. T. P. Smart, C. Fernyhough, A. J. Ryan, and G. Battaglia, *Macromol. Rapid Commun.*, 2008, **29**, 1855–1860.

14. M. I. Angelova and D. S. Dimitrov, *Faraday Discuss. Chem. Soc.*, 1986, **81**, 303–311.

15. S. Mai, J. P. A. Fairclough, I. W. Hamley, M. W. Matsen, R. C. Denny, B. Liao, C. Booth, and A. J. Ryan, *Macromolecules*, 1996, **29**, 6212–6221.

16. *http://mit.edu/sjiang2/www/Resources/Prepare%20Lipid%20Vesicles.pdf*, Retrieved on Sep.17, 2012.

17. *http://www.rpgroup.caltech.edu/courses/aph162/2006/Protocols/vesicle.pdf*, Retrieved on Sep.17, 2012.

18. E. A. Boucher and P. M. Hines, *J. Polym. Sci. Polym. Phys. Ed.*, 1976, **14**, 2241–2251.

19. N. J. Deng, Y.-Z. Luo, S. Tanodekaew, N. Bingham, D. Attwood, and C. Booth, *J. Polym. Sci. Part B Polym. Phys.*, 1995, **33**, 1085–1096.

20. G. Battaglia, C. LoPresti, H. Lomas, M. Massignani, and T. Smart, *J. Mater. Chem.*, 2009, **19**, 3576–3590.

21. G. Battaglia and A. J. Ryan, *J. Am. Chem. Soc.*, 2005, **127**, 8757–8764.

22. M. J. Hope, R. Nayar, L. D. Mayer, and P. R. Cullis, in *Liposome Technology: Entrapment of Drugs and Other Materials*, ed. G. Gregoriadis, CRC Press, Vol. 1, 2nd edn., 1993, vol. I, pp. 123–139.

23. *http://www.avestin.com/lf.html*, Retrieved on Sep. 17, 2012.

24. R. Shaw, *http//149.171.168.221/partcat/wp-content/uploads/Malvern-Zetasizer-LS.pdf. Retrieved Feb. 1, 2014.*, 1–132.

25. *A Basic Guide to Particle Characterization (INFORM WHITE PAPER)*, 2012.

26. P. Russo, 2012, 1–48.

27. *Dynamic Light Scattering : An Introduction in 30 Minutes. (Technical note)*, Malvern Intruments.

28. C. Svanberg and R. Bergman, *Chalmer Univ. Technol.*, 2005, 1–6.

29. B. B. Weiner, *Brookhaven Instruments Corp. White Pap.*, 2010, 1–4.

30. Z.-H. Huang, M. Abkarian, and A. Viallat, *New J. Phys.*, 2011, **13**, 1–16.

31. G. Battaglia and A. J. Ryan, *Nat. Mater.*, 2005, **4**, 869–876.

32. J. R. Howse, R. a L. Jones, G. Battaglia, R. E. Ducker, G. J. Leggett, and A. J. Ryan, *Nat. Mater.*, 2009, **8**, 507–511.

33. Y. Okumura, T. Nakaya, H. Namai, and K. Urita, *Langmuir*, 2011, **27**, 3279–3282.

34. V. a. Parsegian and T. Zemb, *Curr. Opin. Colloid Interface Sci.*, 2011, **16**, 618–624.

35. F. Quemeneur, A. Rammal, M. Rinaudo, and B. Pepin-Donat, *Biomac*, 2007, **8**, 2512–2519.

36. Y. Zhang and P. S. Cremer, *Curr. Opin. Chem. Biol.*, 2006, **10**, 658–663.

37. L. M. Pegram, T. Wendorff, R. Erdmann, I. Shkel, D. Bellissimo, D. J. Felitsky, and M. T. Record, *Proc. Natl. Acad. Sci. U. S. A.*, 2010, **107**, 7716–7721.

38. M. J. Hey, D. P. Jackson, and H. Yan, *Polymer (Guildf).*, 2005, **46**, 2567–2572.

39. E. Florin, R. Kjellander, and J. C. Eriksson, *J. Chem. Soc., Faraday Trans. 1*, 1984, **80**, 2889–2910.

40. G. Battaglia and A. J. Ryan, *Macromolecules*, 2006, **39**, 798–805.

41. B. Lerebours, E. Wehrli, and H. Hauser, *Biochim. Biophys. Acta*, 1993, **1152**, 49–60.

42. J. Israelachvili, *Proc. Natl. Acad. Sci. U. S. A.*, 1997, **94**, 8378–8379.

43. D. Marenduzzo, K. Finan, and P. R. Cook, *J. Cell Biol.*, 2006, **175**, 681–686.

44. Http://web.path.ox.ac.uk/~bioimaging/Documents/neg_stain.pdf, 2010, 1–3.

45. L. Derici, S. Ledger, S. Mai, C. Booth, W. Hamley, and J. S. Pedersen, *Phys. Chem. Chem. Phys.*, 1999, **1**, 2773–2785.

46. N.-J. Deng, Y.-Z. Luo, S. Tanodekaew, N. Bingham, D. Attwood, and C. Booth, *J. Polym. Sci. Part B Polym. Phys.*, 1995, **33**, 1085–1096.

Chapter 3: Preparation of giant vesicles with a new-modified swelling-hydration technique

The author would like to acknowledge the assistance of PhD student Mr. Christopher Tse of Dr Patrick Smith's Inkjet Research Group, Department of Mechanical Engineering of the University of Sheffield. Mr Christopher Tse operated the inkjet printer and assisted in the selection of the control voltages as detailed later. All the other work in this chapter is the author's own work.

3.1 Introduction

In section 1.3.2 of chapter 1, techniques were described for vesicle preparation, all with their own advantages and disadvantages. Primary amongst the drawbacks, in almost all the methods, is the fact that many vesicles are created simultaneously. It would be preferable to create single or a small number of vesicles in a localised area, so that these can be examined and tested *in situ* using a micromanipulator equipment. In this way, different experiments can be conducted such as micropipette aspiration[1,2,3,4] experiments or the study of the fusion[5,6,7,8] event. This chapter describes our attempts to create giant vesicles (GVs) in a controlled and localised manner.

In the present chapter, the inkjet printing technique was used to explore the efficiency of GVs formation using the poly(ethylene oxide)$_{16}$-poly(butylene oxide)$_{22}$ block copolymer ($E_{16}B_{22}$) and the effect of different additives, i.e. sugars and salts, on improving vesicle formation. The copolymer $E_{16}B_{22}$ was synthesised in the group of Dr Colin Booth, Department of Chemistry University of Manchester, and has been widely used in other vesicle studies[9,10,11,12,13]. The aim of using this methodology is to afford a fixed position for vesicle-production where polymersomes can be found and easily collected, for experimental manipulation. This method of reducing the total number of GVs in solution also reduced the chance of GV's fouling the aspiration tubes. In collaboration with Dr Patrick Smith's group in the department of Mechanical Engineering University of Sheffield we undertook experiments to test the suitability of inkjet printing for vesicle (also called polymersomes) formation.

The inkjet method consisted on depositing small drops, e.g. 30 or 60 µm in diameter, of the polymer solution onto a glass slide at well-defined locations. Then, during hydration, each individual polymer microdrop would produce a small number of giant vesicles. As a small number of spots were hydrated each time and the total number of vesicles could, to some degree, be controlled.

Part of the study was to extend the work of Howse *et al.*[9]. These authors determined a protocol based on photolithography of creating well defined micrometer-size vesicles by controlling the amount of block copolymer available for each vesicle. In such a study, polymer solution of 5 %(w/w) $E_{16}B_{22}$ was deposited over micrometer-sizes square islands via spin-casting where the hydration of the films provides controlled size distribution of giant vesicles. The present research was intended to evaluate whether that protocol could be extended to produce giant vesicles. According with literature[9], the diameter of small vesicles can be controlled if the volume of polymer solution is restricted and if there is sufficient space between each GV to allow a free-growing vesicle. In other words, the vesicles are sufficiently well formed before coming into contact, that fusion is avoided.

Also, further research was conducted regarding the preparation of few lamellas structures after the deposition of each microdrop. This will be described in detail in section 3.3.1 of this chapter. Few lamellas are desirable in terms of control of vesicle formation. Furthermore, the inkjet printing technique could be an alternative and may be a more efficient technique for coating polymer films on surfaces compared with other current methodologies, such as spin coating[14,15].

3.2 Methodology

The main physical parameters to be taken into account for printing a polymer solution on a glass slide are viscosity and solution homogeneity. In the case of the latter, the polymer must be completely dissolved in order to avoid aggregation that could prevent vesicle formation on the glass slide. This problem can be solved for this polymer solution by stirring for at least three days. In the case of the viscosity, this was analysed by preparing different solution concentrations of $E_{16}B_{22}$ and comparing them with the range of viscosities affordable for printing.

Therefore, solutions of $E_{16}B_{22}$/water, with concentrations of 0.5, 1, 5 and 10 %(w/w) were prepared and their viscosities determined using an AR-G2 rheometer (TA Instruments Ltd). The dynamic viscosity was determined as a function of the shear rate over the range of 0.1-1000 sec^{-1} at a constant temperature of 25^{o}C. The following table summarises the results:

%(w/w)	*Viscosity (Pa-s)*
0.5	0.00105
1	0.00121
5	0.00408
10	0.00466

Table1. Dynamic viscosities of the polymer $E_{16}B_{22}$ in water at different concentrations.

Usually, samples with a relatively high solution viscosity perform well in printing[16]. The range of viscosities of the block copolymer $E_{16}B_{22}$, determined the preferable working concentration between 5 and 10 %(w/w). For the inkjet experiments, a concentration of 5 %(w/w) was chosen, partly due to the above criteria and partly because literature shows that successful preparation of GUVs were made using this concentration of $E_{16}B_{22}$[9].

The inkjet printer equipment basically consists of a Jetlab®4 table top printing platform, a MicroJet™ III controller (which control the piezoelectric actuator) and a PH-46 drop-on-demand print head (MicroFab Technologies). The equipment is depicted in Figure 1. The core of the printer is the inkjet microdispenser which is comprised of a piezoelectric actuator attached to an glass tube[17]. In general, the basic principle of operation of this printer is as follow[18]. When the piezoelectric actuator receives an electric signal, this rapidly deforms, generating a pressure acoustic wave. This wave travels to the end of the dispenser, i.e. the nozzle, where the wave energy is transformed into inertial energy[19]. In order to generate a drop[18], the voltage needs to rise for a time, then remain constant and then fall, what is known as "unipolar" signal (Figure 2(A)). The piezoelectric actuator deforms only when there is voltage rise or fall. At constant voltage, the actuator is static. Therefore, a sequence of voltage pulses causes a series of waves which unbalance the equilibrium of the fluid at the end of the nozzle, and, as a result, ejects part of the liquid. Then, the surface tension transforms this part of the liquid into a drop sphere[18].

Thus, modifying the timescale at which the voltage rises, stays constant, or falls controls the piezoelectric actuator performance. These parameters can be manipulated using the MicroJet™ III controller software interface, shown in Figure 2(B). Here, the Rise Time, Dwell Time, and Fall Time correspond to the Dwell Voltage elapsed in microseconds. These variables are the minimum elements required to create a drop. Depending of the inkjet solution being used, more complex signal voltages can be employed in order to stabilize the drop generation. For example, a basic signal, i.e. unipolar, can be added to another signal by establishing the Echo Time and Echo Voltage in the controller software. An echo signal can be created by using a negative voltage and the Dwell Voltage can have the same magnitude than the Echo Voltage or different. In our experiments, droplets were optimised with Rise Time: 8 μs, Dwell Time: 6 μs, Fall Time: 6 μs, Echo Time: 12 μs and Voltage: 30 V.

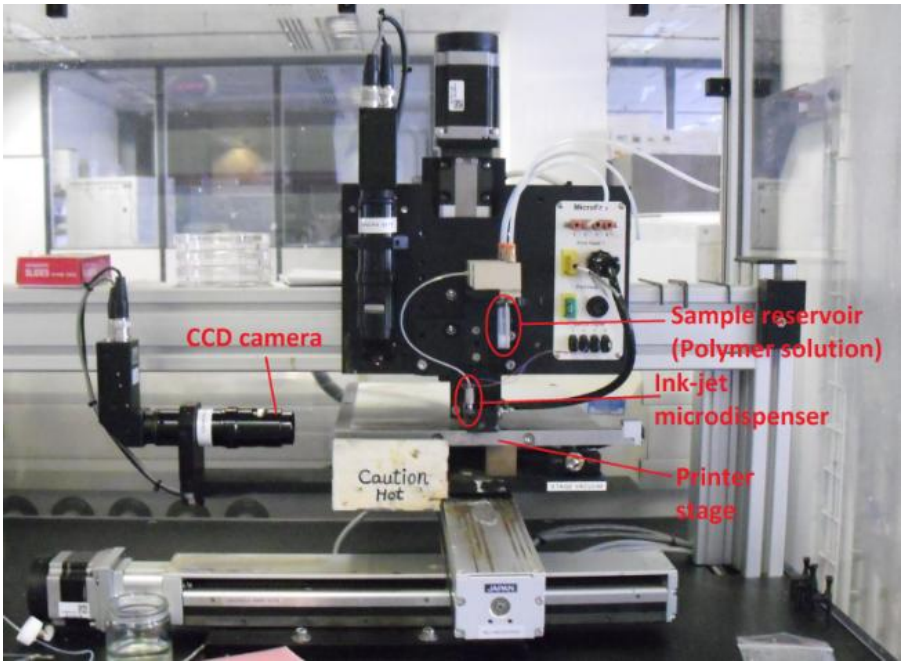

Figure 1. The inkjet printing equipment used in the experiments. The glass slide is placed on the printer stage where the camera on the left is used for imaging during printing.

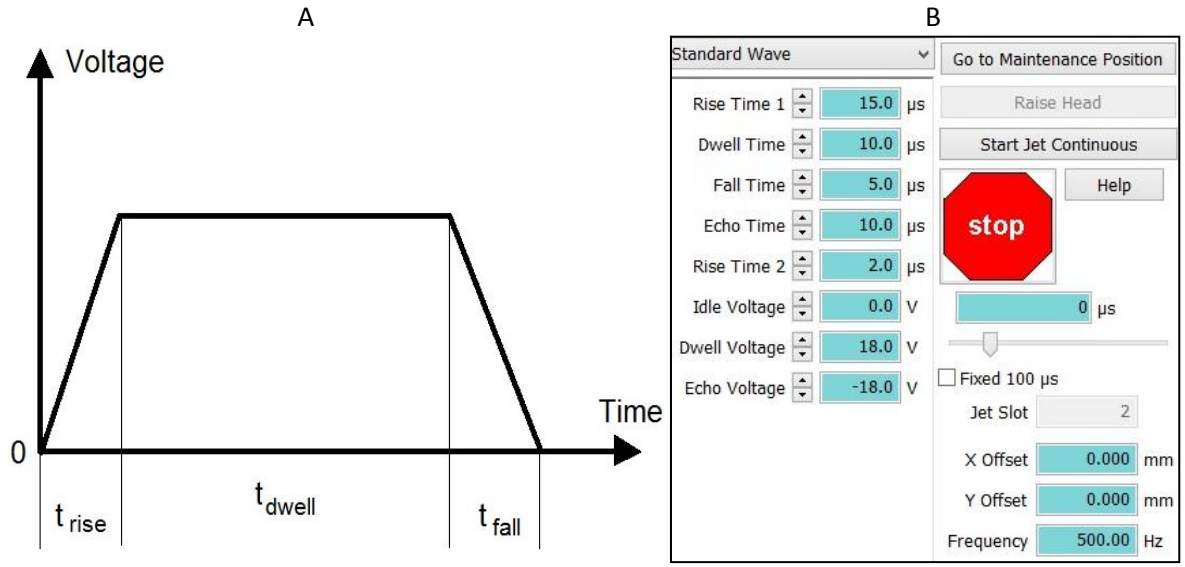

Figure 2. In order to generate a drop, the voltage needs to rise for a time, then remain constant and then fall, what is known as "unipolar" signal[18](A). The quality of the drops dispensed by the printer can be controlled using the jetlab®4 software (B).

In these experiments, the general procedure, from polymer injection to vesicle formation, is as follows:

1) An $E_{16}B_{22}$/water solution of 5 %(w/w) was prepared using ultra high quality water (UHQW) filtered through 0.2 μm PTFE filters. This solution was left stirring for at least three days. This process enables the dissociation of possible clusters of polymers.

2) In some experiments, salts or a sugar were mixed with the block polymer solution in order to obtain molar ratios of either 1:1 or 1:10 or 1:20 (additive/polymer). In most cases, the final concentration of polymer/water was 5 %(w/w). Also, it was used a concentration of 3 %(w/w).

3) The polymer solution was loaded in the inkjet printer sample reservoir and the parameters which control the piezoelectric actuator were adjusted for optimal printing. The polymer solution was printed using an array of 10x10 or 20x20 polymer microdrops, using an inner nozzle diameter of 30 μm, over a microscope glass slide, with approximately 100 μm or 200 μm between each drop. The gap between the drops was to allow free vesicle growth.

4) After printing, the glass slide was place in an inverted light microscope. The time evolution of the experiment was recorded using a CCD camera.

5) Water, or other types of aqueous solutions, were added to the sample and the bilayers grew at the outer edges of the polymer spot. Depending of the type of sample used (with or without additives), hemispherical or spherical giant vesicles started to appear after about 5 minutes of water addition.

The evolution of the giant vesicles (GV's) shows that multiple GV's develop from a single polymer microdrop, in contrast to the results of Howse *et al.*[9]. This is probably related to the hydration process being over supplied with polymer due to the size of the microdrop. The hypothesis being that there is a maximum size of the droplet where each droplet generates only one GV. However this was only a minor setback as the system still provides a small number of GV's in a localised environment. To determine if the surface interaction could be tuned to deliver a reduced number of GV's from each drop, a study of the effect of contact angle was undertaken.

Glass slide surfaces were modified using self-assembled monolayers (SAMs) in order to study the effect of hydrophobic surfaces on the process of vesicle growing when microdrops were hydrated. Depending on the type of substance used to make the SAMs, the surface of the glass slide can changed from hydrophilic to different degrees of hydrophobicity. To determine this degree, a drop of water was deposited over the surface of the glass slide and the angle formed between the solid

surface and the maximum liquid surface of the droplet was measured using a contact angle Goniometer equipment (Rame-Hart, Instrument Co.)

The SAMs were made using the following method. First, a piranha solution was prepared in a Pyrex beaker using a mix of *1/3* volume of H_2O_2 (30 %(w/v)) and *2/3* volume of H_2SO_4 (< 95%), (reagent grades purchased from Fisher Scientific). Then, microscope glass slides were submerged into this solution for 50 minutes. The piranha solution cleaned and activated the glass slide by hydroxilizing (OH addition) onto the surface. Next, the glass slide was rinsed at least 10 times with ultra high quality water (UHQW) in order to remove residual piranha solution. Subsequently, the glass slides were placed into the oven for 4 hrs at a temperature of 80^{o}C to dry. Drying was necessary in order to eliminate any remaining water, as the SAMs are highly reactive to water. In order to obtain a range of different contact angles on the surface, toluene or ethanol was poured into a receptacle, containing the glass slides, and a few drops of either octyltrimethoxysilane (96 %, Aldrich) or 1H, 1H, 2H, 2H-perfluorooctyl-trychlorosilane (97%, FluoroChem) were added to the solvent. The glass slides were allowed to react overnight and then were rinsed with either toluene or ethanol as previous and then water. Table 2 summarises the contact angles obtained.

Contact Angle (^{0})	***Methodology***
0	A microscope slide was cleaned with piranha solution (H_2O_2/H_2SO_4).
16 ±4	Uncleaned microscope glass slide
41 ±4	SAMs of Octyltrimethoxysilane in ethanol as solvent
76 ±5	SAMs of a mixture of octyltrimethoxysilane and perfluoroctyltryclorosilane in toluene as a solvent in a volume ratio of 1:1 (0.1 ml)
86 ±8	SAMs of perfluoroctyltryclorosilane in toluene as a solvent

Table 2. Description of the contact angles obtained by using different procedures of SAM preparations.

As multiple GV's were produced from each drop, the number of copolymer layers within each drop was determined in order to intent a single (or few) layer-coated slide. For calculation purposes (section 3.3.2), the height of the microdrop was determined (Figure 3). This was achieved by using Z-sectioning from microphotographs taken using a *Zeiss LSM 510 NLO* confocal laser scanning microscope with a 1 mW HeNe laser (543 nm). The images of the droplets were analysed using the *Zeiss LSM Image Browser (Version 4.2.0.121)* software which allows orthogonal projections of the XZ and YZ planes. As a result, the relevant spatial distances are possible to be measured. The

microdrops were imaged by mixing 5 ml of 5 %(w/w) $E_{16}B_{22}$ polymer solution with a small amount (0.1 %(w/w)) of rhodamine B octadecyl ester perchlorate as a dye.

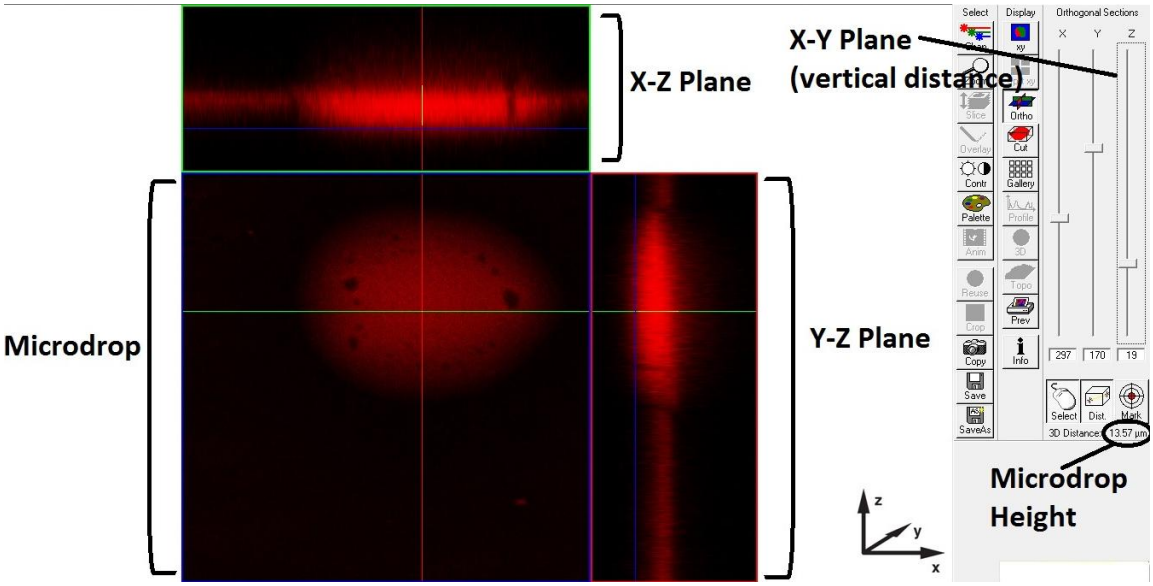

Figure 3. Measuring of the microdrop height using orthogonal images. The vertical distance of the droplet was determined by moving the X-Y plane in the "Z" direction.

3.3 Results and discussion

In the inkjet printer experiments, broadly speaking, the size of the nozzle controlled the range of the diameters of the microdrops deposited on the surface. The printer's piezo electric device controlled the position where each droplet is placed; allowing the required space for vesicles to grow without fusing. The hypothesis was that modifying these factors facilitates control over the size distribution of polymersomes by depositing small amount of a polymer solution, i.e. picoliter drops, into a place that can be tightly specified.

The concept of microprinting a polymer solution over glass slides for making vesicles is based on the mechanism of vesicles formation. According to literature[20], liposomes made of charged phospholipids can be formed if there is separation of an individual bilayer from a multilayer lamellar phase. The initial hydration among polar amphiphilic groups contributes to both separation and bending of the bilayer in a bulging-like shape. Further separation occurs when water diffuses through the outer layers, increasing the interbilayer separation in lamellae. Then, defects or gaps along the lamellar structure's length, (or agitation) induce detachment and subsequently, close the blisters to form a liposome.

The mechanism of formation for polymersomes is similar to that of liposomes. After printing the polymer $E_{16}B_{22}$ on a glass slide, the microdrops (5 %(w/w) polymer/water) dried and formed small spots, as it can be seen in Fig. 4. These spots contain many layers of block copolymer, i.e. lamellar stacks, arranged one above the other, which in the presence of water go through morphological transitions in a polymer/water equilibrium system. When the lamellar structure is hydrated[9], the hydrophilic (PEO) and hydrophobic (PBO) parts of the block copolymer undergo internal microphase separation in the lamellar phase where tubular or hexagonal rod structures form. The lamellar phase is still present but just in the outer surface. Further hydratation separates the layers of the lamellar phase more because the hydrophilic domains generate steric repulsion against each other. This separation creates a free space in the upper layer where a lamellar structure can grow[9,20] in a globular-like shape, until the bilayer closes in order to achieve a minimal energy surface[21], i.e. a sphere.

The following picture shows a typical array of microdrops used in experiments. The diameters of the microdrops are around 40 µm from a nozzle size of 30 µm. Also, the microdrop sizes can be controlled by modifying the printing parameters of the MicroJet™ III software (Figure 2(B)). The horizontal and vertical distances between spots are around 80 µm.

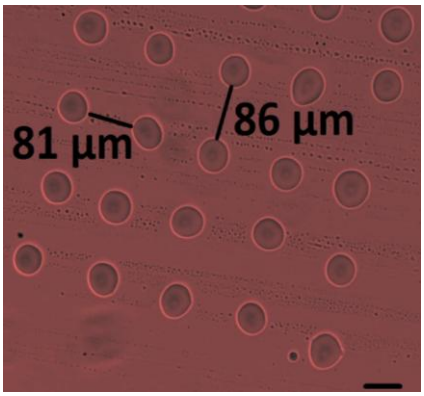

Figure 4. An image taken using a 4x objective, showing the microdroplet array on the glass slide. The scale bars at the bottom-right is 60 µm.

3.3.1 Effect of different hydrophobic surfaces over vesicle growing

Figure 5 shows the evolution of microdrop hydratation through time on a glass surface with a contact angle of 0^{o}. During a period of 20 minutes after water addition, Figure 5(A), several bilayers grew around the polymer microdrop. These vesicles are hemispherical, apparently not completely formed, with sizes of approximately 9.6 µm and are close together. They continue to grow with time (Figure 5(B)). The hemispherical vesicle with a size of 9.6 µm, in Figure 5(A), increased in size to 10.4 µm in Figure 5(B). This increase is due to the continuing hydration of the lamellae since there was no

membrane separation from the microdrop lamellar phase. After 60 minutes, Figure 5(C), a large hemispherical vesicle of 19.3 µm was observed. It seems that two growing polymersomes in Figure 5(B), with sizes of 10.8 µm and 10.4 µm, fused together to form a larger hemispherical polymersome, probably of initial radius around 15 µm that subsequently grew to 19.3 µm. This is probable due to the close proximity of the two bilayers. After 80 minutes, Figure 5(D), hemispherical vesicle sizes were between 10-17 µm. Finally, after 90 minutes, Figure 5(E), another large vesicle, 16.1 µm, can be seen which could be the product of the fusion of others two hemispherical polymersomes with sizes of 12 and 10.3 µm, Figure 5(D).

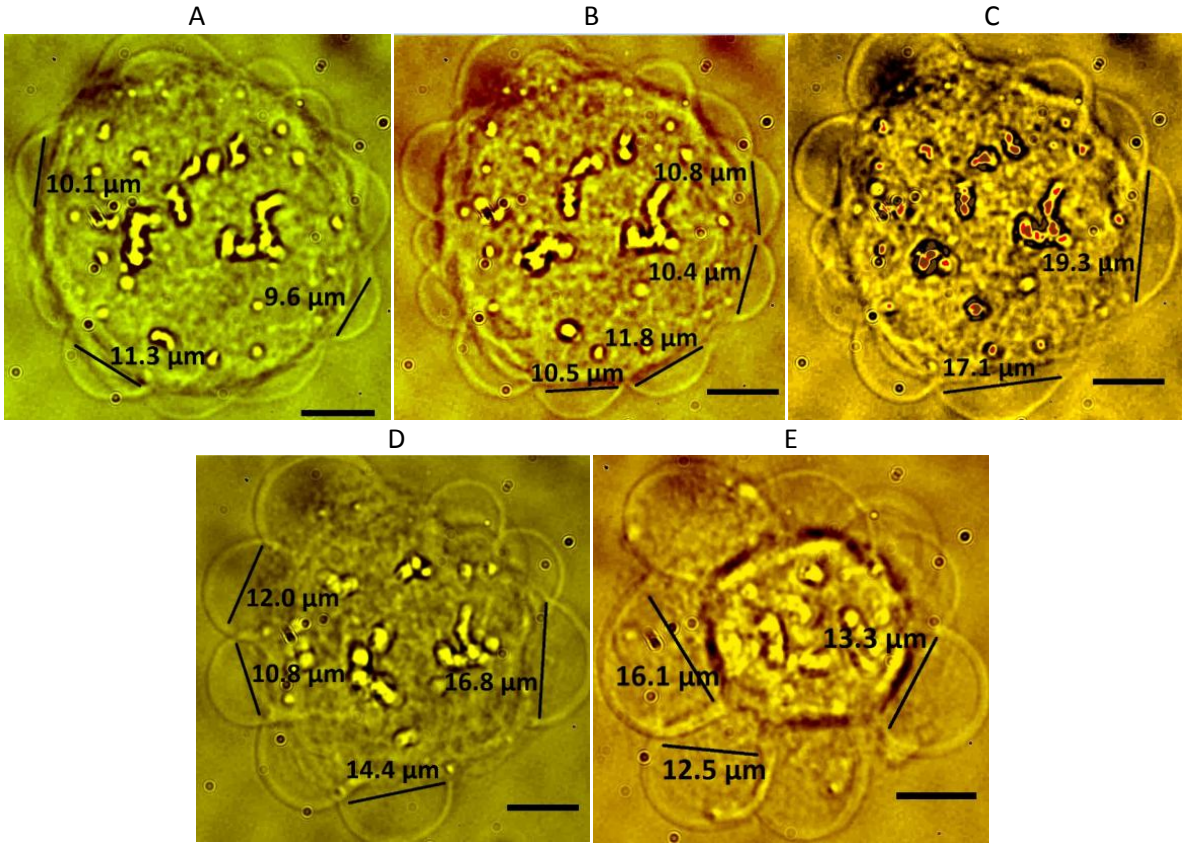

Figure 5. Microphotographs of $E_{16}B_{22}$ microdrop hydration, at 60x magnification, prepared with the inkjet printing technique using a nozzle size of 30 µm on a glass surface with a contact angle of 0^{o}. The pictures were taken at different times after water addition: 20 min (A), 40 min (B), 60 min (C), 80 min (D) and 90 min (E). The scale bar at the right-bottom corner represents 10 µm.

In Figure 6, the polymer solution was deposited on a glass-surface slide with a contact angle of 16^{o} $\pm 4^{o}$. In Figures (A) and (B), 5 and 10 minutes after water addition, respectively, the diameter of the swollen polymer spot increases from 40.9 to 44.8 µm. However, vesicles formation around the polymer dot is not as clearly visible, compared to Figure 5. In Figure 6(A), a hemispherical polymersome of 12.1 µm, can be identified 5 and 10 minutes after water addition. This

hemispherical vesicle can be observed embedded into the polymer substrate. Figures (C), (D) and (E) show the evolution of a large hemispherical polymersome after 20, 35 and 45 minutes. This hemispherical bilayer can be seen to be above other forming vesicles which are into the swollen polymer substrate. This suggests that water has permeated under the polymer dot and is releasing the dot from the surface. However, encouragingly the diameter of 33.2 µm increases through time, eventually reaching a diameter of 34.8 µm. Unfortunately, this large hemispherical vesicle is still fouled by excess polymer material.

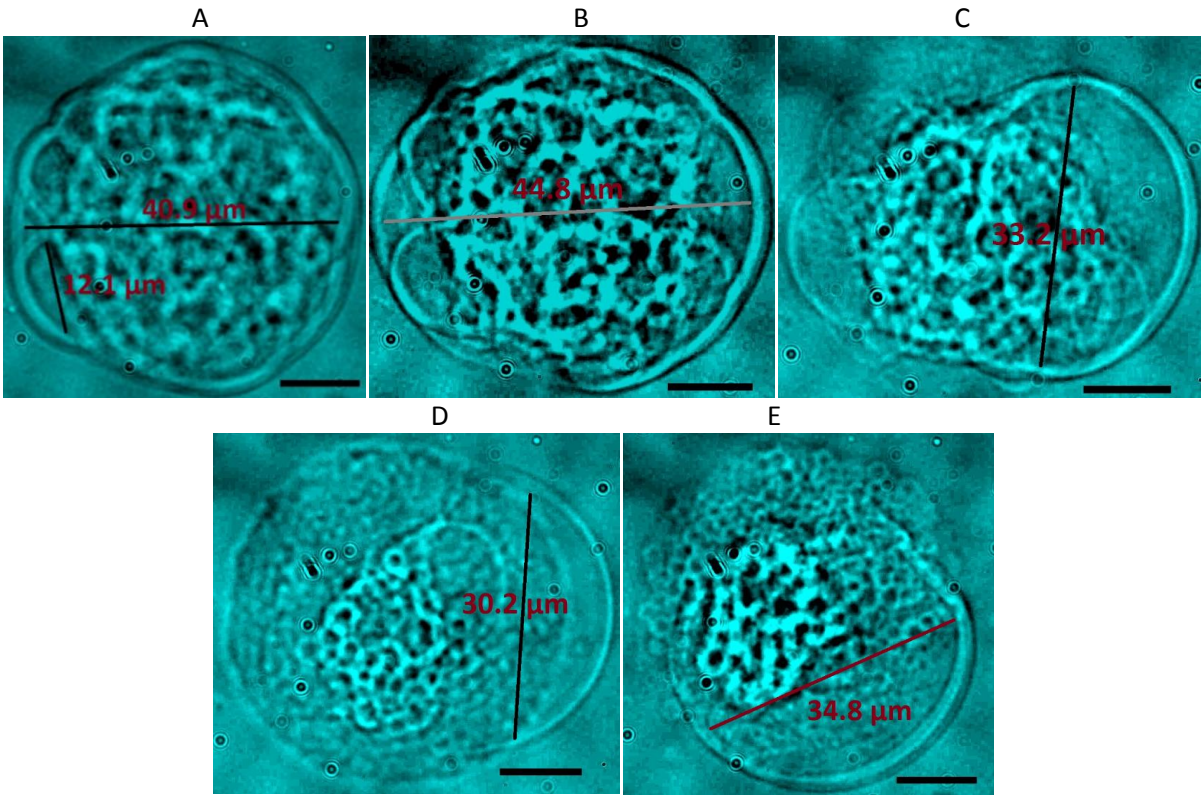

Figure 6. Microphotographs of $E_{16}B_{22}$ microdrop hydration, at 60x magnification, prepared with the inkjet printing technique using a nozzle size of 30 µm on a glass-surface slide with a contact angle of 16^{o} ±4^{o}. The pictures were taken at different times after water addition: 5 min (A), 10 min (B), 20 min (C), 35 min (D) and 45 min (E). The scale bar at the right-bottom corner represents 10 µm.

At a contact angle of 41^{o} ±4^{o}, many overlying vesicles were formed (Figure 7). However none of these vesicles could be isolated. The problem could be the water diffusing under the polymer microdot or with dust contamination of the surface or polymer solution. For example, it has been found that when the polymer solution or the glass slide contain small particles of dust, this can hinder polymersome formation. Also, a lack of stirring in polymer solution can bring problems. In this case, when a polymer solution of 5 %(w/w) $E_{16}B_{22}$ was not mixed well enough, the solution became turbid. When it was deposited on the glass slide, the microdrop exhibited small lumps or lamellar

structure imperfections, after drying, which can lead to problems in vesicle formation. However, stirring the polymer solution for at least two days was enough to avoid this problem.

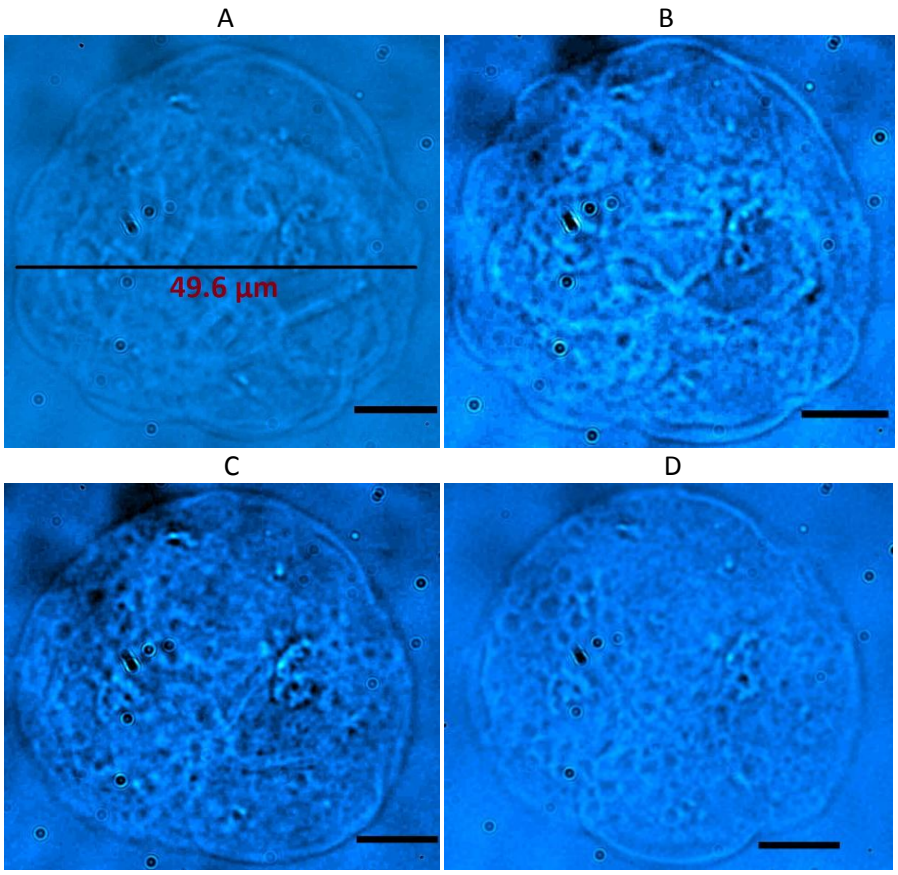

Figure 7. Microphotographs of $E_{16}B_{22}$ microdrop hydration, at 60x magnification, prepared with the inkjet printing technique using a nozzle size of 30 µm on a glass-surface slide with a contact angle of 41^{o} ±4^{o}. The pictures were taken at different times after water addition: 10 min (A), 20 min (B), 40 min (C), and 60 min (D). The scale bar at the right-bottom corner represents 10 µm.

At higher contact angles (e.g. 76^{o} ±5^{o} i.e. a hydrophobic surface) several vesicles of different sizes could be found around the polymer spot (Figure 8). After 20 minutes from water addition, Figure 8(A), a large hemispherical vesicle of 38.8 µm in diameter could be seen in the sample with three other smaller hemispherical vesicles, indicated by arrows, inside, above or below the larger one (the microscope images do not allow us to determine which). There was also a hemispherical vesicle of 13.7 µm of diameter growing with an adjacent vesicle of about 15 µm (top-right of the picture, indicated by an arrow). After 40 minutes, Figure (B), the large vesicle described above remained and, in addition, another hemispherical vesicle became visible with a size of 15.2 µm. After 60 minutes, Figure (C), this last vesicle "disappeared", maybe either fusing with the neighbouring bilayer of 35.7 µm, since this increased in size, or probably the vesicle detached from the lamella structure after complete formation. After 80 minutes, Figure (C), three tiny spherical polymersomes with diameter

of 1.9 µm (blue arrow), 2.6 µm (black arrow) and 3.7 µm (red arrow) became visible. These spherical bilayers were unusually small because previously most of the vesicles had diameters of about 10 µm. A possible explanation could be a better hydration of the sample in this experiment. After 100 minutes, Figure (E), a giant vesicle of 45 µm could be clearly seen, maybe the product of the fusion of 41.3 and 31.8 µm polymersomes although the new size is not much bigger than before. Also, small vesicles (indicated with the big arrow) were attached over the membrane of the big polymersome.

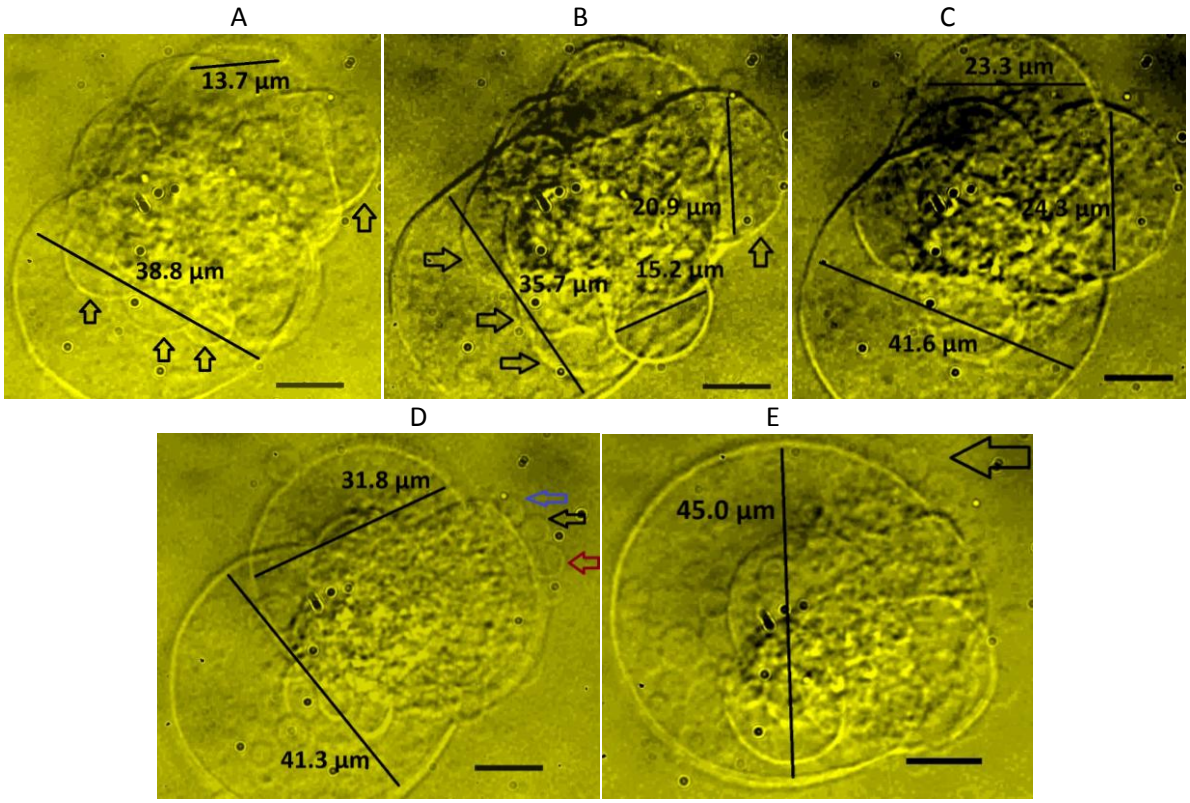

Figure 8. Microphotographs of $E_{16}B_{22}$ microdrop hydration, at 60x magnification, prepared with the inkjet printing technique using a nozzle size of 30 µm on a glass-surface slide with a contact angle 76° ±5°. The pictures were taken at different times after water addition: 20 min (A), 40 min (B), 60 min (C), 80 min (D) and 100 min (E). The scale bar at the right-bottom corner represents 10 µm.

In Figure 9, a hydrophobic surface of 86° ±8° contact angle was used for the inkjet printing experiments. Thus, 20 minutes after water addition, several vesicles were growing around the polymer spot, Figure 9(A). Then, after 40 minutes, Figure 9(B), typical polymersome sizes were around 10 µm. From Figure (C) to (F), 60 to 75 minutes, it seemed that all vesicles around the polymer microdrop merged and yielded just one vesicle of 21.4 µm of diameter. A droplet of this size could generate a single polymersome of about 20 µm, but this one still fouled by excess polymeric material. However, of all the conducted experiments, that was the only occasion where all the

vesicles around a polymer spot fused and created a single visible vesicle. It appeared that in order to obtain one vesicle many conditions needed to be met, only some of which we were able to control.

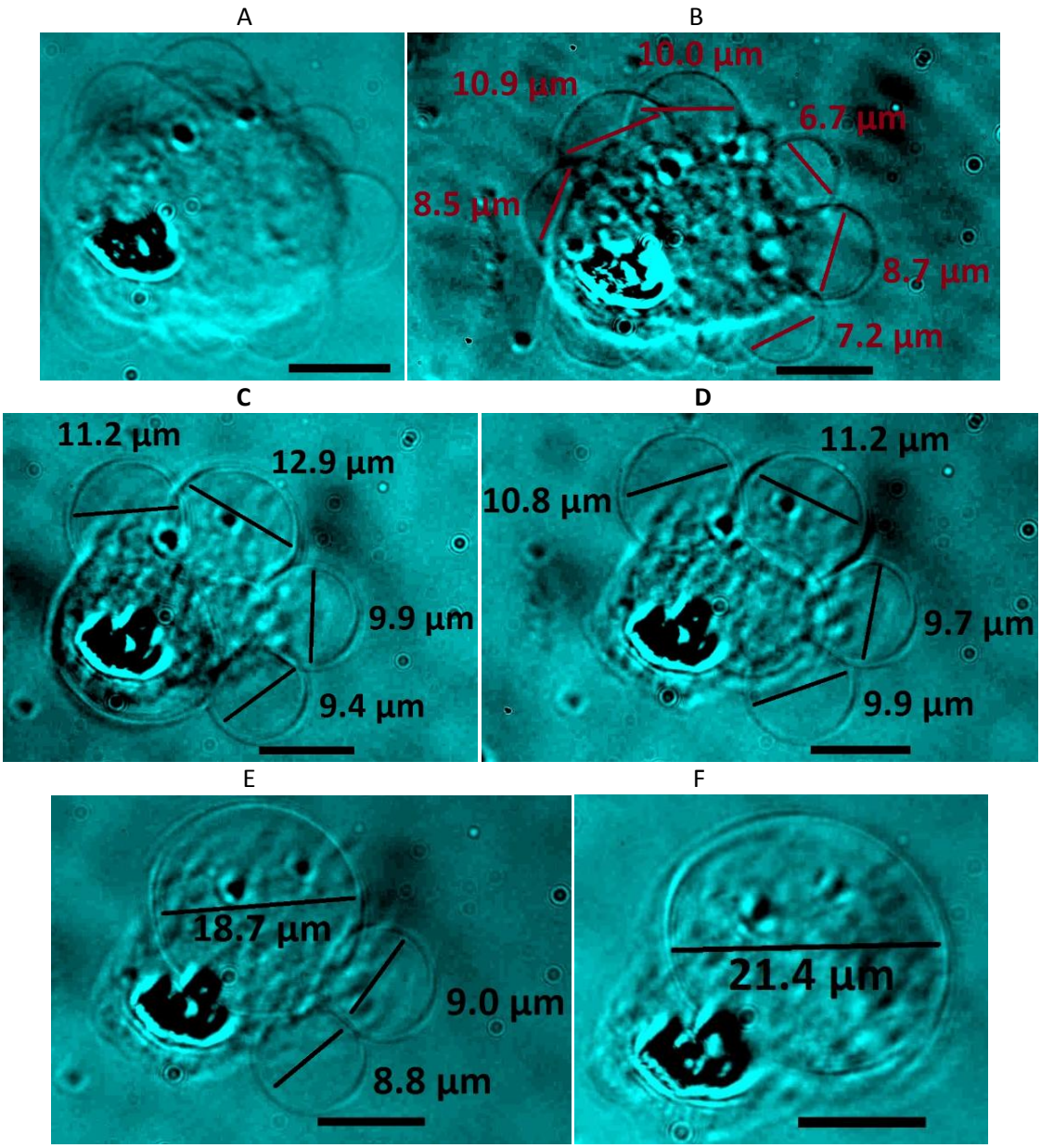

Figure 9. Microphotographs of $E_{16}B_{22}$ microdrop hydration, at 60x magnification, prepared with the inkjet printing technique using a nozzle size of 30 µm on a glass-surface slide with a contact angle of $86^{o} \pm 8^{o}$. The pictures were taken at different times after water addition: 20 min (A), 40 min (B), 60 min (C), 65 min (D), 70 min (E) and 75 min (F). The bar at the right-bottom corner has a dimesion of 10 µm.

It does seem that the nature of the glass surface, increasing from hydrophilic to hydrophobic, encourages the formation of larger vesicles due to an improve of the hydration process in the polymer substrate. Also, it is not clear if large vesicles are the result of membrane fusion since

vesicles were close each other as can be seen in Figure 5, 8 and 9, or were the result of the swelling of the polymer layer after a time. The results are not widely reproducible and often contamination by dust has a dominating influence. One major issue is that in the Howse et al[9] work, the layer thickness was much small than that observed here. Therefore the gradient of hydration from top to bottom of the film is not likely to be as the Howse et al work[9]. According with a simple calculation presented in secction 3.3.1, the polymer microdrop comprises about 1000 layers or lamellar structures. Therefore, apparently, water hydration influenced more top layers than bottom layers. This is further discussed at the end of this chapter.

Figure 10 displays vesicles with a tethered morphology. These structures were seen after the addition of more drops of water to the sample. Very probably, the hydration forces caused by water addition promoted polymersome detachment from around the polymer microdrops. For example, Figure (A) depicts a tethered vesicle which is attached to the microdrop, that is at the bottom of the picture. In another part of the sample, Figure (B) shows a chain of vesicles which surrounded a fragment of polymer which separated from a larger segment. Also, images (C) and (D) represent isolated tethers which were removed from the polymer spot. They can form a vesicle network that can be several hundreds of micrometers long. At the present time, there is no clear idea about why the tethered morphology is produced although there has been a recent hypothesis[22]. When vesicles stick to one another and then subsequently separate, they can form tethers. The tethers in Figure 10 may be a result of the fusion and then separation of vesicles because these tethered were observed just after the addition of more droplets of water to the sample. Water could cause hydrodynamic forces that could promote vesicle movement and possible collision and fusion of polymersomes.

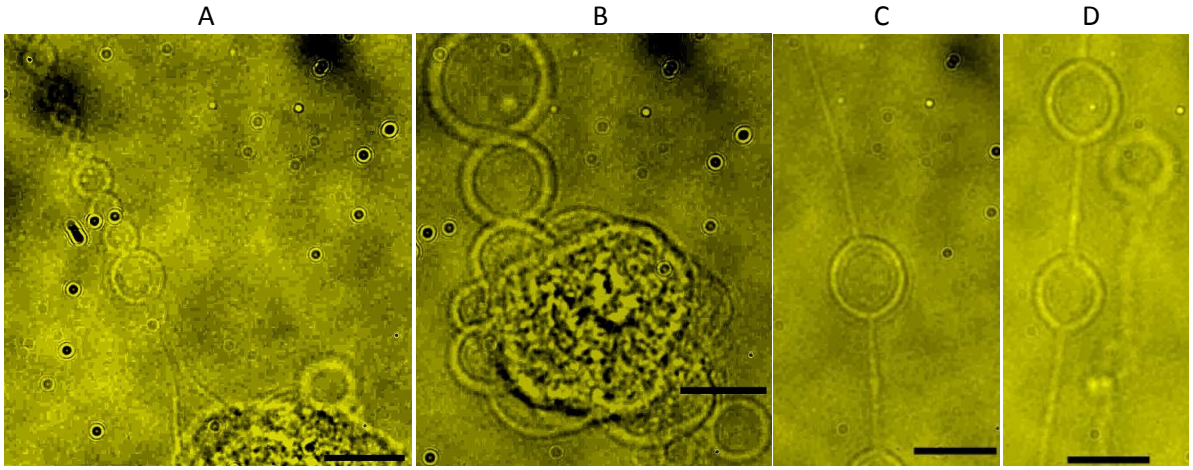

Figure 10. Microphotographs of tethers formation when more drops of water were added to the sample at a specific time: 100 min (A) and 122 minutes (B), (C) and (D). The bar at the right-bottom corner has a dimesion of 10 µm at 60x magnification.

3.3.2 Calculation of the number of layers per polymer microdrop

A single giant vesicle can be obtained if just one layer of polymer is deposited on the glass slide. Since the layer thickness depends on the polymer solution concentration, at a certain concentration, the printer can place a single lamellar structure on the glass surface. Thus, the number of layers at 5 %(w/w) concentration can be calculated and, by extrapolating data, the concentration at which a single layer is formed can be determined. This data will be used to prepare a polymer concentration which could print few layers and, in this way, control the number of giant vesicles in each microdrop.

A lamellar structure was formed when a microdrop of polymer solution was deposited on the glass surface as shown in Figure 11*:*

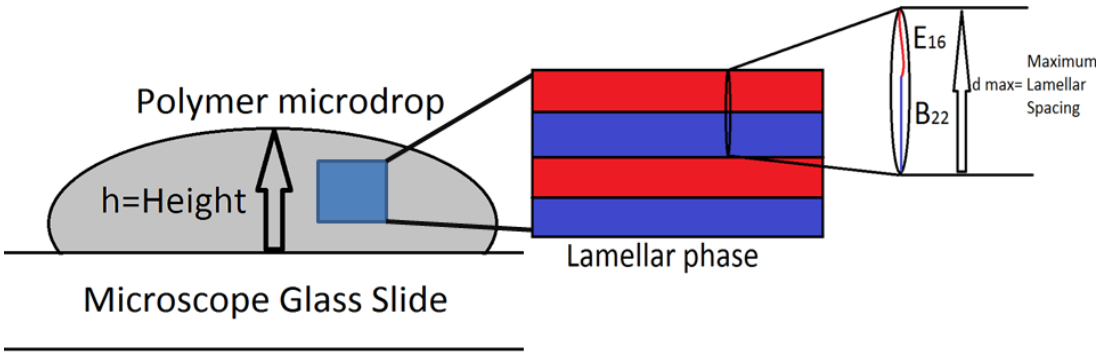

Figure 11. The polymer microdrop of a certain height is on a glass slide. On the right side of the sketch, the lamellar structure of the $E_{16}B_{22}$ is represented with the maximum lamellar space between layers.

The number of layers in a microdrop is:

$$No.of\ layers = \frac{h}{d(polymer)}$$

Where h is the height of the microdrop and d is the maximum lamellar spacing for the $E_{16}B_{22}$ block copolymer. The height of the microdrop was determined by confocal laser scanning microscopy (Figure 3) with an average of 19.11 *μm* (± 7.9 *μm*) for three microdrops in two different samples (13.3 *μm*, 26.6 *μm*, 17.4 *μm*).

The maximum lamellar spacing can be estimated using the following equation[23]*:*

$$d/\text{Å} = 0.95\ Z_E + 1.21\ Z_B$$

Where Z_E and Z_B are the numbers of carbon and oxygen atoms in the ethylene and butylene chain parts, respectively:

$$\frac{d}{\text{Å}} = 0.95\ (3)16 + 1.21(5)22 = 178.7\ \text{Å} = 0.01787\ \mu m$$

Therefore, the number of layers deposited on the glass slide*:*

$$No.of\ layers = \frac{19.11\ \mu m}{0.01787\ \mu m} = 1\ 069.4\ \approx 1069\ layers$$

Thus, the concentration in order to deposit one layer is:

$$\frac{5\ \%(w/w)}{1069\ layers} = 0.00467\ \%(w/w)$$

An attempt was made to prepare a single layer by preparing a polymer solution of 0.3 %(w/w) $E_{16}B_{22}$. The method previously discussed was used to prepare vesicles with further addition of a small amount of Rhodamine B (from Laboratory Reagent BDH Chemicals LTD.), as a dye, to the polymer solution. However, when water was added to the sample, no vesicles were detected using light microscopy. It seemed that water dispersed the microdrops on the glass surface avoiding any vesicle formation.

3.3.3 Improvement the hydration process on polymer microdrops

As it was seen above, inkjet printing the polymer solution on a glass slide can produce bilayers. However, most these structures (Figure 5-9) were hemispherical vesicles, and embedded into the polymer substrate, i.e. vesicles are tighly attached to the substrate, and, as a consequence, difficult to pick up when conducting micropipette aspiration (MPA) experiments. For example, a small sucction pressures did not unbind vesicles and large pressures has the effect of detaching the polymer substrate both cases make it difficut to insolate them. A carefull and control rehydration, e.g with a syringe pump, can help to detach some vesicles. However, in most cases either the rehydration process did not affect the vesicle unbinding or the polymer substrate detached from the surface of the glass slide. Moreover, longer hydration times (Figure 12) did not have great effect over the process of vesicle growth and did not provide more vesicles. Therefore, slightly modifications to the hydration methodology are necessary in order to promote complete formation of polymersomes.

The inkjet printing method used to produce vesicles is related to the lipid film hydration method cited in literature[24], also know as gentle hydration[25] or hydration-rehydration[26] or spontaneous swelling technique[27]. This method is based on the formation of a phospholipid film over a solid

surface, usually a glass surface, via the evaporation of an amphiphilics/organic solvent mixture[24]. Then, the hydration of the sample provides giant vesicles.

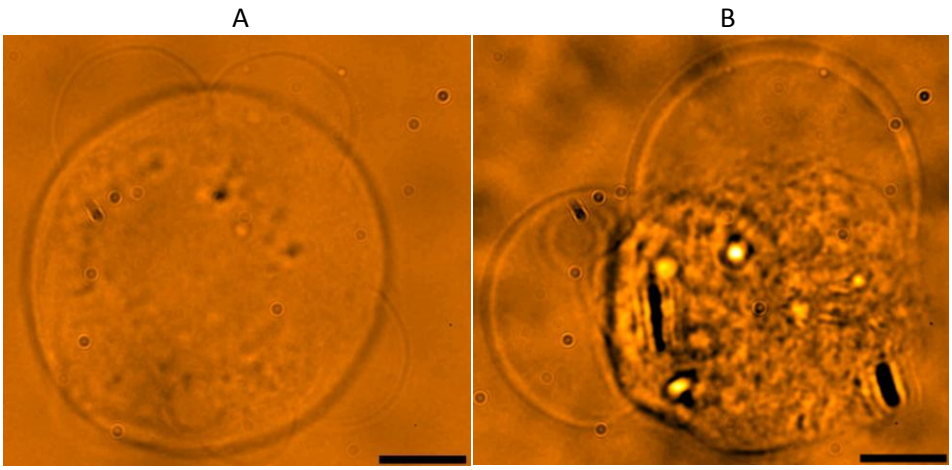

*Figure 12. Water hydration of polymer films on a glass surface (*86^{o} ±8^{o} contact angle) *after about 12 hrs. Basically, there were no differences in both vesicle sizes and the number of vesicles in comparison with short period of times (2 hrs hydration). The scale bar is 10 µm.*

The gentle hydration is widely used to prepare both liposomes or polymersomes using either sugars or salts aqueous solutions as the subtances of hydration[28]. The similarities of this technique with inkjet printing procedure is the hydration of a polymer film which is deposited over a glass surface. So far in experiments, we have hydrated the samples using just water. However, in theory, it follows that it could be feasible to form polymersomes by addition of sugars or salts to the inkjet-printed polymer microdrops. The importance of using refractil solutes in polymersome production is derived from the necessity of enhancing the membrane contour visibility in MPA experiments. For instance, typically in the gentle hydration method, a thin film is hydrated with sucrose solution and, after both vesicle formation and enventually sucrose encapsulation, vesicles are resuspended in a glucose solution. So, in this way, a difference of refractive index can be created, at least temporarily, between the inside and outside of the polymersome.

Therefore, the following experimental secctions will describe two groups of tests: either experiments with different concentrations of sugars and salts added to the vesicle solution (“additive in solution”) or mix into the deposited polymer substrate (“additive in film”) and then hydratated, in order to promote vesicle growing. All the glass slides used in these experiments had a contact angle of 86^{o} (± 8^{o}).

3.3.4 "Additive in solution" experiments

According to literature, non-electrolyte solutions are recomended to hydrate films made of neutral amphiphilics[29], i.e. phospholipids and block copolymers, with typical sugar concentrations in the range of 0.1-0.3 M using the gentle hydration technique[30]. Therefore, testing these cases in our experiments, different sugar solutions at different concentrations were employed to hydrate polymer microdrop samples. At low concentrations, the addition of either 0.1 M sucrose or 0.1 M glucose solution produced similar results, as can be seen in Figure 13(A) and 13(B) respectively. Both images are almost identical after 24 hrs of sugar addition. So, the hydration power of these substances is similar either sucrose or glucose are suitable for inkjet printing. Incrementing glucose concentration to 0.2 M (Figure 13(C)) and 0.5 M (Figure 13(D)) did not provide any improvements in vesicle growth after times of 24 hrs and 12 hrs respectively. Moreover, the process of film hydration with 0.1 M sucrose followed for 6 hrs and, then, rehydration with 0.1 M glucose in a lapse time of 2 hrs, seems to inhibit vesicle growth, i.e. few and small hemispherical vesicles (Figure 13(E)). In general in these experiments, the addition of sugars at low and high concentrations did not cause an improvement on polymersome formation and, actually, the same problems persist, such as hemispherical-not-completly formed and bound vesicles.

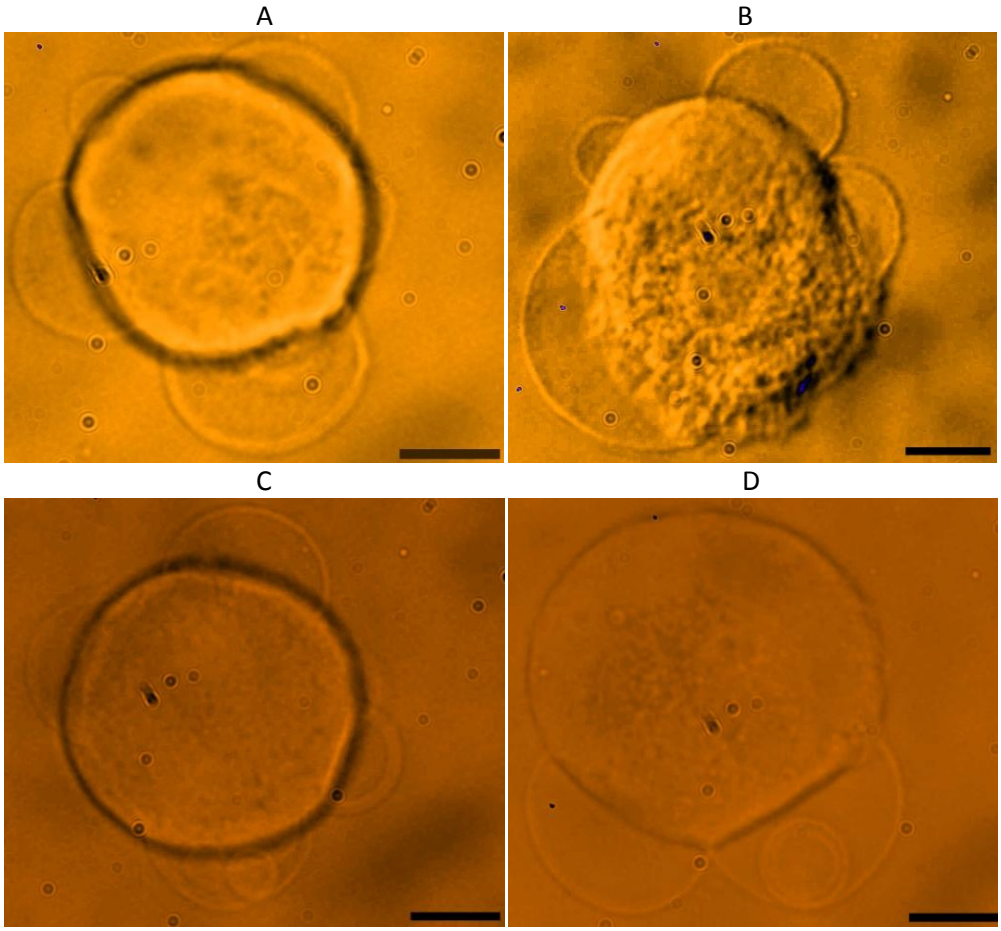

E

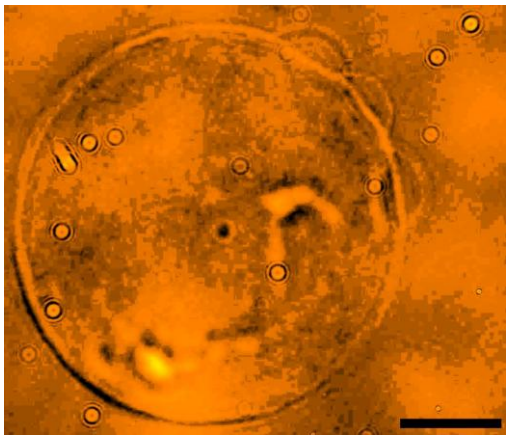

Figure 13. Hydration of polymer films using different concentrations of sugar aqueous solutions: 0.1 M sucrose (A), 0.1 M glucose (B), 0.2 M glucose (C), 0.5 M glucose (D), and 0.1 M sucrose and then re-hydration with 0.1 M glucose (E). Microphotographs (A), (B), and (C) were taken 24 hrs after hydrated the samples and (D) after 12 hrs and (E) after a total hydration time of 8 hrs (6 hrs hydration with 0.1 M sucrose and 2hrs rehydration with 0.1 M glucose). The scale bar is 10 µm.

Figure 14(A-F) shows the hydration of inkjet printing samples using two different concentrations of NaH_2PO_4. At relatively low ionic strength and after two hours of hydration, the addition of a 0.3 M salt solution did not produce vesicles in most parts of the glass slide (Figure 14(A)). However, a very small number of microdrops, such as in Figure 14(B), contained what seemed to be evidence of bilayers (indicated by arrows) embedded into the polymer substrate. Longer hydration times did not improve vesicle formation. For example, after 24 hrs (Figure 14(C)), two protruding membranes (indicated by arrows) seem to be uncompleted polymersomes. Similar results can be obtained a higher concentration of NaH_2PO_4 solution. At 1 M and after 2 hrs of hydration, most of the polymer microdrops do not present any evidence of vesicles (Figure 14(D)) and others present some highly flexible parts of bilayers (Figure 14(E)). Again, these polymersomes seemed not to be fully formed. After 5 hrs (Figure 14(F)), there are formations of two spherical vesicles (indicated by arrows) which are fouled by the substrate. Though this was the first time that this was observed, completely formed polymersomes after just hydration, these vesicles were rarely observed and, also, their sizes were small (about 6 µm), not large enough for MPA experiments. Therefore, few polymer microdrops showed fragments of bilayers (Figure 14(B-C) and (E)) and even less showed spherical vesicles (Figure 14(D)) in this series of experiments.

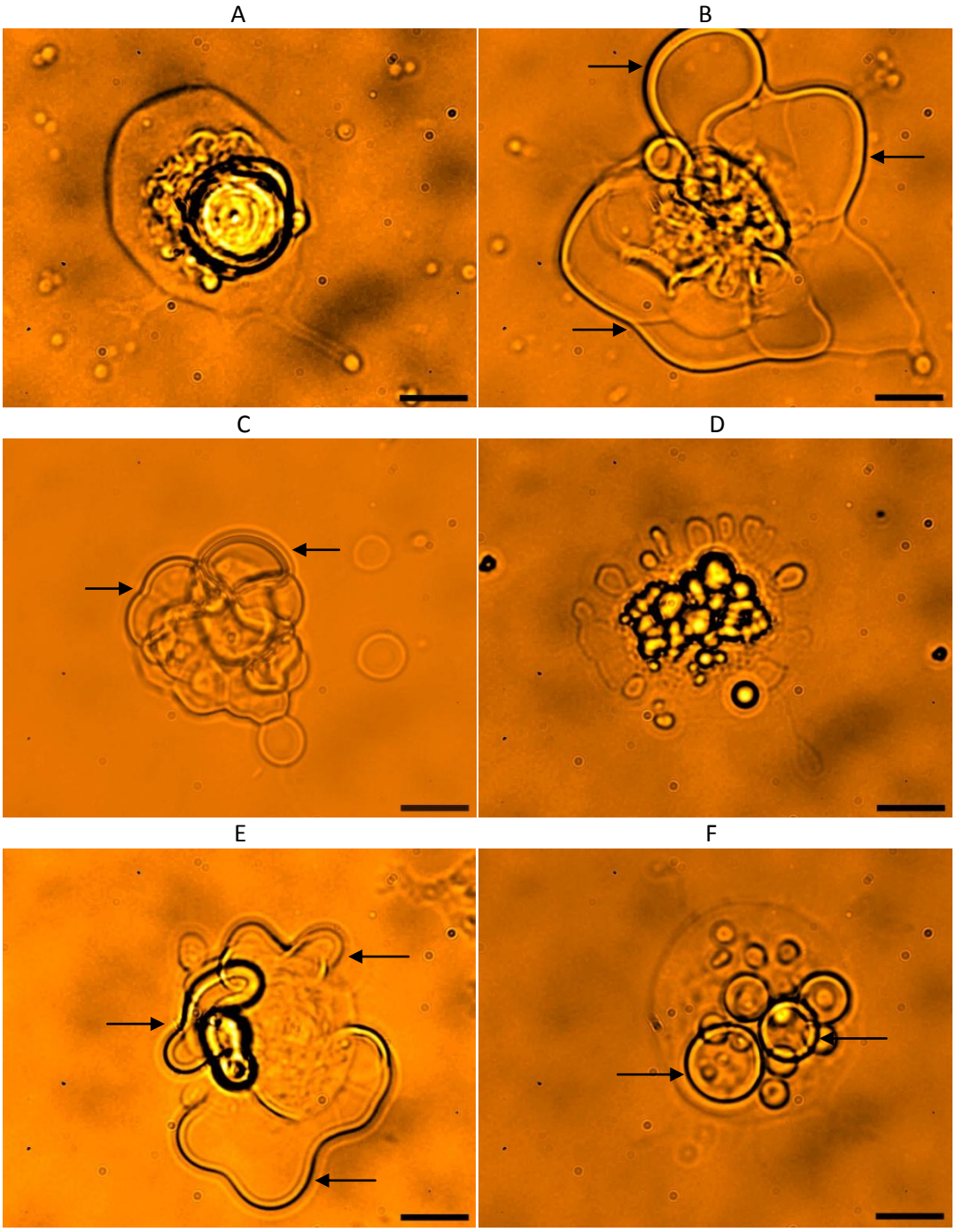

Figure 14. Hydration of polymer films at different NaH_2PO_4 concentrations: 0.3 M (A-C) and 1 M *(D-F). Microphotographs (A), (B) and (D) were taken after 2 hrs hydration time and (E) and (F) after 5 hrs and (C) after 24 hrs. The scale bar is 10 µm.*

It is quite difficult to obtain vesicles with neutral-charged amphiphilics under a salt solution environment. Usually, what is done in liposome formation is that a small percentage of charged-phospholipids (≥ 10 % mol) are used to create the thin film. In this way, after salt hydration, there exist an repulsions between lamellae and, as a result, liposomes can form at physiological salt concentrations(≈ 0.1 M)[31] and, if the repulsion is large enough, at higher (2 M)[32] salt concentrations.

So, in our case, the lack of a force which does not overcome the interbilayers adhesion may be the main cause of the inefficiency swelling using either water with/without sugars or salts.

3.3.5 "Additive in film" experiments

Based on studies on the efficient formation of vesicles using the gentle hydration method[33,34], a manner was determined to increase the interbilayer distances and as a result enhance vesicle formation. This approach consists of mixing an additive with the polymer aqueous solution before inkjet printing the sample. In this way, after microdrops deposition over the glass slide, the additive will be within the film. Then, addition of water to the samples will generate bilayers and eventually spherical giant vesicles. The additives used in these experiments were NaI, NaH_2PO_4 and glucose which were mixed with the viscous block copolymer at different molar concentrations.

The first case of "additive in a film" was the mixture of NaI with polymer at a molar concentration of 1:1 and with a final polymer concentration in water of 5 %(w/w) for inkjet printing, i.e. 5 %w/w $E_{16}B_{22}$(1)-NaI(1). The results are shown in Figure 15(A) and (B). In these microphotographs, one can observe hemispherical vesicles still embedded into the polymer substrate after 2 hrs hydration. Although the water exposure time was not particularly long, it can be suggestted that most of the NaI entrapped within bilayers leaked into the solution and there should not be further membrane growing. Therefore, the main cause of inefficient formation of polymersomes is the low molar ratio. Basically, at low amounts of NaI, there was no improvement in vesicle formation with respect to water or glucose addition since vesicles are still attached to the substrate. Increasing molar ratio to 1:10 ($E_{16}B_{22}$/NaI), one can observe completly formed polymersomes around the polymer substrate after 2 hrs of hydration (Figure 15(C-D)). However, the yield is quite low, i.e. most microdrops did not present sings of any vesicles formation.

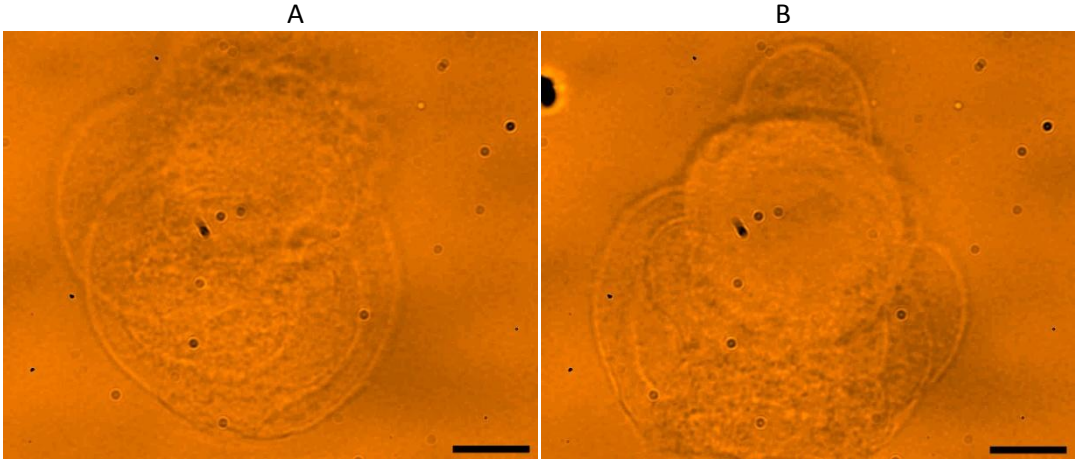

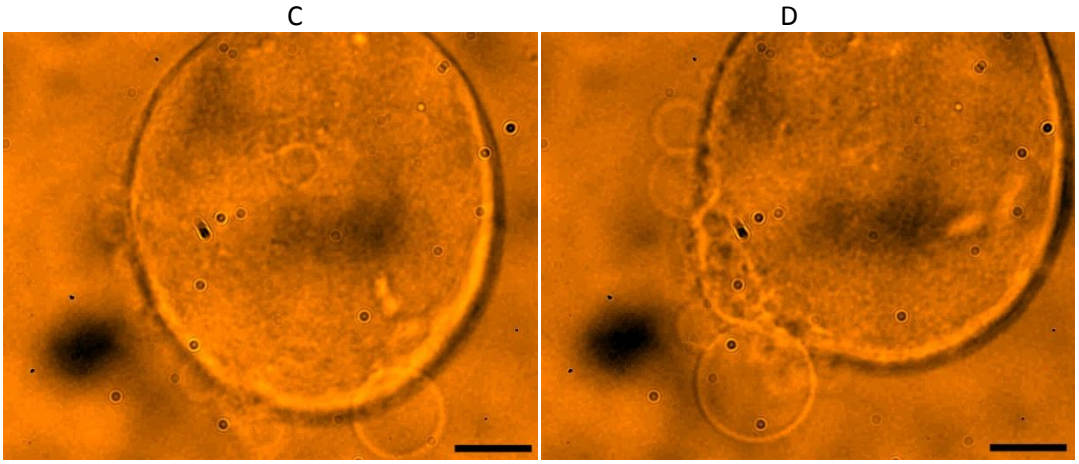

Figure 15. Polymer films contained different concentrations of NaI ("Additive in film"). Microphotographs (A) and (B) represent microdrops which were prepared with a molar ratio polymer/salt of 1:1 (5 %(w/w) EB(1)-NaI(1)) and (C) and (D) correspond to a molar ratio of 1:10 (5 %(w/w) EB(1)-NaI(10)) after 2 hrs of addition of water. The scale bar is 10 µm.

A change in the type of salt can improve substantially the bilayer separation in the polymer film. The additon of NaH_2PO_4 to the polymer solution at a molar ratio of 1:10, i.e. 5 %w/w EB(1)-NaH_2PO_4(10), enhances both the vesicle production and sizes after 2 hrs of water addition, as can be seen in Figure 16(A-C). Also for the first time in experiments, vesicles unbound from the polymer substrate. This makes it easier to collect them using a micropipette. In general, it can be observed many vesicles of small diameters (D_v < 10 µm) and some large vesicles such as in Figure 16(C) with a sizes of 33.9 µm. Specially, these sizes of vesicles are suitable for MPA experiments since are large and are loosely attached to the polymer dots.

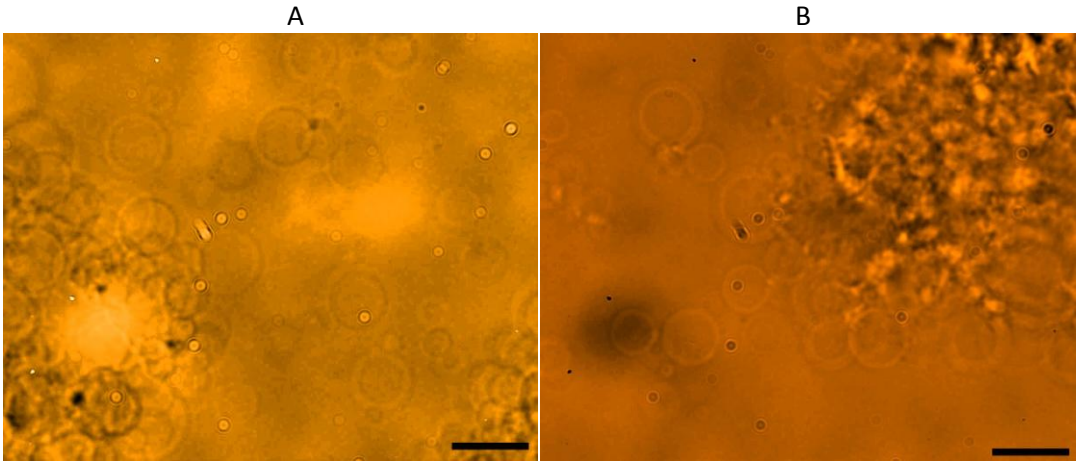

C

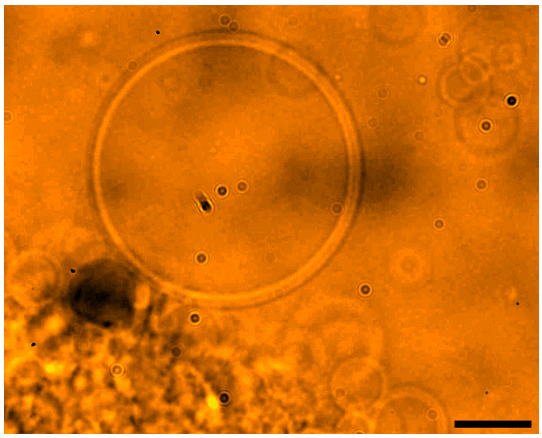

Figure 16. Polymer films prepared with a molar ratio polymer/salt of 1:10 using a 5 %(w/w) EB(1)-NaH2PO4 (10) samples after 2 hrs of addition of water. The scale bar is 10 µm.

Similar resuts can be obtained using glucose instead of NaH_2PO_4 in molar rations of 1:10 and 1:20, i.e. 5 %w/w $E_{16}B_{22}$(1)-Glucose(10) and 5 %w/w $E_{16}B_{22}$(1)-Glucose(20) respectively. In the case of 5 %w/w EB(1)-Glucose(10) samples, the evolution of vesicles was monitored through time. So, just after 5 minutes of water hydration, some vesicles are relative big and spherical and continue to grow over time. For example, it was noticed a vesicle of a size of 15.2 µm (indicated by an arrow) together with others small vesicles around (Figure 17(A)). This vesicle continue to grow from 15.3 µm to 24.6 µm (Figure 17(B)) after 2 hrs. Another charateristic in these experiments was vesicle unbinding from the polymer substrate (Figure 17(C)). It was observed that these unbiding vesicles are bigger than vesicle using a sample of 5%w/w EB(1)-NaH_2PO_4(10) (Figure 16(A-B)). Also, after 20 hrs of hydration, an inspection of the sample provides evidence that the vesicle sizes did not change considerably with respect to short times. For instance, the polymersome size in Figure 17(D) is 30.5 µm, after 20 hrs of water hydration, which did not vary significantly after 2 hrs (Figure 17(B)). It appears that in a time of 2-3 hrs most of the glucose leaks out of the vesicle, i.e. sugar diffusivity throughout time, and, then, the vesicle size stabilizes. At higher molar ratio, i.e. 5 %w/w $E_{16}B_{22}$(1)-Glucose(20), vesicles yield was improved and sizes were increased. For example, after 3 hrs of water hydration, Figure 17(E-F) presents a great number of vesicles with sizes between 5-15 µm which in turn are "entrapped" in big vesicles with diameters of 45.7 and 46.7 µm respectively. Roughly speaking, at the same molar ratio and hydration times, bigger vesicles were observed using glucose than NaH_2PO_4 but higher yields using NaH_2PO_4 than glucose. This may be caused by the difference in osmotic pressures among sugar and the salt.

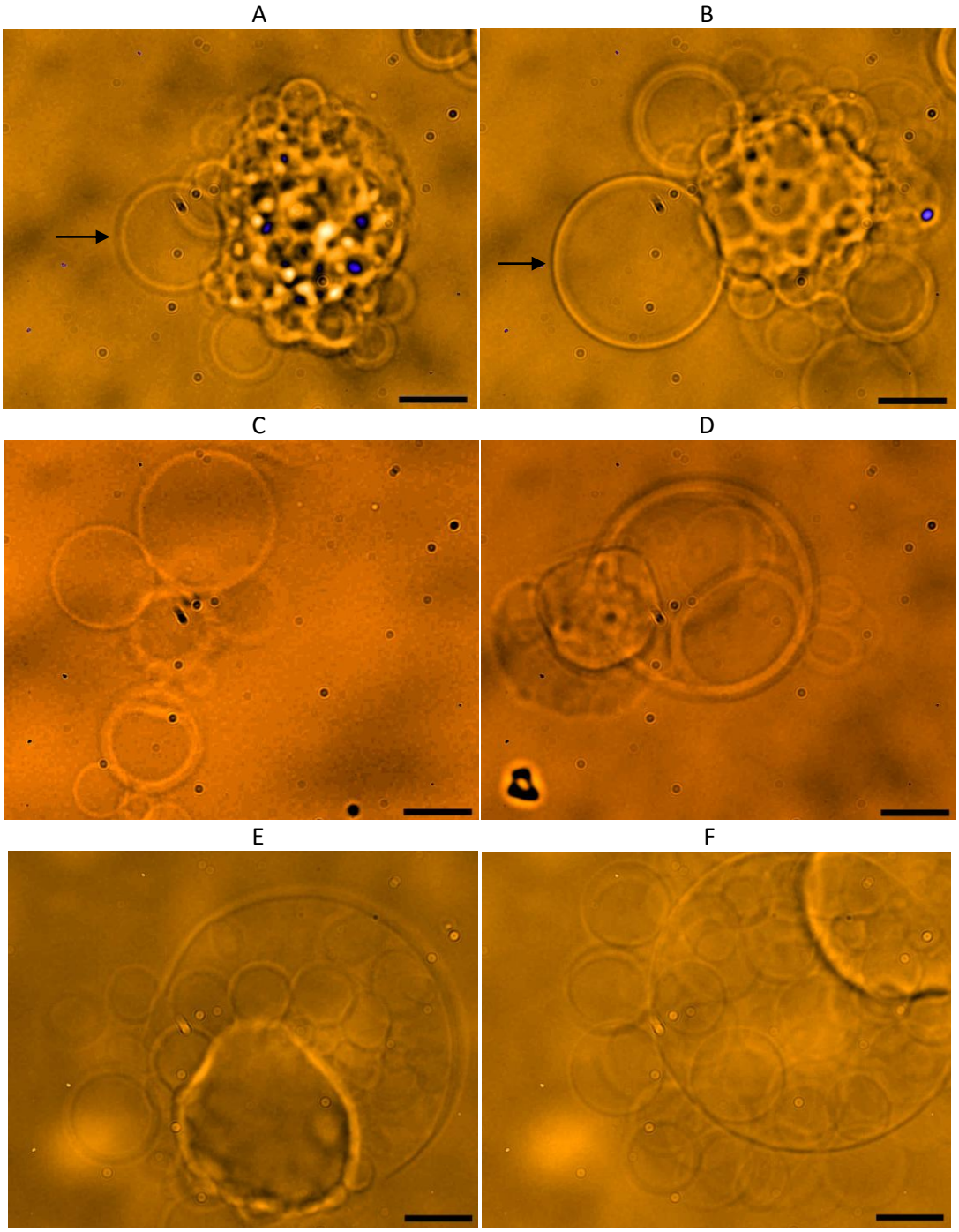

Figure 17. Polymer substrate prepared with 5 %w/w $E_{16}B_{22}$(1)-Glucose (10) (A-D) and 5 %w/w $E_{16}B_{22}$(1)-Glucose(20) (E-F) samples. At a molar ratio of 1:10 (polymer/glucose), different microphotographs were taken at different water hydration times: 5 min (A), 2 hrs (B), 3 hrs (C) and 20 hrs (D), 3 hrs (E) and 3hrs (F). The scale bar is 10 µm.

The number of polymersomes can be reduced if the polymer concentration is also reduced. For example, at a molar ratio of 1:20 ($E_{16}B_{22}$/Glucose) and decreasing the content of polymer in water from 5 %(w/w) to 3 %(w/w), polymersomes decreased in number (Figure 18(A-B)). So, according

with this result, the amount of polymer deposited over the glass slide partially control the number of vesicles. Together with the type of substace within the film. Also, it is interesting to notice that nonetheless the glucose content into the film was relative high (1:20), most polymersomes exhibit hemispherical shape and strong attachement to the substrate. In this case, glucose did not exert a great effect in interbilayer separation in comparison with 5 %w/w EB(1)-Glucose(20) samples. However, this results should be taken with caution since it has been noticed in several experiments that inkjet-printed samples used after several weeks of preparation decrease the quality and yield of vesicles. Thus, this implies that glucose degraded into the film and this explain the poor swelling behaviour into the film in these experiments.

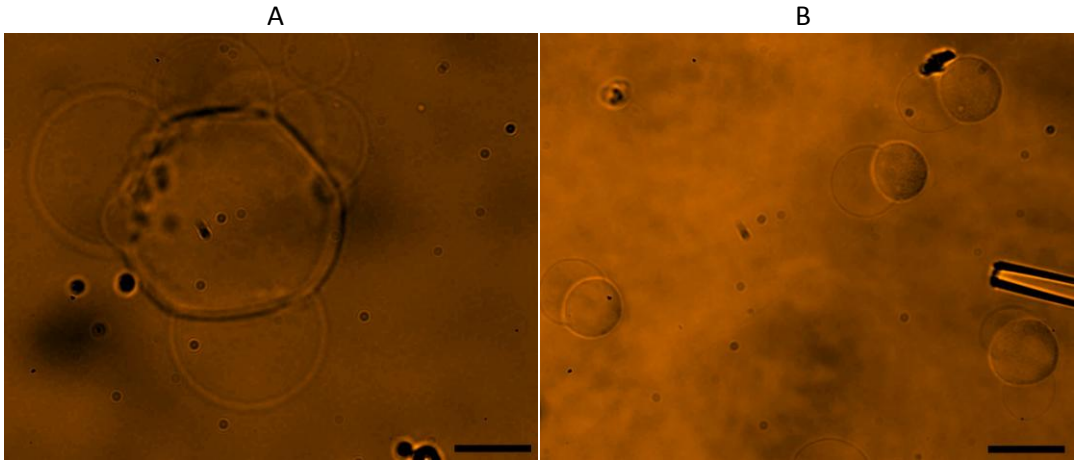

Figure 18. Polymer substrate prepared with 3 %w/w $E_{16}B_{22}$(1)-Glucose (20). Microphotograph (A) was taken with an objective of 60x and (B) with an objective of 20x. The scale bar is 10 µm in (A) and 30 µm in (B).

3.3.6 Effect of different salt environments on "additive in film" samples

The purpose in these series of experiments was to study the feasibility of polymersomes formation, via the "additive in film" method, under either hydrating or re-hydrating with different type of salts and concentrations. Most of the experiments were conducted using 5 %w/w $E_{16}B_{22}$(1)-Glucose(20) samples and some using $E_{16}B_{22}$(1)-NaH_2PO_4(10) samples. The importance of vesicle formation under salt conditions lies in the possibility of create prototypes of cell-like structures or polymersomes as microreactors under salt conditions.

In this sequence of tests, 0.1 M NaH_2PO_4, 0.1 M NaBr and 0.1 M NaI were used to hydrate 5 %w/w EB(1)-Glucose(20) samples after a time of 12 hrs. Figure 19(A) was hydrated with 0.1 M NaH_2PO_4. In this image, one can observe what seems to be bilayer(s) pulled off from the substrate. This image is quite similar with membranes of Figure 14(B) but even more deformed. Similar results can be observed when employed 0.1 M NaBr (Figure 19(B)). According with the overall picture of

deformations in images, the flexibility along the membrane changed, varying more drastically for NaH_2PO_4 than NaBr. So, it seems that salts affected the bilayer flexibility, i.e. bending rigidity, since such parameter indicates the weak forces required to bend a bilayer and form a curvature structure. At 0.1 M NaI, the quality of swelling behaviour decrease dramatically. In this sample, most polymer microdrops were not affected by the salt and, some of them, formed small membrane protrusions (Figure 19(E)). Therefore, complete formation of vesicles are not possible at 0.1 M of NaH_2PO_4, NaBr and NaI. These results are similar than the addition of salt solutios to the polymer substrate without glucose. It is interesting to notice that the addition of NaH_2PO_4 affected substantially the flexibility of bilayers in samples without/with glucose (Figures 14(B) and (E) and Figure 19(A), respectively) but, at the same time NaH_2PO_4 promote certain degree of swelling which is maximized when the salt was into the film (Figure 16(A-C)), whereas NaI has a very poor effectiveness on swelling bilayers (Figure 15(A-D) and Figure 19(C)) if compared with NaH_2PO_4 at the same conditions.

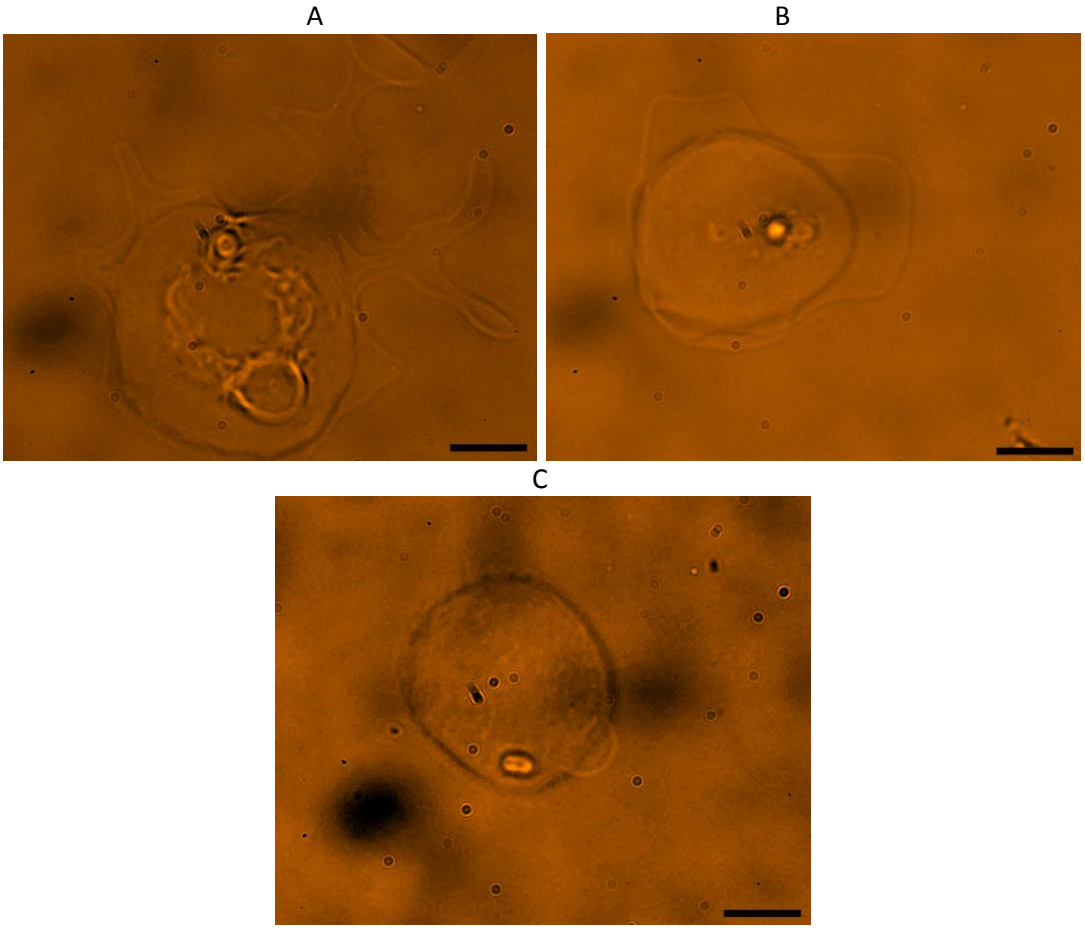

Figure 19. Polymer films prepared from a 5 %w/w EB(1)-Glucose(20) sample. After microdrops deposition over the glass slide, different salts were used to hydrate: 0.1 M NaH2PO4 (A), 0.1 M NaBr (B), and 0.1 NaI (D). These microphotographs were taken after a total hydration time of 12 hrs. The scale bar is 10 µm.

At even lower concentrations, the hydration with 0.01 M of either NaH_2PO_4 or NaI to the inkjet-printed sample prevented vesicle growing, Figure 20(A-B) respectively (3 hrs hydration). Alternatively, samples can be hydrated using water and then rehydrated using salt solutions. In this case, detachment of polymer substrate usually occurred since the first addition of water swollen and eventually loosen the microdrops from the glass slide after a certain time. Then, the second addition of salt commonly separated part of the microdrop, avoiding a natural vesicle growing. However, some experiments can be analysed. Figure 20(C) shows 2 hrs of water hydration of $E_{16}B_{22}$(1)-NaH_2PO_4(10) and then addition of 0.1 M NaH_2PO_4 just some seconds after (Figure 20(D)). One can observe the immediate collapsing of vesicles after the addition of 0.1 M NaH_2PO_4 (Figure 20(D)). In this case, the salt solution maybe exerted a higher osmotic pressure over the spherical vesicles which subsequently deflated. So, ions entraped into the membrane was overcome by the osmotic pressure exerted with the salt solution. Similar results can be expected for glucose samples, i.e. 5 %w/w EB(1)-Glucose(10) and 5 %w/w EB(1)-Glucose(20). Moreover, after 3.5 hrs of water hydration and then addition of 0.01 M NaI to a sample of 5 %w/w EB(1)-Glucose(20), this salt seems did not affect the shape of polymersomes which were detached from the polymer substrate (Figure 20(E)) but caused a sort of shrink in polymersomes linked to the polymer microdrops (Figure 20(F)). Microphotographs of Figure 20(E-F) were taken after about one hour of salt addition. Therefore, it is expected that after a certain time bilayers attached to the polymer fragment in Figure 20(F) will be continue to grow.

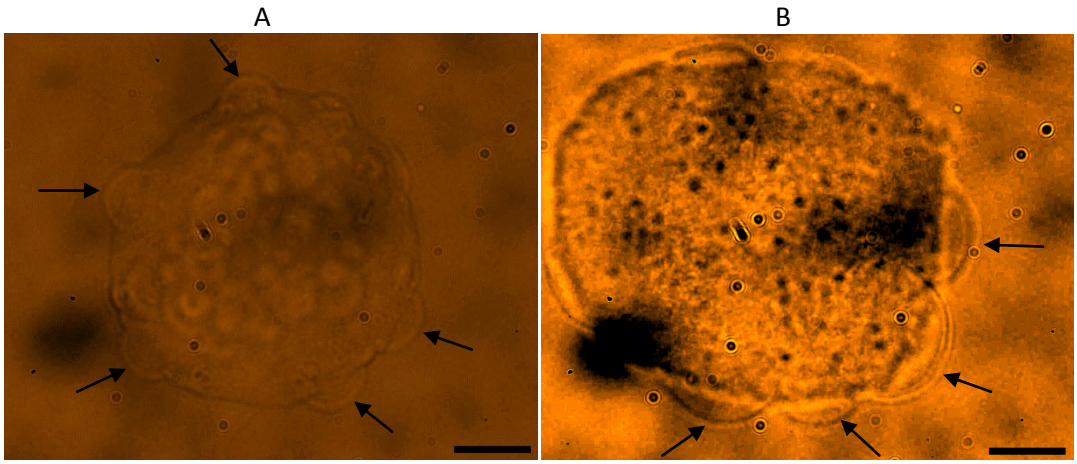

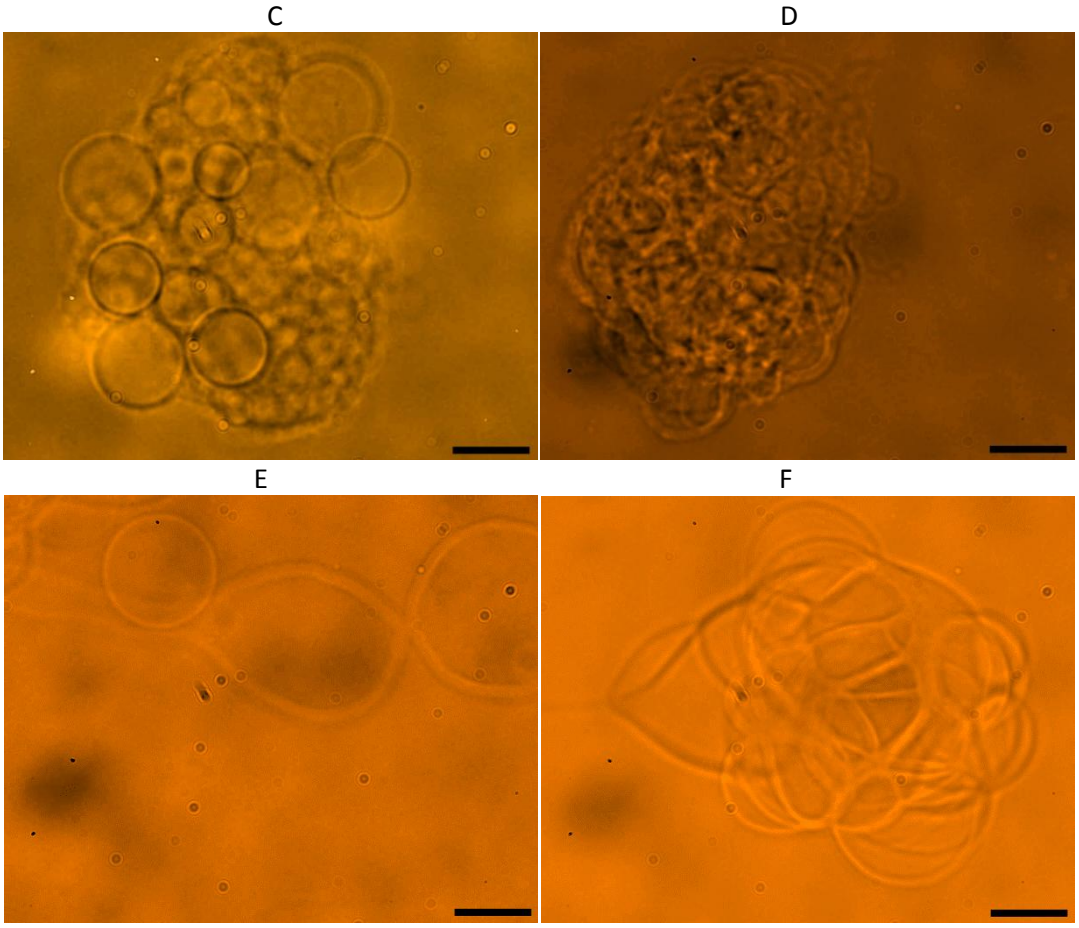

Figure 20. Polymer films prepared from a 5 %w/w EB(1)-Glucose(20) and $E_{16}B_{22}$(1)-NaH_2PO_4(10) samples. Microphotographs (A) and (B) represents the hydration of a sample of 5 %w/w EB(1)-Glucose(20) using 0.01 M of NaH2PO4 and 0.01 M NaI, respectively, after a time of 3 hrs. Then, (C) correspond to 2 hrs water hydration of a $E_{16}B_{22}$(1)-NaH_2PO_4(10) sample and (D) refers to a rehydration process using 0.1 M NaH_2PO_4. Finally, (E) and (F) represent 3.5 hrs hydration with water of a 5 %w/w EB(1)-Glucose(20) sample and then re-hydration using 0.01 M NaI. The scale bar is 10 µm.

3.3.7 Analysis of results

The hydration of inkjet-printed samples using water or different aqueous solutions such as sugars or salts revealed a lack of spherical formation of giant vesicles. Possible reasons of this problem may have been caused by some characteristics of the sample. For instance, the inkjet printing equipment is able to deposit microdrops which form individual disk films of about 30 µm of diameter and about 19 *µm* of thickness over a hydrophobic glass slide. In a similar study of vesicle preparation[9] using 5 %(w/w) $E_{16}B_{22}$ via a film hydration method and described in secction 3.1, the polymer bilayer thickness was some hundreds of nanometers since thin films are recommend for vesicle formation[35]. Apparently what happened in this series of experiments was that the disk films were thick and dense

which avoided deep hydration[35] than would occur using a much thinner film. So, the aqueous solutions used to hydrate the sample did not provoke sufficient bilayer separation required for vesicle formation. This was in part because the hydration forces partially overcame the interbilayers adhesiveness. This in turn reflected the poor swelling behaviour in the sample since vesicles were still embeded into the polymer substrate. The polymer aqueous concentration and the hydrophobic surface used for inkjet printing should influence in the disk-film thickness. In the first case, a relative high concentration of polymer (5 %(w/w)) was used and, in the second case, microdrops (polymer/water) deposited over a hydrophobic surface leaves thick films since there is a high contact angle between the solvent and the glass surface[29].

Also, the hydration process is important. For example, vesicles sucessfully prepared via the gentle hydration method, a polymer or phosholipid film covers a much greater area of the glass where the film is deposited, i.e. covers all the surface base of the recipient, than using the inkjet printing method. In this way, when a solution is added to the large film, the hydration, begining in a top-down direction. In the present experiments, since the film is enclosed in a disk-like form, water or any other aqueous solution hydrates the bottom bilayer at approximatly the same time than the top. So, the hydration forces cannot per se overcome the compactness of the microdrop since the bottom layers cannot swell before the top layers. This can derive, the entire drop to be removed and a lack of vesicle formation.

The addition of eitheir sugars or salts into the polymer film promoted spherical-shape giant vesicles which is a way to help bilayer separation in the lamellar structure. A possible explanation of the efficient swelling of these samples can be explained in the following way. Consider a lamellae structure as in Figure 11 after sample deposition over the surface, molecules of the additive possibly held between bilayers. Then, hydration with water begins to dissolve the additive molecules and form an excess with respect to the exterior. This provokes a difference in osmotic pressure and induces more water to coming into lamellae spaces which eventually separate and form vesicles. Thus, the additive provides an artificial repulsion between bilayers that drastically changed the swelling film efficiency. According with present experiments, the molar ratio concentration between polymer/additive should be at least 1:10 in order to form spherical vesicles. The type of additive within the film also influenced the vesicle development. Better results were shown using either NaH_2PO_4 or glucose instead of NaI when comparing the same molar ratios.

References

1. M. L. Longo and V. L. Hung, in *Methods in Membrane Lipids*, ed. A. M. Dopico, Humana Press Inc, Totowa, NJ, 2007, pp. 421–437.

2. V. Heinrich and W. Rawicz, *Langmuir*, 2005, **21**, 1962–1971.

3. R. Kwok and E. Evans, *Biophys. J.*, 1981, **35**, 637–652.

4. J.-Y. Shao and J. Xu, *J. Biomech. Eng.*, 2002, **124**, 388–396.

5. J. Heuvingh, F. Pincet, and S. Cribier, *Eur. Phys. J. E. Soft Matter*, 2004, **14**, 269–276.

6. J. Lehn, R. Lipowsky, C. K. Haluska, K. A. Riske, and R. Dimova, *Proc. Natl. Acad. Sci. U. S. A.*, 2006, **103**, 15841–15846.

7. F. M. Menger and S. J. Lee, *Langmuir*, 1995, **11**, 3685–3689.

8. T. Tanaka and M. Yamazaki, *Langmuir*, 2004, **20**, 5160–5164.

9. J. R. Howse, R. A. L. Jones, G. Battaglia, R. E. Ducker, G. J. Leggett, and A. J. Ryan, *Nat. Mater.*, 2009, **8**, 507–511.

10. G. Battaglia and A. J. Ryan, *J. Am. Chem. Soc.*, 2005, **127**, 8757–8764.

11. G. Battaglia and A. J. Ryan, *J. Phys. Chem. B*, 2006, **110**, 10272–10279.

12. G. Battaglia and A. J. Ryan, *Macromolecules*, 2006, **39**, 798–805.

13. G. Battaglia, A. J. Ryan, and S. Tomas, *Langmuir*, 2006, **22**, 4910–4913.

14. D. T. W. Toolan and J. R. Howse, *J. Mater. Chem. C*, 2013, **1**, 603–616.

15. N. Sahu, B. Parija, and S. Panigrahi, *Indian J. Phys.*, 2009, **83**, 493–502.

16. *Microdispensing in http://www.microfab.com*, Retrieved on August 28, 2013.

17. *http://www.microdrop.de/microdrop.html*, Retrieved on August 28, 2013.

18. *Man. Ink-Jet microdispensing, a basic set-up http//www.microfab.com*, Retrieved on August 29, 2013.

19. D. Wallace, D. Hayes, T. Chen, V. Shah, D. Radulescu, P. Cooley, K. Wachtler, and A. Nallani, *Ink-jet as a MEMS manufacturing tool*, .

20. D. D. Lasic, *Biochem. J.*, 1988, **256**, 1–11.

21. G. Battaglia and A. J. Ryan, *Nat. Mater.*, 2005, **4**, 869–876.

22. B. Nasseri and A. Fasciolo, *J. Drug Target.*, 2005, **13**, 471–477.

23. S. Mai, J. P. A. Fairclough, K. Viras, P. A. Gorry, I. W. Hamley, A. J. Ryan, and C. Booth, *Macromolecules*, 1997, **30**, 8392–8400.

24. A. Laouini, C. Jaafar-Maalej, I. Limayem-Blouza, S. Sfar, C. Charcosset, and H. Fessi, *J. Colloid Sci. Biotechnol.*, 2012, **1**, 147–168.

25. K. Akashi, H. Miyata, H. Itoh, and K. J. Kinosita, *Biophys. J.*, 1996, **71**, 3242–3250.

26. *http://mit.edu/sjiang2/www/Resources/Prepare%20Lipid%20Vesicles.pdf*, Retrieved on Sep.17, 2012.

27. R. Dimova, S. Aranda, N. Bezlyepkina, V. Nikolov, K. a Riske, and R. Lipowsky, *J. Phys. Condens. matter*, 2006, **18**, S1151–S1176.

28. D. E. Discher and A. Eisenberg, *Science (80-.).*, 2002, **297**, 967–973.

29. D. Needham and E. Evans, *Biochemistry*, 1988, **27**, 8261–8269.

30. H. Bermudez, A. K. Brannan, D. A. Hammer, F. S. Bates, and D. E. Discher, *Macromolecules*, 2002, **35**, 8203–8208.

31. N. F. Morales-Penningston, J. Wu, E. R. Farkas, S. L. Goh, T. M. Konyakhina, J. Y. Zheng, W. W. Webb, and G. W. Feigenson, *Biochim. Biophys. Acta*, 2010, **1798**, 1324–1332.

32. Y. Yamashita, M. Oka, T. Tanaka, and M. Yamazaki, *Biochim. Biophys. Acta*, 2002, **1561**, 129–134.

33. K. Tsumoto, H. Matsuo, M. Tomita, and T. Yoshimura, *Colloids Surf. B. Biointerfaces*, 2009, **68**, 98–105.

34. N. L. Yamada, M. Hishida, H. Seto, K. Tsumoto, and T. Yoshimura, *Europhys. Lett.*, 2007, **80**, 48002–p1(6).

35. F. J. Szoka and D. Papahadjopoulos, *Annu. Rev. Biophys. Bioeng.*, 1980, **9**, 467–508.

Chapter 4: The MPA technique and the mechanical properties of $E_{16}B_{22}$ giant polymersomes

4.1 Introduction: Membrane elasticity in MPA experiments

The micropipette aspiration (MPA) technique is a widely used methodology to measure the mechanical properties of liposomes, polymersomes and cells. This technique consists on capturing a giant vesicle or biological membrane (with sizes between 10-100 μm) using a small glass capillary (commonly called a micropipette with a diameter between 1-10 μm) and exerting a stepwise increment in the suction pressure, e.g. 1-2000 Pa, over the membrane which causes a protrusion into the glass tube. The data fitting of tension versus area strain at low and high pressure provides the bending modulus, k_C, and the area expansion modulus, K_A, respectively. The tension can be calculated from the pressure exerted over the membrane and the area strain can be estimated from the effect of the pressure on the geometrical properties of vesicles or cells. Other mechanical parameters that can be quantified using MPA are lysis tension[1], shear surface viscosity[2], cell adhesion strength[3], elastic shear modulus[4] and interlayer friction[5]. Moreover, with a slightly modification in the methodology, the MPA technique can be used to conduct experiments such as fusion studies[6], membrane-shape modification (e.g. oligovesicular[7] and tether formation[8]), and used to perform microreactions in vesicles, when the MPA technique is used in parallel with a microinjection equipment[9].

The deformation analysis of natural and synthetic membranes can be described using basic mechanics and taking into account the change in the overall geometry of the bilayer throughout different steps in the suction process. This elasticity can be illustrated considering giant vesicles in terms of the liquid-drop model[10]: an encapsulated fluid with a very thin bilayer, which behaves according to Newton's laws, with uniform surface tension over the whole enclosed system, and without any resistance to flow into the micropipette.

Figure 1*(A)* depicts the different forces that can act over a giant vesicle. These forces are: the internal (P_i) and external (P_o) pressures which operate over a surface area, and the water surface tension ($\boldsymbol{\sigma}$) that acts along the membrane circumference. The analysis of these three forces over a vesicle can be better described by cutting the vesicle in half. So, in such a system *(Figure 1(B))*, two equivalent opposite forces in equilibrium with each other can be indentified[10]. The first force pushes

the membrane outwards as the result of a gradient in pressures, i.e. $P_i > P_o$, depends on the area [11] and can be represented as: $F_p = (P_i - P_o)\pi R^2$, where R is the radius of the vesicle[10]. The second force, which is of the same magnitude as F_p, pushes the bilayer inwards due to membrane surface tension and depends on the circumference length[11]. Its algebraic relation is $F_t = \sigma 2\pi R$, where $2\pi R$ is the circumference where the surface tension is developed[10].

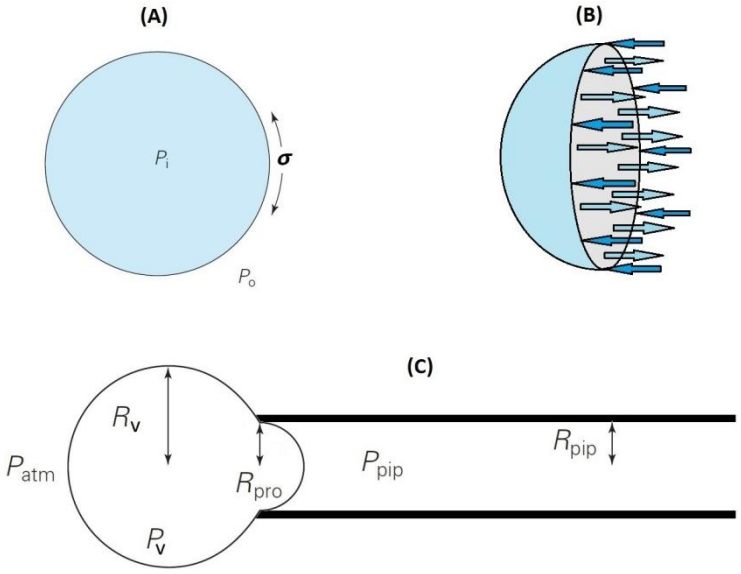

Figure 1. Diagrams of forces acting over a vesicle. The forces which interact with a spherical enclosed bilayer are internal and external pressures, P_i and P_o respectively, as well as the surface tension σ (A). A vesicle cut in half is equilibrated by P_i, P_o and σ forces (B). A vesicle aspirated into a micropipette with the parameters that define the MPA process (C). Where P_{atm} is the atmospheric pressure, P_v is the vesicle pressure, R_v is the radius of the vesicle, R_{pro} is the radius of the vesicle protrusion, P_{pip} is the pipette pressure and R_{pip} is the pipette radius.

According with Newton's second law, the two forces of pressure and surface tension are equal, $F_p = F_t$, and, consequently, this leads to the Laplace equation[10]: $P_i - P_o = 2\sigma/R$. So, applying the Laplace law to a giant vesicle, the hydrostatic surface tension exerted over a spherical closed bilayer is proportional to the gradient in pressures that exists among the membrane and to the specific radius of the vesicle[10].

The parameters that define the evolution of elastic forces in a micropipette aspiration experiment are illustrated in Figure 1(C), where P_{atm} is the atmospheric pressure, P_v is the pressure within the vesicle, R_v is the vesicle radius, R_{pro} is the radius of the part of the vesicle inside the micropipette or protrusion radius, P_{pip} is the suction pressure and R_{pip} is the pipette radius. Thus, according with Laplace and considering a homogenous surface-tension (σ) along the whole membrane, two

equations that describe both the outside vesicle tension; $P_v - P_{atm} = \frac{2\sigma}{R_v}$, and inside micropipette tension, $P_v - P_{pip} = \frac{2\sigma}{R_{pro}}$, can be derived. In Figure 1(C), shows that the radius of the protrusion is equal to the radius of the micropipette. So, combining the last two equations, considering $R_{pro} = R_{pip}$, and solving for σ:

$$P_{atm} - P_{pip} = \Delta P = 2\sigma\left(\frac{1}{R_{pip}} - \frac{1}{Rv}\right) \quad (1)$$

And finally:

$$\sigma = \frac{\Delta \mathrm{P}\, R_{\mathrm{pip}}}{2\left(1 - \frac{R_{\mathrm{pip}}}{R_v}\right)} \quad (2)$$

The above equation is used to calculate the membrane tension in MPA experiments. R_{pip} and R_v can be measured by optical microscopy and ΔP from the difference in height of water in a water reservoir system. Such system exerts a suction pressure over the membrane according with the following equation:

$$P = \Delta h\, \rho\, g \quad (3)$$

Where Δh is difference in height in the water reservoir, ρ is the density of the fluid (i.e. water, 1000 kg/m^3) used to exert the pressure and g is the gravitational acceleration, which is a physical constant (i.e. 9.8 m/s^2).

Another important parameter which describes the system and needs to be calculated in MPA experiments is the area strain (α), also known as the relative area change of the membrane or apparent area expansion or relative area dilation. Based on purely geometrical factors, and considering the volume of the vesicle as constant and total surface area as variable[12], the change in membrane area (ΔA) to a zero membrane deformation ($A_o = 4\pi R_v^2$) can be estimated using the following expression[13]:

$$\alpha = \frac{\Delta A}{A_o} = \frac{A - A_o}{A_o} = \frac{2\pi R_{pip}\Delta L}{A_o}\left(1 - \frac{R_{pip}}{R_v}\right) \quad (4)$$

Where ΔL is the increment of the projection length of a giant vesicle inside the glass capillary tip. The change of ΔL (with respect to a pressure reference) provides the means to measure the change in the total membrane area[14] and hence the area strain.

The fundamental elastic modes of deformation in a fluid bilayer, i.e. bending and stretching, are calculated by basically specifying σ and α. The mechanical parameter estimated in this research work was the area expansion modulus (K_A), also known as area compressibility, area elastic[15] or area stretch modulus[16]. K_A is determined by conducting a linear fitting of equation (5) at high tension regime (σ > 0.5 mN/m), where the slope of the graph σ vs α is the stretching modulus. K_a is commonly reported in units of mN/m or dyn/cm.

$$\sigma = K_a \alpha \quad (5)$$

A more refined calculation of K_A will introduce a factor of correction for thermal bending undulations since these persist at high tension[16]. This can be done by recalculating α via equations (6) and (7) and then carrying out a linear regression of α' vs σ which will provide a revised value for the stretching modulus[16], i.e. $K_{A,\,corr}$.

$$\alpha'(i) = \alpha(i) + \Delta\alpha(i) \quad (6)$$

$$\Delta\alpha(i) = -\left(\frac{k_B T}{8\pi k_c}\right) \log\left(\frac{\sigma(i)}{\sigma(1)}\right) \quad (7)$$

In equation (7), k_B is the Boltzman constant, T is the absolute temperature, k_c is the bending modulus and σ the membrane surface tension. Basically, equation (7) is a function of σ and takes into account the bending fluctuations of the membrane, through the term k_c. Equation (6) smoothes these undulations by adding a factor of correction ($\Delta\alpha(i)$) to a relative area dilation ($\alpha(i)$). In this way, the new area dilation, or direct area dilation ($\alpha'(i)$), considers each ith data pair of α and σ relative to an initial tension ($\sigma(1)$).

All giant vesicles in micropipette aspiration (MPA) experiments were made by a method of hydration which consisted of using a modify inkjet printer which deposits microdroplets of a polymer/glucose solution over a hydrophobic glass slide. This methodology was described in detail in chapter 3. Most of the MPA experiments were conducted in the University of Sheffield and a small number of experiments in the University of Exeter. In Sheffield, an automated MPA system was created by assembling, setting, programming and calibrating all the electric equipment thereby required. The use of MPA equipment in Exeter was necessary in order to collect some crucial data, i.e. the observation of the vesicle projection length into the micropipette, which could not be obtained in the University of Sheffield.

4.2 Methodology: MPA equipment in Sheffield

The MPA equipment used in the University of Sheffield is depicted in Figure 2 and, with greater detail, in Figure 3. Basically, it consists of an anti-vibration workstation *isolate system 2000* from *INTRACEL*, an *Olympus* inverted microscope model *IX71* equipped with bright-field and phase contrast microscopy, a B700 PixeLINK camera of 1.3 megapixels with a compatible version for LabVIEW Vision software, motorized and manual micromanipulators from *Sutter Instrument Company* models *MP-225* and *MP-33* respectively, and a homemade-automated pressure system. In addition to MPA experiments, this micropipette setup was also designed for conducting experiments of vesicle fusion in the future.

4.2.1 Pressure System

Such a system is divided into two mainly parts: the equipment that controls the water manometer height and the equipment that allows the recollection of pressure data.

In the first part, the water manometer is held using an aluminium bar with a rectangular plate as a base. The manometer is made of a water filled plastic tubing which one end is fixed at the top-side of the supporter structure and the other end is attached to a slide carriage (Figure 2). This furniture is mounted onto a threaded bar which when rotates the moving end upwards or downwards. The revolutions of the threaded bar are control by a stepper motor (*SM*) from *Danaher Motion* placed at the top of the holder. The interface between the *SM* and the personal computer (*PC*) is the stepper drive (*SD*) which allows running the *SM*. In our case, a High Performance Micro-Stepping Drive model *P70530* from *DANAHER MOTION PACIFIC SCIENTIFIC* was used. However, in order to have a functional automatic system, it was necessary to use *LabVIEW™* programming language. This software was created by National Instruments Corporation and is a powerful tool that allows the control of electric equipment and the measurement, processing and analysis of physical signals coming from a sensor. The interface between the SD from *DANAHER MOTION* and the *LabVIEW™* software from National Instruments is the *NI-9512* stepper drive interface module and the *NI-compactRIO-9073* real time controller. These two hardware components permit to control the *SM* and give access to programming in *LabVIEW™*. It should be mentioned that one of the main difficulties in running the *SM* using LabVIEW™ 2010 was found the software compatibility of National Instruments with *DANAHER MOTION*. Although the proper hardware was used, several software patches and drivers were needed in order to cover a number of errors in the software LabVIEW™ 2010. The required patches and drivers will depend on the LabVIEW and *NI-cRIO* versions. In the case of LabVIEW™ 2010, the recommended software is: 2010sp1-Real Time Engine,

NI LabVIEW 2010 sp1, NI LabVIEW 2010 Real Time Module, NI-RIO 3.2.0 or later, LabVIEW NI SoftMotion Module 2010, and LabVIEW 2010 sp1 NI softmotion module.

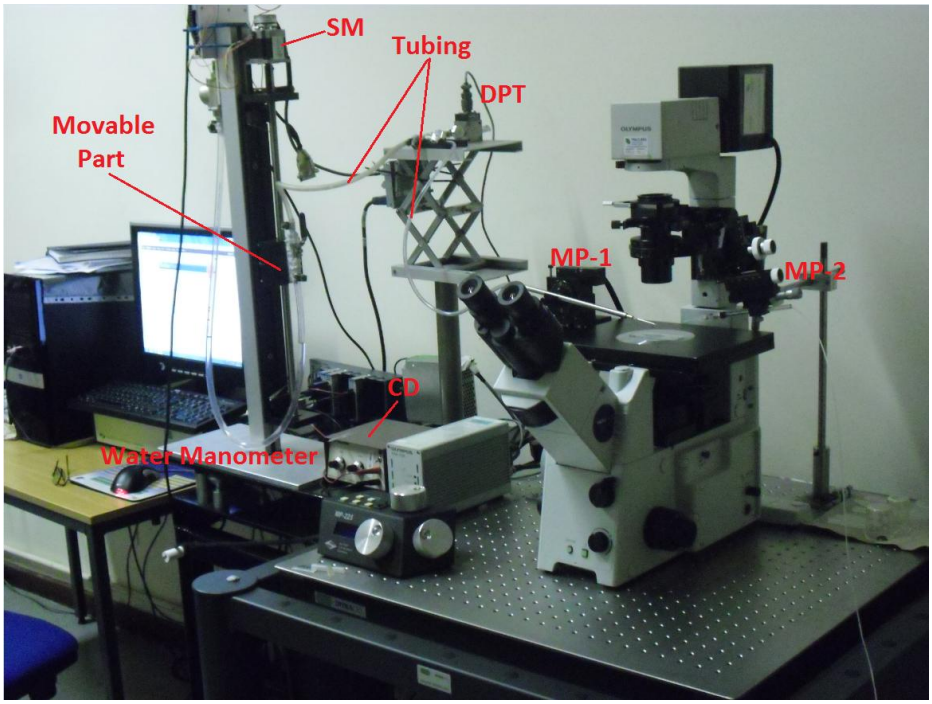

Figure 2. MPA equipment in Sheffield. The main parts of this equipment consist of a optical microscope, an active antivibration table, automated (MP-1) and manual (MP-2) micromanipulators, a water manometer with a movable part, a stepper motor (SM) and signal conditioning in the form of a carrier demodulator (CD).

In the second section of the pressure system, the water manometer is connected to a differential pressure transducer (*DPT*) and micropipette holder using different plastic tubing diameters (Figure 2 and 3). In this way, a change in water height exerts a pressure along the plastic tubing whose ends include the *DPT* and the micropipette (Figure 3). Both pressures should be similar because the system is hermetic seal and the sensor is near to the micropipette. The equipment and hardware used in measuring and processing the pressure signal will be described in the following way. Firstly, the *DPT* (model *DP15-32* from *Validyne*) detects a mechanical force and transforms it into an electrical signal. This signal passes through a carrier demodulator (model no. *CD15-C-1-A-1* from *Validyne Engineering*), which main task is to filter the noise, and then sends the signal to both a data acquisition device (*NI-9215*) and real time controller (*NI-cRIO-9073*) and finally to the *PC*.

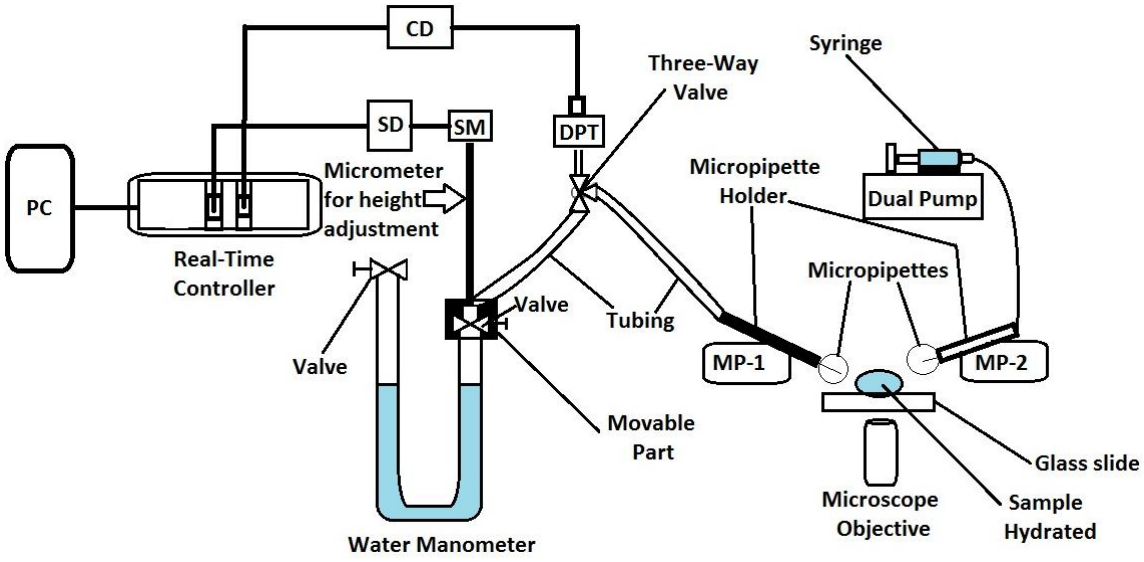

Figure 3. Equipment and experimental set-up of MPA experiments. The labels in this diagram are: MP-1= automated micromanipulator, MP-2= manual micromanipulator, DPT= differential pressure transducer, CD= carrier demodulator, SM= stepper motor, SD= stepper drive and PC= personal computer. Briefly, a height difference in the water monomer causes a change in pressure that can be used to aspirate vesicles into the micropipette. The program LabVIEW is used to control water height, by means of the SM and SD, and process pressure data, via DPT and CD. MP-1 is used to pick up giant vesicles and MP-2 is used to hydrate the sample using a syringe and controlled by a dual pump.

The next table summarised all the equipment used to control the pressure system.

Equipment	Model and Manufacturer	Function
Stepper Motor	T21NRLH-LDN-NS-00 (Pacific Scientific T-series)	Move the water reservoir
Stepper Drive	P70530 (Danaher Motion)	Connectivity Accessory
Stepper Drive Interface Module	NI-9512 (National Instruments)	Connectivity Accessory
Differential Pressure Transducer	DP15-32 (Validyne)	Transducer
Carrier Demodulator	CD15-C-1-A-1 (Validyne)	Signal Conditioning
Analog Input Module	NI-9215 (National Instruments)	Data Acquisition Device
Real-Time Controller	NI-CompactRIO-*9073* (National Instruments)	Connectivity Accessory

4.2.2 The LabVIEW program and the pressure system calibration

The LabVIEW code, also called virtual instrument (VI), that controls the pressure system is shown in Figure 4. The top box controls the movable part of the manometer in the VI with the following four input variables: *Position, Velocity, Acceleration and Acceleration Jerk*. The *Position* indicates the number of steps or counts of the SM, (200 steps equal one revolution). For example, for a target position of 5 000, the SM moves vertically about one centimetre from a zero position. The others parameters control the *Velocity, Acceleration and Acceleration Jerk* of the SM. The bottom box in Figure 3 collects voltage data from the DPT and, then, transforms voltage into pressure using the calibration equation of the manometer and presents this data into a graph of *Pressure* (Pa) vs *Time* (ms). Moreover, this program has two subroutines that average voltage and pressure measurements with the purpose of further reducing the noise of the DPT. For a complete explanation of the specific function of each icon see the National Instrument web page.

The calibration equation of the manometer was made with the help of a cathetometer. This instrument consists of a sliding telescope attached on a half millimetre Vernier graduated vertical bar. To improve the measuring accuracy, the metallic graduate bar is mounted on a tripod base which has a small circular spirit level and, also, the bar is fitted with a 0.01 mm precision vernier scale. Moreover, the telescope lens has a cross-hair mark inside which facilitates measurement of the water level in the manometer. In the pressure system calibration, the water reservoir was elevated in the range of 0-80 000 *Position* and the difference in heights and voltage were recorded every 10 000 *Position*, i.e. steps of about 2.280 cm. Then, the pressure was calculated using equation (3). All this process was repeated two more times. Finally, average values of voltage and pressure were plotted obtaining a straight line which equation was used to transform voltage to pressure. The general characteristics of the pressure systems can be summarized in the following way: working distance: 0-18.7 cm, *position* working distance: 0-80 000 and maximum suction pressure: about 1840 Pa. The uncertainties in the pressure system was determined by calculating the standard error (S.E.), S.E.= ±6.6 Pa, based on taking 5 measurements of data pressure every centimetre along the 18.7 cm total vertical length.

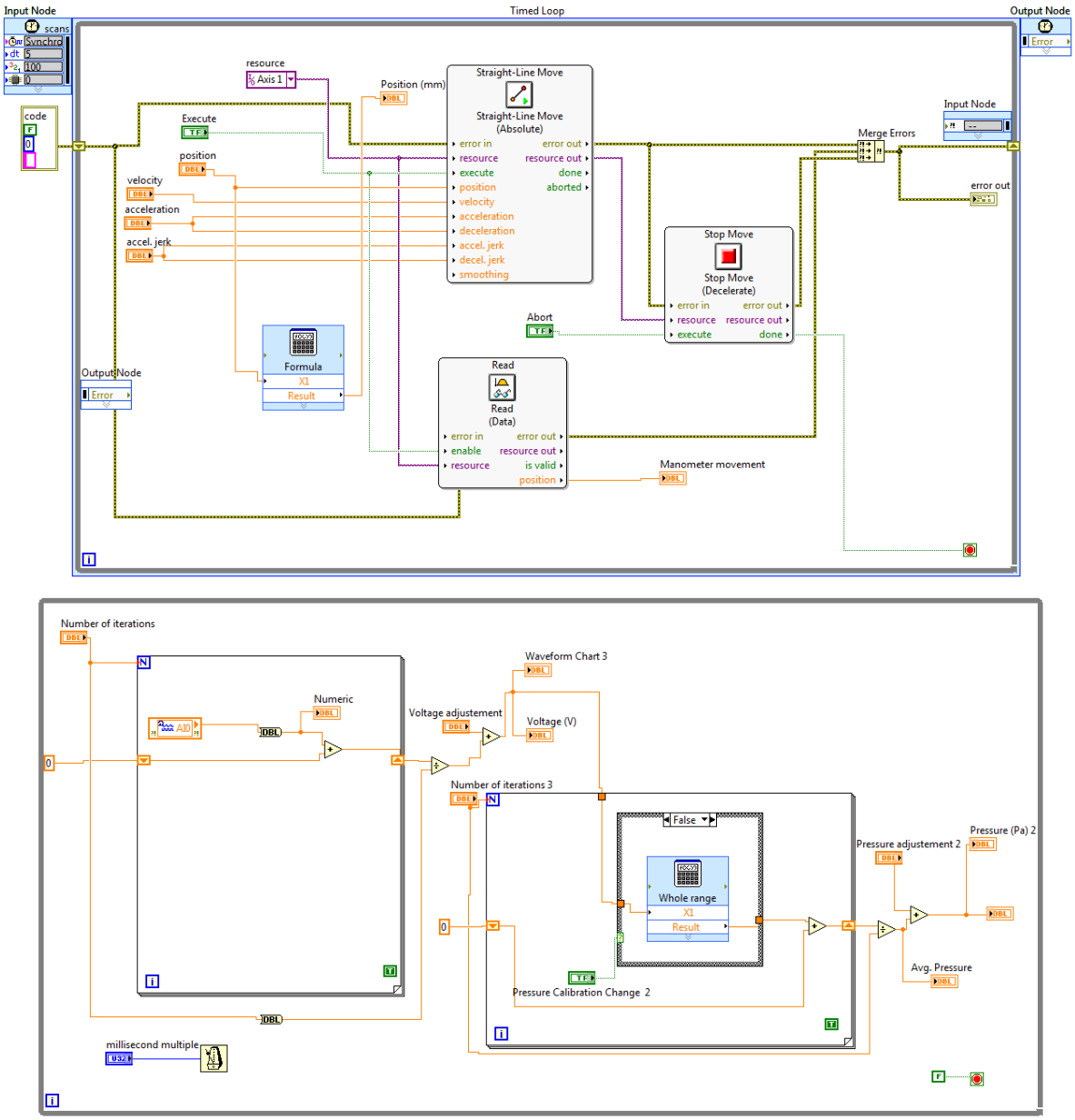

Figure 4. Block Diagram which controls the pressure system in MPA experiments. The top box controls the water column and the bottom box collect the pressure data. For a detail description of the function of each icon, consult the National Instrument web page.

4.2.3 Glass micropipettes elaboration

Micropipettes were made using borosilicate glass capillaries of 1.5 mm O.D. and 1.17 mm I.D. (*Harvard Apparatus LTD)*. The advantage of this material, borosilicate, is that provides both toughness and flexibility of micropipette tips. The capillaries were pulled employing two different apparatus. The first equipment (*Narishige* puller model *PC-10*) creates small micropipette tips (1-10 µm) by heating and pulling the glass with the aid of weights. An example of a micropipette tip made using this equipment is shown in Figure 5(A). However, pipettes for MPA experiments are required

to have specific geometry characteristics such as long parallel walls and small diameters. So, a laser-automated puller system was employed (*Sutter Instrument* model *P-2000*) which has a better control over the pipette geometry by modifying certain input parameters in the equipment. These parameters were determined by trial and error and are presented in the following table:

HEAT	FILAMENT	VELOCITY	DELAY	PULL
450	5	40	200	50
430	5	0	60	0

After having obtained the micropipette with the P-2000 puller, polishing of the microcapillary with a microforge equipment (MF-900 Narishige) is required, in order to eliminate the small imperfections and non-homogenous surfaces around the pipette tip. Figure 5(B) shows a typical micropipette used in MPA experiments.

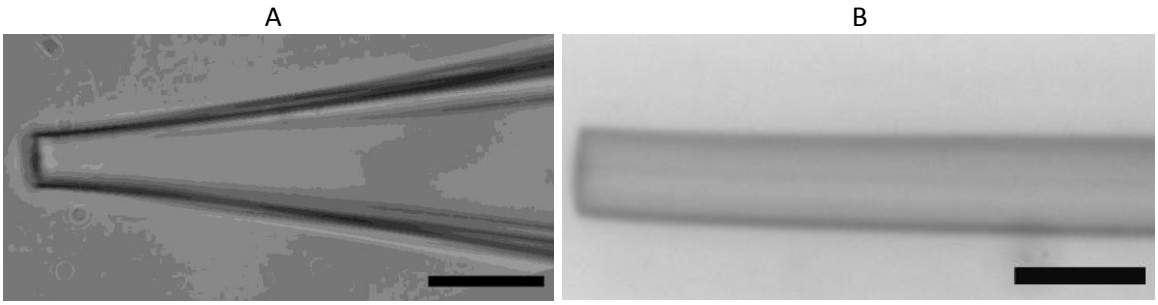

Figure 5. Comparison of two micropipettes using different pipette pullers but the same glass material, i.e. borosilicate. PC-10 puller provides micropipettes with very small diameters and wide tapers (A) while the P-2000 puller afford a better control over the morphology allowing micropipettes with long tapers and small diameters (B). Long tapers are preferred for the MPA technique due to the uniform cross section along the tube. The scale bar is 10 µm.

4.2.4 Preparation of $E_{16}B_{22}$/Nile Red dye sample

A Nile Red dye (Sigma-Aldrich) and $E_{16}B_{22}$ block copolymer in a weight ratio of 1:100 (Nile Red:$E_{16}B_{22}$), were mixed in a vial glass using chloroform ($CHCl_3$) as solvent. A relative high concentration of Nile Red was used (1 %w/w) in order to ensure dye entrapment within the membrane. The sample was placed in a glass sample vial on a stirring stage for about 8 hrs then, put into a vacuum oven throughout the weekend in order to dry. After this time, at the bottom of the glass vial was observed a thick film where Nile Red was mixed with the block copolymer. Then, ultrahigh quality water was added in order to prepare a polymer solution of 5 %(w/w). This sample was used for preparing giant vesicles using the inkjet printing technique. The methodology described

above was based on a study where Nile Red was introduced inside the hydropobic part of a block copolymer, (polybutadiene-b-poly(ethylene oxide))[17]. According with their results, Nile Red was successfully loaded within the vesicle bilayer which vesicles were produced using the hydration method.

4.3 Methodology: MPA equipment in Exeter

The MPA equipment in the University of Exeter (Figure 6) consists of an Olympus microscope model IX50 with bright field, phase contrast and differential interference contrast microscopy. The microscope is on an antivibration table (THORLABS) and has a CCD camera (ALLIED Vision Technologies) with a source of light coming from the Polychrome V monochromator illumination system (TILL Phothonics). The micromanipulator is a manual one from THORLABS. The pressure system consists of a slider water reservoir mounted on a wooden bar with a tripod base. Along the surface of this bar, a metric tape with millimetre accuracy is attached. The water reservoir is connected to the micropipette using a small diameter plastic tubing. The micropipette is fit into a pipette holder which is put on the micromanipulator. Images were taken using the TILL Photonics Live Acquisition software.

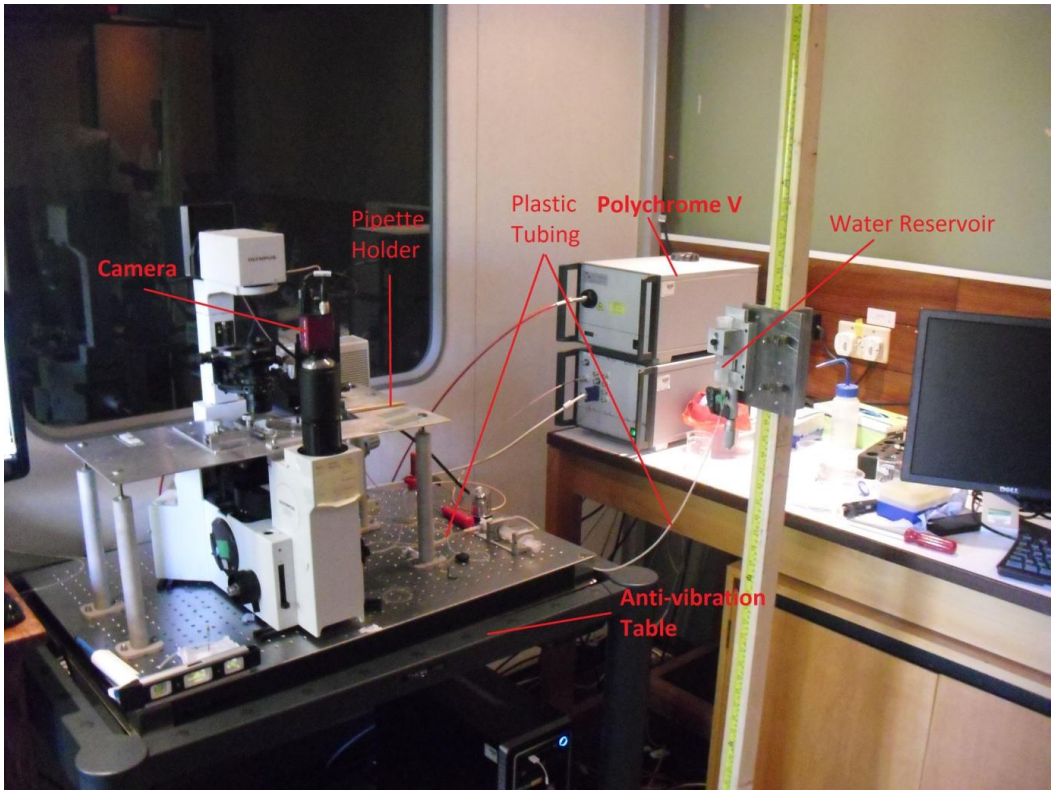

Figure 6. MPA aspiration equipment used in the University of Exeter. For details of this equipment, see above paragraph.

4.3.1 Experimental protocol of MPA experiments

The following methodology was followed in order to obtain the area compressibility modulus. Giant vesicles were prepared with a polymer aqueous solution mixed with glucose in a molar ratio of either 1:10 or 1:20 (polymer/glucose). The diameter of polymersomes, the projection length and the micropipette diameter were determined using ImageJ software.

1. Micropipettes were obtained from the puller P-2000 and these pipettes were polished and cut giving flat micropipette tip surfaces. The typical final diameters were between 5 and 12 µm.

2. Pipettes tips were coated with a siliconizing fluid (SurfaSil^{TM}) in order to reduce vesicle adhesion. Pipettes were place in an oven for about an hour in order to dry. Then, in three small vials, Surfasil^{TM} (1 ml)/Toluene(50 ml), Toluene and Methanol were poured. (The concentration recommended[18] for Surfasil^{TM}/Toluene solution is 1-10 %V). The pipettes were taken from the oven and were gently swirl for about 1 minute in Surfasil^{TM}/Toluene solution, then were rinsed in Toluene (for removing excess of Surfasil^{TM}) and in Methanol (for neutralising the SurfaSil^{TM} against water). Finally, the micropipettes were put into the oven for about 24 hrs in order to dry them and then put into a plastic storage container.

3. With a non-metallic flexible syringe needle (MicroFil^{TM} -28G, World Precision Instruments), pipettes were backfilled using the same liquid that was used to hydrate samples.

4. A micropipette was connected to the water manometer using a small diameter plastic tubing that was fitted into the micropipette holder which in turn is mounted to the micromanipulator.

5. Hydrophobic microscope slides with a printed polymer solution were carefully hydrated with water using a pipette Pasteur. Cautious water addition was necessary as forcing water with a relative large force from the pipette Pasteur can wash off the printed polymer dots. Alternately, a syringe pump (World Precision Instruments) can be used in order to hydrate samples.

6. Commonly 2-3 ml of water was poured over the glass slide. The hydrophobic surface allows the formation of a raised drop of held in place by surface tension, facilitating MPA experiments. After about 2-3 hrs, vesicles are formed using a 5 %w/w EB(1)-Glucose(10 or 20 molar units) polymer solution.

7. The micropipette was introduced into the vesicle solution and was brought down carefully to the bottom of the glass slide, where vesicles are formed.

8. Then, small negative and positive pressures were applied until the vesicle was static and touched the micropipette tip. This was taken as the “zero pressure”.

9. A small suction pressure was applied to the vesicle with the purpose of picking it up. After capturing a vesicle, the vertical position of the pipette is raised and the glass slide is moved some hundreds of microns using the microscope stage. This step is necessary in order to detach the vesicle and cut tethers.

10. Data collection begins by applying a suction pressure of –2 cm of water to the vesicle and after 90 seconds a picture was taken and the experimental observables were obtained. This step is repeated several times until the vesicle is aspirated.

11. For calculation purposes, vesicles with a diameter at least three time larger than the pipette diameter were chosen and the slope of the $\boldsymbol{\sigma}$ vs $\boldsymbol{\alpha}$ graph were obtained with at least four points.

4.4 Results and discussion of MPA experiments in Sheffield

The independent variables which define the mechanical properties of vesicles, i.e. bending modulus and area compressibility modulus, in MPA experiments are: the difference in vesicle suction pressure (ΔP), the vesicle projection length into the micropipette (ΔL), vesicle radius (R_v) and pipette radius (R_{pip}). ΔP can be estimated with a manometer by measuring differences of vacuum pressure with respect with a zero reference pressure. Moreover, ΔL, R_v and R_{pip} can be determined by observing and analysing lengths in the images of the aspirated vesicles. One of the main problems that were encountered in experiments was the difficulty in observing the vesicle protrusion into the glass micropipette. The next following sections describe the attempts to solve this drawback and the solution as well as the determination of the area expansion modulus.

In these series of experiments, the water manometer connected to the pipette exerts a sequence of several vacuum pressures every two minutes over a giant vesicle (GV). Bright field and phase contrast microscopic techniques were used in experiments, as well as several polymer solutions with different additives in order to prepare GVs, in an attempt to have a better contrast of the vesicle protrusion in the images. All images were analysed using ImageJ or LabVIEW Vision software. Also, the brightness and contrast of images were adjusted using the aforementioned software since the vesicle contour can be enhanced and some details become clearer. The best images were selected from a large number of experiments in order to facilitate the interpretation of results.

4.4.1 Vesicles prepared with 5 %(w/w) $E_{16}B_{22}$

First MPA experiments were conducted using a polymer aqueous solution of 5 %(w/w) printed over a glass slide for vesicle preparations. At this stage of early experiments, the shape of micropipette tip, i.e. with small diameters and wide tapers, did not affect the results since the main purpose of these tests was to observe the projection length. However, pipettes with these features were only used in the first stage of tests and then modified according with methodology described in section 4.2.1.3. It should be mentioned that in these series of experiments, few vesicles were aspirated by the micropipette. Later, this technique of producing enclosed bilayers was abandoned because vesicles were usually not fully formed and tightly attached to the polymer substrate, i.e. formation of hemispherical structures. So, when a relative high vacuum pressure was applied to such polymersomes in order try to detach them, most of the time the polymer microdrop was also attracted to the pipette which complicates vesicle capture and isolation. All these problems made it difficult to pick up single giant vesicles into the micropipette, without contamination by excess polymer. This methodology would be replaced by the polymer/glucose solution samples because of its high efficiency in producing spherical polymersomes.

Figure 7 depicts a successful experiment of vesicle capture, where a pipette with a diameter of 3.5 µm captured a vesicle of 19.7 µm size with a suction pressure of about 200 Pa. Then, after applied a vacuum pressure in the range of 200-330 Pa, the vesicle was aspirated. Examining Figure 7, it can be seen that although a tension of 0.213 mN/m was exerted over the vesicle, there were no signs of the typical hemispherical cap of the projection length inside the micropipette. A further examination reveals that the glass capillary is not entirely transparent. Some polymer residues of past attempts of vesicle aspiration remained into the micropipette and absorbed light. This fact can explained the random “stains” along the pipette tip.

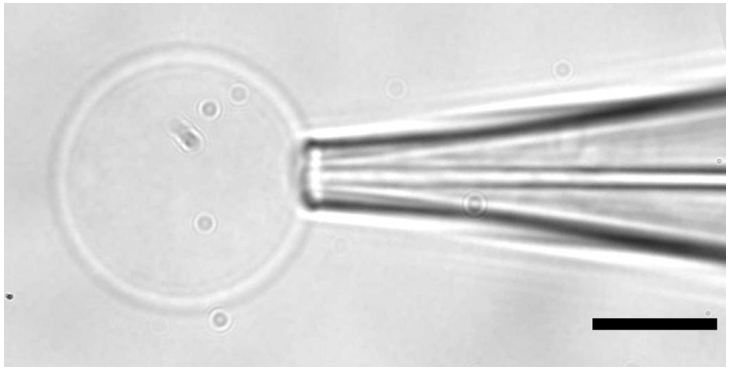

Figure 7. A micropipette with a diameter of 3.5 µm captured a giant vesicle of 19.7 µm after a suction pressure of 193 Pa, σ = 0.213 mN/m. This image was taken using the bright field microscopic technique. Bar scale is 10 µm.

4.4.2 Vesicles prepared with 5 %(w/w) $E_{16}B_{22}$/Nile Red dye

This sample was prepared according with section 4.2.1.4. In these experiments, Nile Red was loaded within the bilayer of a vesicle in order to provide better membrane contrast. Nile Red is a strong fluorescent dye that is frequently used to stain lipids in the analysis and study of hydrophobic structures in cells[19]. Therefore, nonetheless this dye works by using a fluorescence microscope, Nile Red inside the vesicle membrane could cause more light absorption and, as a result, enhance its definition.

Figure 8 shows different stages of the experiment in a wide range of suction pressures: 210 Pa (A), 317 Pa (B), 430 Pa (C), 538 Pa (D), 647 Pa (E), 867 Pa (F), and above 867 Pa (G). The pipette and vesicle have diameters of 4.1 µm and 21.1 µm respectively. Image Figure 8(G) was taken just a moment after the pressure was increase above 867 Pa, when a destabilization of the vesicle was noticed, and, some seconds later, the vesicle was completely aspirated (entirely sucked into the capillary). At relative low (Figure 8(A-C)) and high suction pressures (Figure 8(D-G)), the vesicle protrusion was not observed throughout the glass capillary. In successful MPA experiments (section 4.3.2.1), the projection length was observed for pressures of about 160 Pa and tensions of about 0.5 mN/m using differential interference contrast microscopy rather than bright field microscopy. Therefore, an absence of a vesicle protrusion in the images suggests a very poor resolution of the aspirated part of the vesicle with this microscopy technique. In the images of Figure 8, in the background there are some small vesicles that had adhered to the large vesicle because, in the process of picking a vesicle, usually, small spherical and long tubular structures stuck to the big one. However, this did not cause interference in observing the vesicle protrusion.

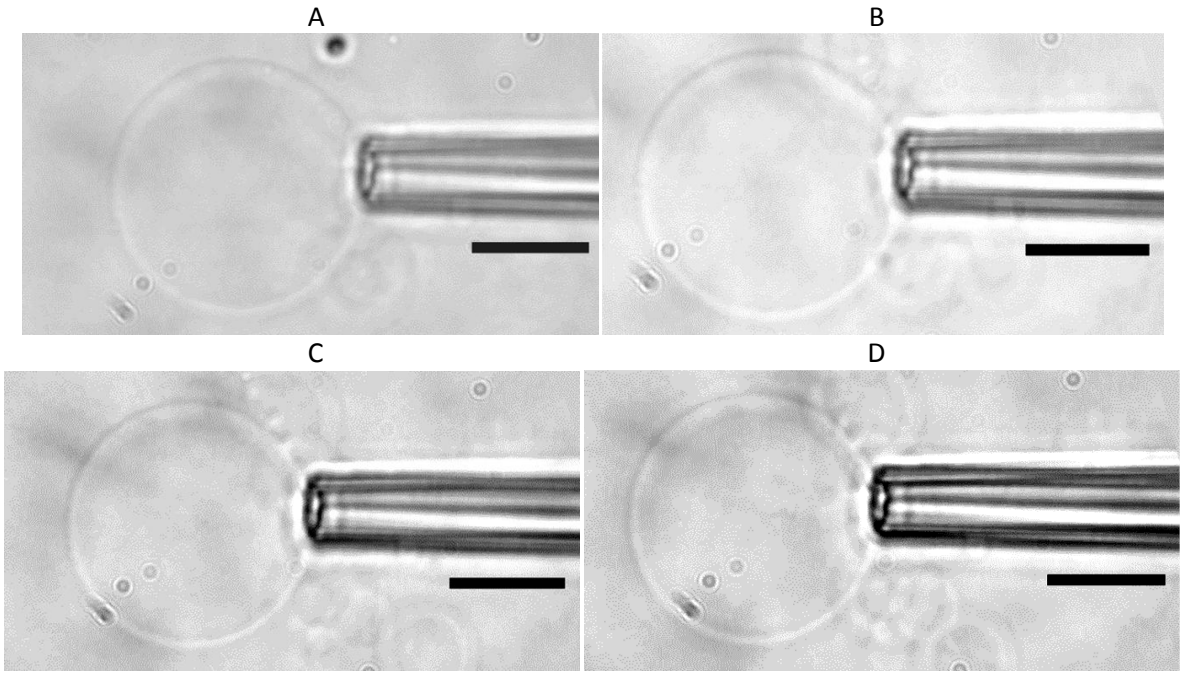

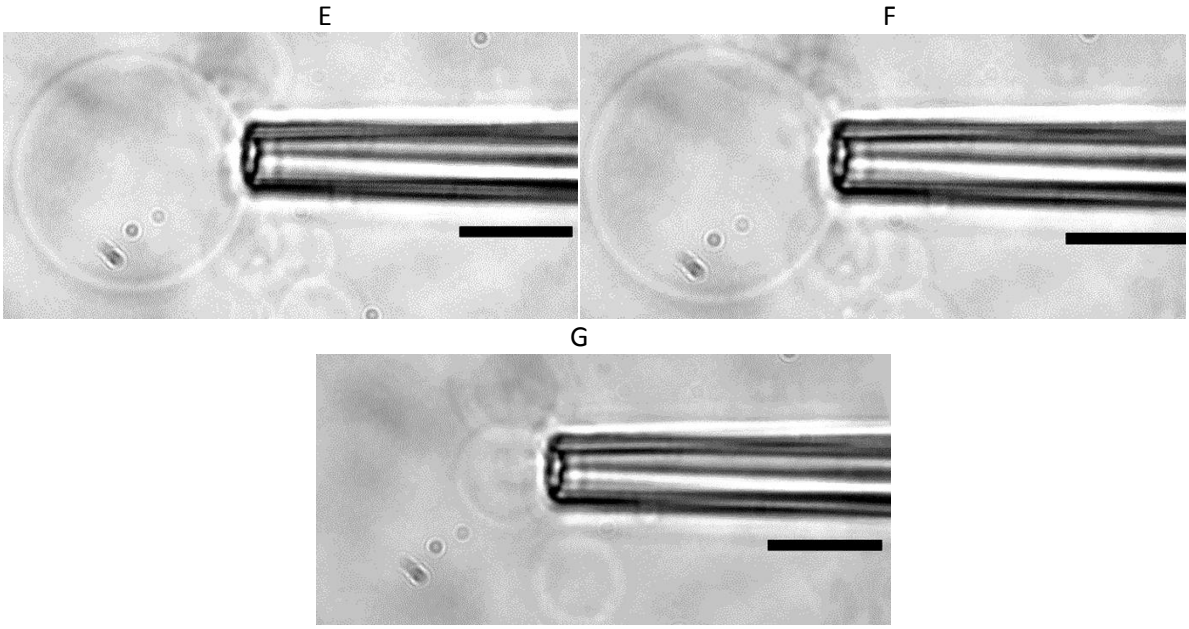

Figure 8. A giant vesicle of 21.1 µm, which Nile Red was encapsulated within the membrane, aspirated with a pipette of 4.1 µm at different suction pressures: 210 Pa (0.267 mN/m) (A), 317 Pa (0.403 mN/m) (B), 430 Pa (0.547 mN/m) (C), 538 Pa (0.684 mN/m) (D), 647 Pa (0.823 mN/m) (E), 867 Pa (1.103 mN/m) (F), and above 867 Pa (G). The scale bar is 10 µm.

4.4.3 Vesicles prepared with $E_{16}B_{22}$/Glucose

Based on chapter 3, the best results to prepare giant vesicles was employing a polymer aqueous solution mixed with glucose in a molar ration of either 1:10 or 1:20 (EB/glucose). The resulting vesicles are very amenable to MPA experiments. So, a sample of 5 %w/w $E_{16}B_{22}$(1)-Glucose(10) was used, where the number in brackets represent the molar ratio of polymer and glucose.

Figure 9(A-D) represents the difference stages of the experiment from 48 Pa to 440 Pa suction pressures using a pipette of 4.8 µm size. At low suction pressures, i.e. 48 Pa and 146 Pa (Figure 9(A-B)) the vesicle diameter was 10.2 µm. Then, increasing suction pressures at 315 Pa (Figure 9(C)) and 440 Pa (Figure 9(D)), the diameter visibly reduced to 9.2 µm and 8.3 µm respectively. This reduction can be originated because a small fragment of the polymersome was aspirated inside the pipette. However, a close inspection of all images reveals that the membrane bilayer was not detected inside the glass capillary, even for Figure 9(C-D) which had a visibly decrement in vesicle diameter. In the interval pressure from 462 to 485 Pa, the vesicle was completely aspirated. Also, similarly to Fig. 8, at the bottom of the micropipette tip, a small vesicle can be seen attached to the big one (Figure 9(B-D)). However, this tether did not hinder the observation of the vesicle protrusion.

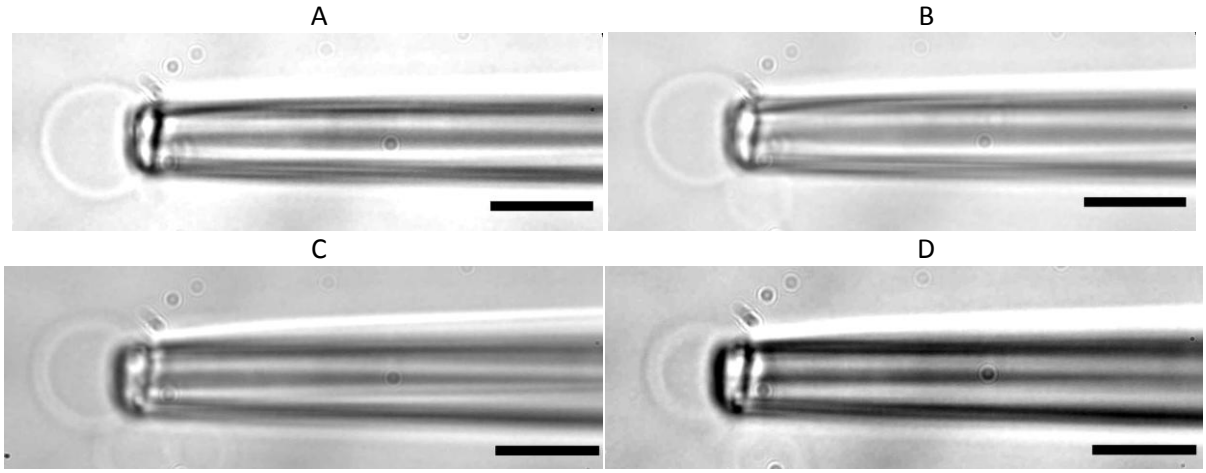

Figure 9. A small vesicle been aspirated by a pipette of 4.8 µm at different suction pressures: 47.5 Pa (0.108 mN/m) (A), 146 Pa (0.331 mN/m) (B), 315 Pa (0.79 mN/m) (C) and 440 Pa (1.252 mN/m) (D).These images were taken using the bright field microscopy technique and the GV was prepared using a 5 %w/w EB(1)-Glucose (10) solution. Scale bar is 10 µm.

In another test, a larger vesicle of 27.6 µm was captured with a vacuum pressure of 133 Pa (Figure 10(A)). Then, stepwise increments of about 100 Pa was applied every 2 two minutes using a pipette of 5.7 µm. Also in this experiment, vesicle diameter (D_v) decreased as the pressure increased. For example, at relative low suction pressures, diameters are the same (at 113 Pa and 220 Pa of Figure 10(A) and 10(B) respectively have a vesicle diameter of 27.6 µm), but began to decrease at 305 Pa (D_v= 26.7 µm, Fig. 10C) and 432 Pa (D_v= 25.9 µm, Figure 10(D)). If one compares the vesicle diameter of Figure 10(A) (D_v = 27.5 µm) with Figure 9(D) (D_v= 25.9 µm), the reduction in size is 1.6 µm. This drop in diameter, in a range pressure of 299 Pa with respect with Figure 10(A), could have been possibly caused by vesicle fragmentation because of formation of membrane micropores. In the first case, according with literature, the projection length of cells[20] and liposomes[21] can be pulled away from the original material when applying relative low pressures. This can lead to a reduction of vesicle material[20]. Assuming this possibility, it is likely vesicle size reduction because of polymersome sectioning. Finally, in Figure 10(D) after had applied a pressure of 432 Pa, some seconds later the vesicle was completely aspirated into the pipette.

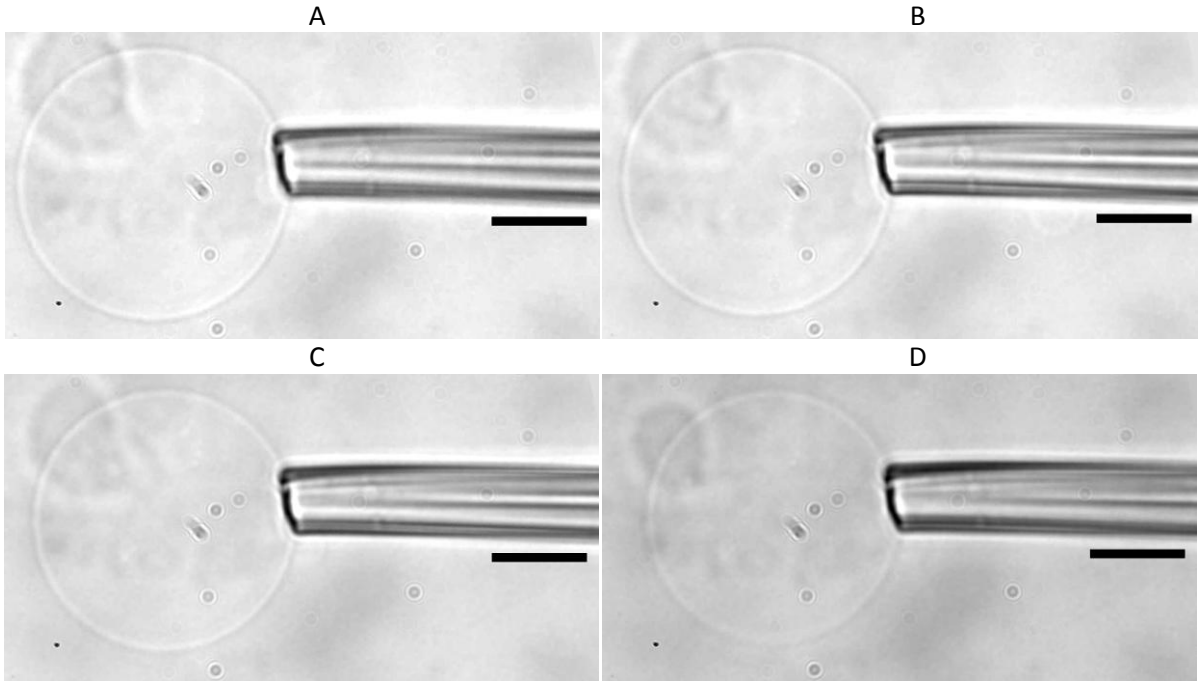

Figure 10. A vesicle been aspirated by a pipette of 5.7 µm at different suction pressures: 133 Pa (0.239 mN/m) (A), 220 Pa (0.395 mN/m) (B), 305 Pa (0.552 mN/m) (C), and 432 Pa (0.789 mN/m) (D). These images were taken using the bright field microscopy technique and the GV was prepared using a 5 %w/w EB(1)-Glucose (1:10) solution. Scale bar is 10 µm.

In experiment of Figure 11, vesicles were observed using the phase contrast microscopy technique. Since vesicles were prepared based on the osmotic pressures differences between the inner glucose concentration within polymer lamellar structures and the outside aqueous solution (chapter 3), vesicles could entrap a small part of glucose molecules into the lumen. This gradient in concentration can allow to have a difference in refractive indices which could be an advantage using the phase contrast technique. Figure 11(A) shows the pipette of 5.3 µm picking up a giant vesicle of 24.8 µm with a suction pressure of 58 Pa. At 188 Pa (Figure 11(B)), the vesicle protrusion could not be seen and it is the same for the next suction pressures of 288 Pa (Figure 11(C)), 374 Pa (Figure 11(D)), and 502 Pa (Figure 11(E)). Then, the suction pressure was increased sharply up to 1072.5 Pa and after about 1 minute, the vesicle burst or went inside the micropipette. It should be noticed that through the experiment, the diameter remained constant.

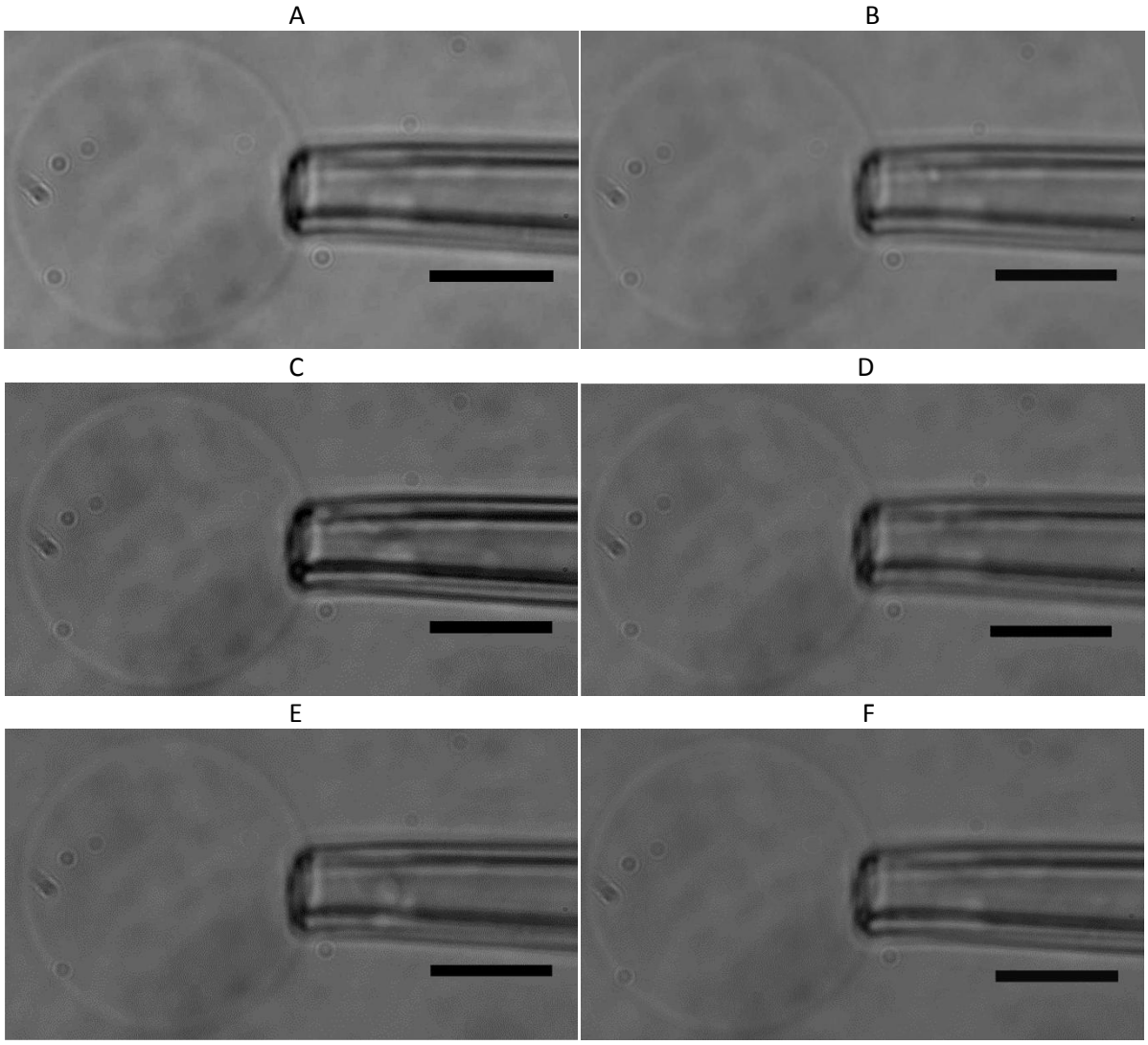

Figure 11. A vesicle aspirated by a pipette of 5.3 µm at different suction pressures: 58 Pa (0.097 mN/m) (A), 188 Pa (0.317 mN/m) (B), 288 Pa (0.485 mN/m) (C), 374 Pa (0.63 mN/m) (D), 502 Pa (0.846 mN/m) and 1073 Pa (1.808 mN/m) These images were taken using the phase contrast microscopy technique and the GV was prepared using a 5 %w/w EB(1)-Glucose (10) solution. Scale bar is 10 µm.

In another alternative experiment, glucose was mixed, in a higher molar concentration than the previous sample, with a 3 %w/w $E_{16}B_{22}$(1)-Glucose(20), i.e. ratio of 1:20 corresponding $E_{16}B_{22}$/Glucose respectively. The idea was to increase the difference in refractive indices by adding more glucose. The series of images in Figure 12 represents different experimental stages in a wide range of suction pressures: 267 Pa (Figure 12(A)), 482 Pa (Figure 12(B)), 712 Pa (Figure 12(C)), 940 Pa (Figure 12(D)), 1165 Pa (Figure 12(E)) and 1395 Pa (Figure 12(F)). Along the micropipette tip can be seen some polymeric material that remained from early suctions, which also was the case of Figure 11. When picking a vesicle, sometimes the vacuum pressure attracts part of the polymer substrate

where the vesicle is attached. Nonetheless a large positive pressure is applied in order to “clean” the micropipette after each experiment, in some cases, the polymeric material is not expelled at all. The polymer remainders are difficult to get rid because they adhere to the micropipette walls and the manometer does not exert enough pressure to eject them. In this case, a new pipette is needed. There is no effect of the remaining polymer obscuring the projection length. However, as was verified in MPA experiments of section 4.3.2.1, for a correct measurement of the expansion modulus, the micropipette tip needs to be “clean” since the residual polymer can adhere to the vesicle protrusion and lead to a small increment of the vesicle protrusion. This affects the accuracy of results since such value does not correspond to the real projection length.

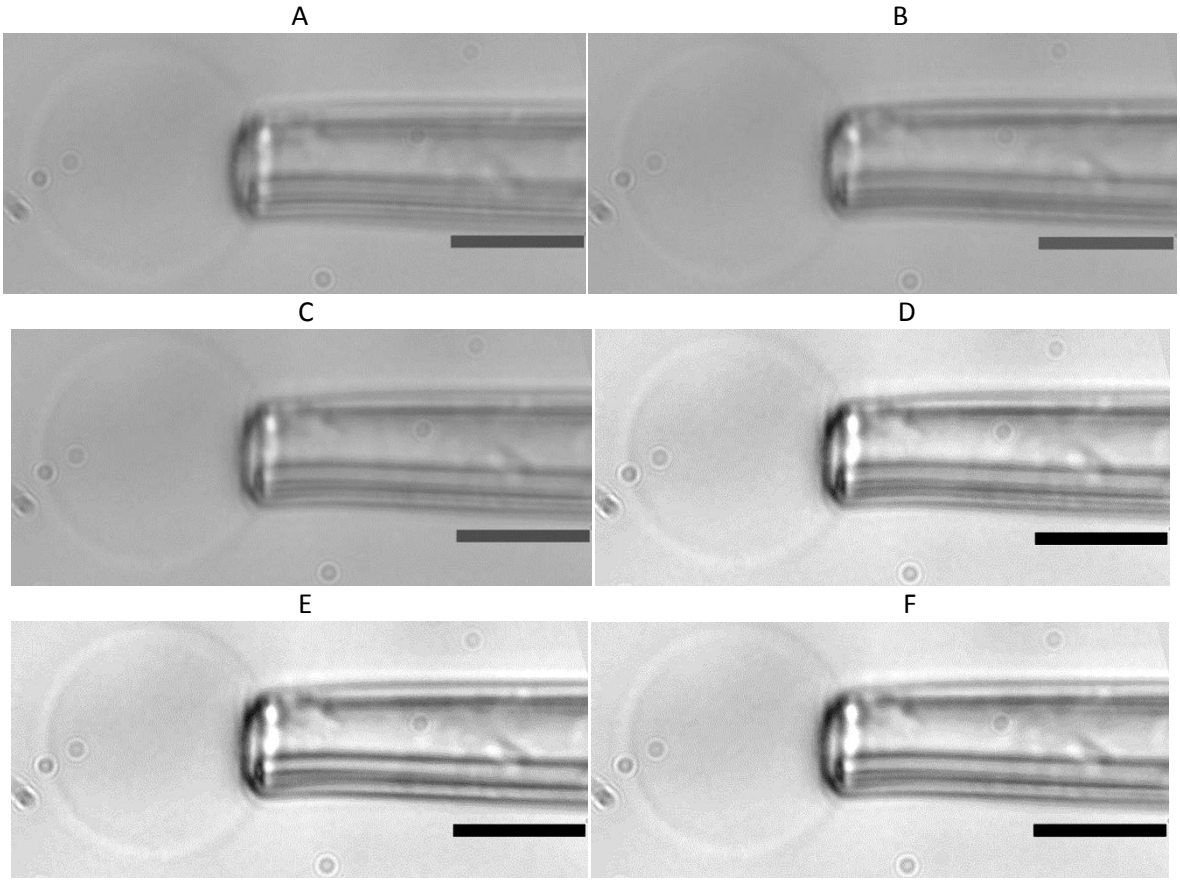

Figure 12. A vesicle been aspirated by a pipette of 6.4 µm at different suction pressures: 267 Pa (0.667 mN/m) (A), 482 Pa (1.204 mN/m) (B), 712 Pa (1.779 mN/m) (C), 940 Pa (2.348 mN/m) (D), 1165 Pa (2.910 mN/m) (E) and 1395 Pa (3.485 mN/m) (F). These images were taken using bright field microscopy technique and the GV (17.8 µm) was prepared using a 3 %w/w EB(1)-Glucose (20) solution. For comparison purposes, the brightness and contrast was adjusted for second half (C-F) of the images. Scale bar is 10 µm.

In all the above experiments, the vesicle projection length could not be observed into the glass capillary. So, one might think that the pressure system did not work correctly or experimental artefacts affected the visibility through the micropipette. However, a clear evidence of the presence of the projection length was carried out in the next experiment. With a suction pressure of 20 Pa, a small vesicle of 9.4 µm was aspirated using a pipette of 4.5 µm (Figure 13(A)). At 145 Pa (Figure 13(B)), the vesicle protrusion was not completely visible. Then, in the subsequence pressure increments of 188 Pa (Figure 13(C)), 225 Pa (Figure 13(D)), 320 Pa (Figure 13(E)) and 365 Pa (Figure 13(F)), the membrane was more visible since one can identify the typical hemispherical cap of vesicle elongation. Also, some sort of material can be seen inside the micropipette which is being pushed as the pressure increases. This material was identified as bacteria that grew after a pipette was initially used after about a week. The bacteria could be easily recognized in this experiment since they independently and constantly moved out of the micropipette. However, owing the pipette tip was blocked by the vesicle, microorganisms were accumulated on the border of the projection length which prevented them from escaping. This allows more contrast with the membrane since bacteria absorbed more light. So, in this case, it was an indirect way of observing the projection length. However, the vesicle protrusion free movement was obstructed by bacteria along the pipette which did not allowed a free development of the experiment. Therefore, this test of observing the protrusion is not reliable in measuring the mechanical properties of this vesicle.

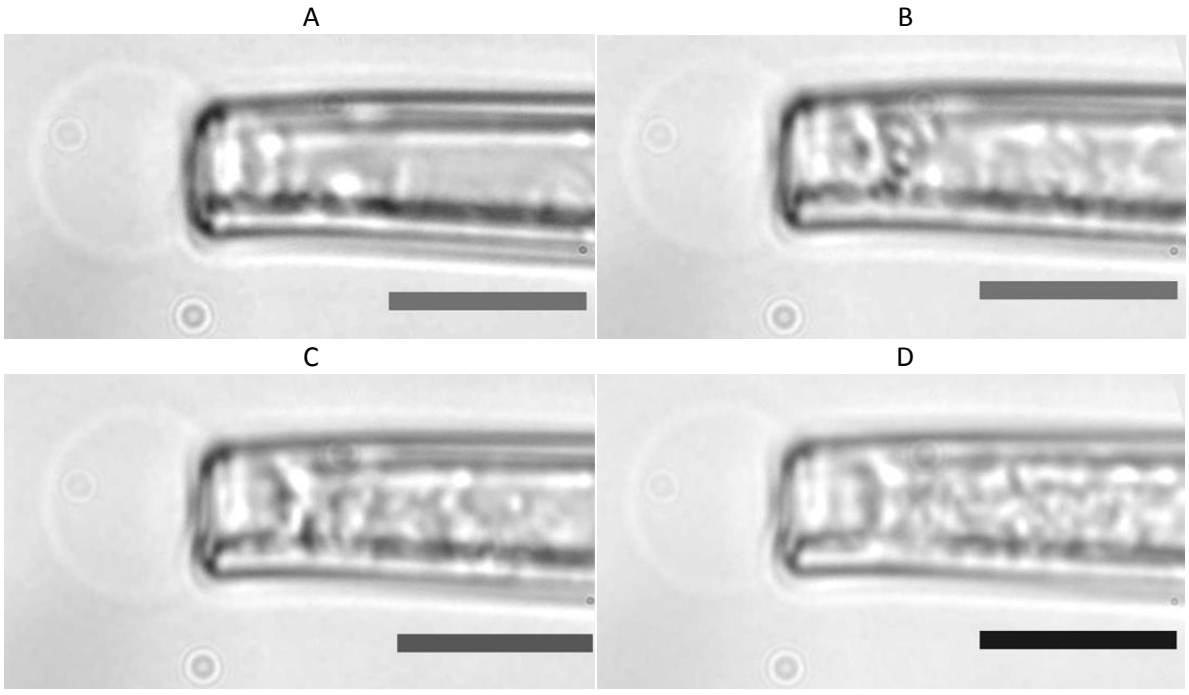

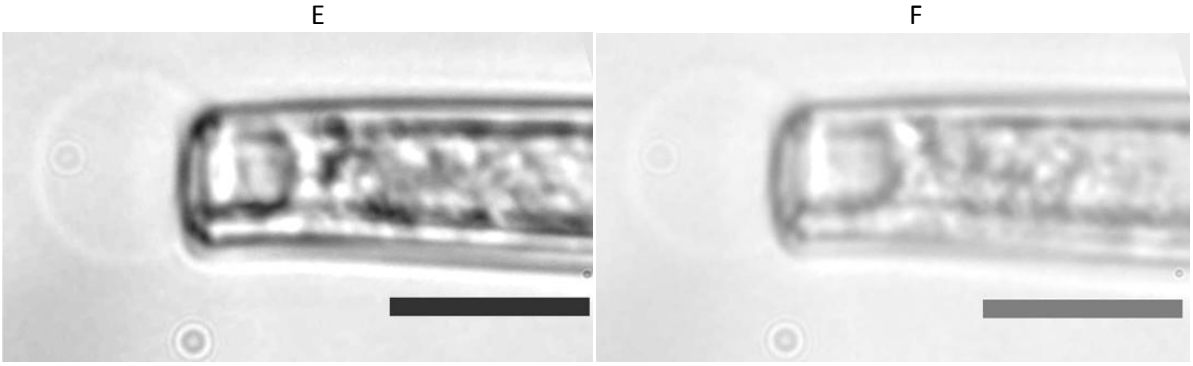

Figure 13. A vesicle been aspirated by a pipette of 4.5 µm at different suction pressures: 20 Pa (0.043 mN/m) (A), 145 Pa (0.313 mN/m) (B), 188 Pa (0.406 mN/m) (C), 225 Pa (0.485 mN/m) (D), 320 Pa (0.690 mN/m) (E) and 365 Pa (0.788 mN/m) (F). These images were taken using bright field microscopy technique and the GV (9.4 µm) was prepared using a 5 %w/w EB(1)-Glucose (10) solution. Scale bar is 10 µm.

The bacteria contamination provided inspiration for an alternative experiment: backfilling the micropipette with a pigment in order to provide a contrast with the membrane. In this case, the pigment red 122 (FUJIFILM) made of Quinocridone was used with particle sizes of about 1 µm, which are much more bigger than membrane interstices, avoiding the particles going through the membrane, and allows more light absorption. So, this pigment was dissolved in water in a stirring plate overnight and, then, backfilled into the micropipette. However, after a certain time, this dye formed small aggregates and block the micropipette, making impossible to conduct the experiments (Figure 14).

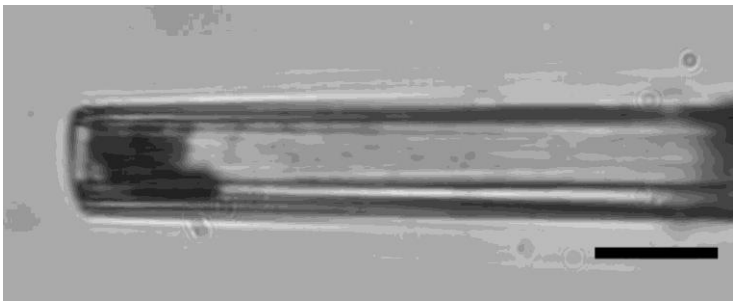

Figure 14. A micropipette backfilled with water/ pigment red 122. Some lumps can be seen along the pipette which blocked it. Scale bar is 10 µm.

4.4.4 Analysis of Results

Bright field microscopy did not solve the problem of observing the vesicle protrusion. Commonly, when using this technique, samples are dense or need to be stained in order to provide them the appropriate contrast[22]. In Figure 7, the projection length could not be observed because polymersomes did not absorb light and as a consequence there was not an increment in optical resolution, leaving the vesicle basically invisible inside the micropipette[23]. So, the membrane was stained with Nile Red (Figure 8). According with literature[17], Nile Red can be incorporated within the hydrophobic membrane of block copolymers if the appropriate method is used for sample preparation (section 4.2.1.4). So, encapsulating this dye can enhance light absorption with the membrane. However, this absorption increment was very small and did not allow the observation of the vesicle projection length (Figure 8). So the effect of membrane staining was insignificant. Another way to enhance contrast using the bright field illumination technique is increasing the refractive index in the system[24]. In Figures 9, 10 and 12, vesicles were prepared by the method of mixing glucose with the polymer aqueous solution (chapter 3). In this case, the way of vesicle preparation permits a small amount of glucose to be encapsulated within the bilayer which can cause a difference in refractive indices with respect with the outside water solution. However, this difference was again insufficient to provide a better sufficient resolution of vesicle protrusion in the images.

Another microscopy technique frequently use in MPA experiments is phase contrast microscopy. This technique takes advantage of difference in refractive indices in the specimen structure in order to enhance the optical resolution[25]. So, vesicles images can be improved using refractile solutes, e.g. using a isotonic solution of 100 to 300 mM with an interior sucrose solution with an exterior glucose solution, which provide the require gradient in refractivity[26]. However, the inkjet printing method for vesicle preparation is sensitive to the addition of others compounds to the vesicle aqueous solution. Even addition of small concentrations of solute refractive solutions, e.g. 0.01 M of NaI or NaH_2PO_4, can prevent vesicle formation, making difficult to have a better polymersome resolution. In Figure 11, phase contrast microscopy was used. However, owing the tiny amount of glucose encapsulated and the impossibility of increasing further the refractive indices, there was not an improvement in vesicle projection length resolution.

As it will be seen in the next section, the projection length was observed by differential interference contrast microscopy (DIC). Unstained[27] and transparent[28] samples are suitable for being analysed with DIC, permitting the resolution of structure details in high contrast that the bright field technique did not reveal. DIC works by altering the phase wavefront of light when the bean of light

passes through the sample, i.e. phase shifts are sensitive to refractive index and the specimen thickness. So, phase changes are converted into amplitude changes which causes the contrast[28]. A part of the DIC microscopy, the projection length can be observed using others techniques such as Hoffman modulation contrast optics[29] or using both[26] phase contrast and enhancing the refractive index, or with specific dyes combined with fluoresce microscopy[26], i.e. high detail structural-specimen spectroscopy.

4.5 Results and discussion of MPA experiments in Exeter

4.5.1 Determination of experimental parameters

As was described in section 4.2.2, the MPA equipment in Exeter consists of a microscope with phase contrast and differential interference contrast microscopy equipped with a monochromator and a xenon light source. This unit, i.e. the Polychrome V, provides high and stable luminous flux density in the plane of the object and, consequently, supplies excellent control of the brightness of the specimen[30]. So, DIC with the annexed light equipment allows the observation of the projection length, suitable for our sample conditions of a small refractive index gradient, as can be seen in Figure 15. However, even with this technique the contrast is very low.

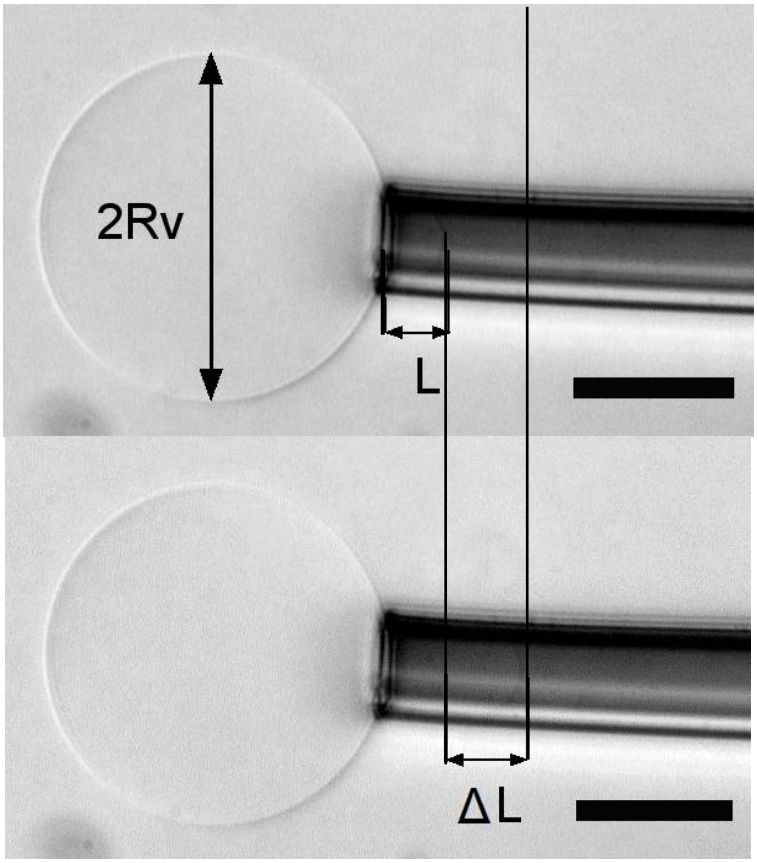

Figure 15. A image taken, with a 40x objective , by differential interference contrast microscopy. In the top image, the vesicle protrusion (L) can be observed when applying a tension of 0.49 mN/m. There was an increase in the projection length (ΔL) when the tension increased to 2.92 mN/m (bottom image). Scale bar is 20 µm.

A stage micrometer (Edmund optics) was used to carry out the spatial calibration. In our case, using an objective of 40x, the calibration constant was 1 µm = 6.35 pixels. The diameter of the vesicles was estimated by rotating the image 90°, in order to avoid selecting the micropipette tip which introduces noise into the plot profile, and making a rectangular selection in the middle of the vesicle (Figure 16(C)). The diameter results from measuring the distance in pixels in the "X" axis (Figure 16(D)) since the contour of the vesicle is represented by a pixel of different intensity with respect with the background intensity. Once the diameter is determined, the image was rotated to its original position and the predetermined value of diameter was used to "find" the beginning of the projection length into the micropipette tip. Then, the protrusion length is estimated from a square section of the projection length and by measuring of the corresponding peak intensities (Figure 16(E-F)).

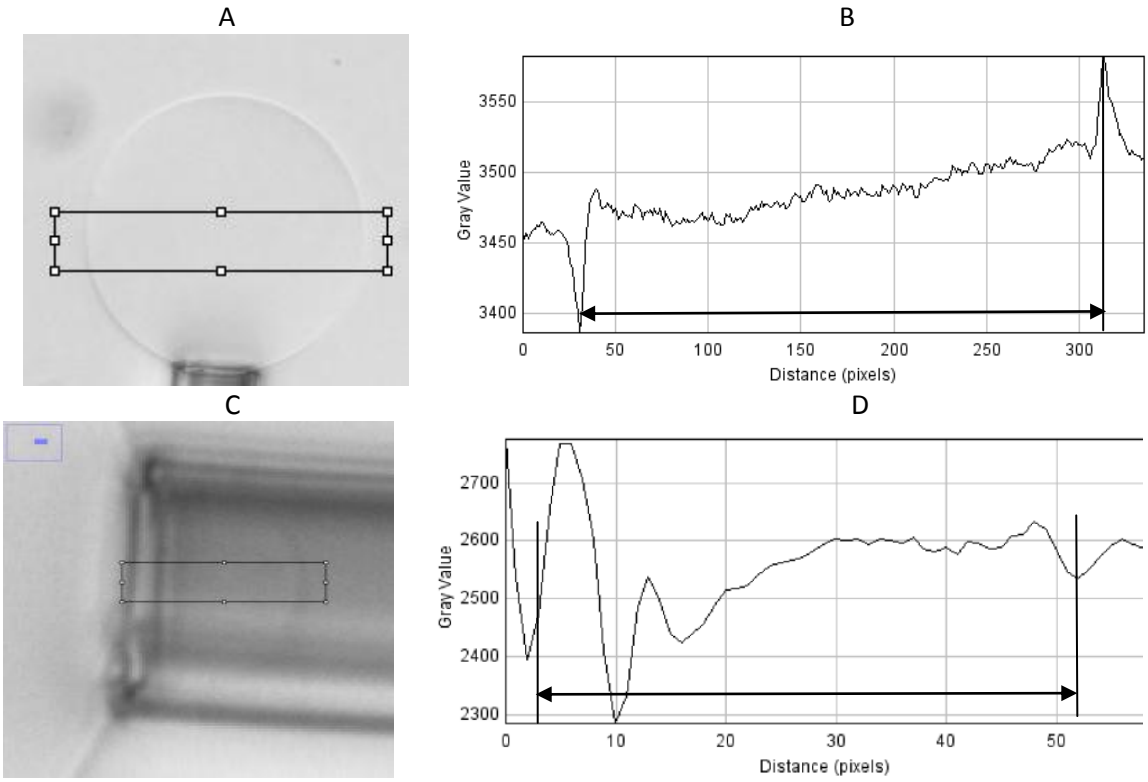

Figure 16. Measure of the diameter (A) and the projection length (C) of a vesicle using a rectangular selection and analyzing them with surface plots ((B) and (D) respectively).

The pipette radius was determined taking into account two spatial references inside the micropipette. The first reference corresponds to the hemispherical cap of the projection length with a value of 9.13 µm (Figure 17(A)). The second reference is the internal edges of the pipette tip with a value of 10.23 µm (Figure 17(B)). So the inner pipette diameter was considered to be the average of these two magnitudes, i.e. 9.68 µm ≈ 9.7 µm.

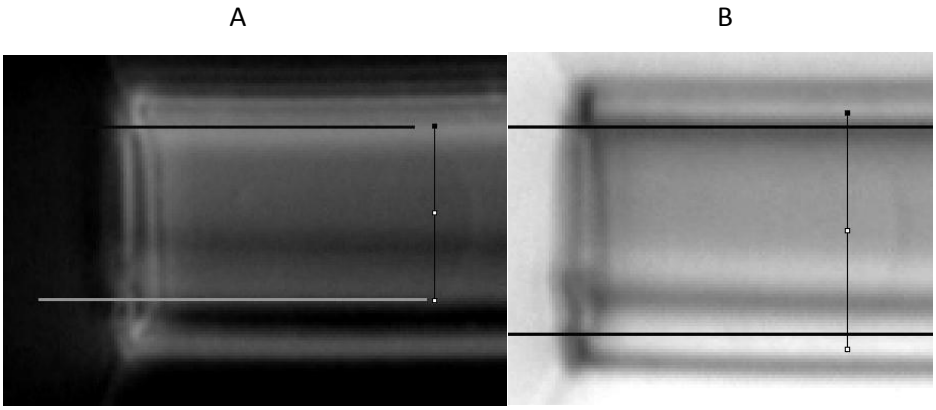

Figure 17. Measurement of the micropipette radius based on projection length edges (A) and pipette thickness (B).

4.5.2 Analysis of results

Membrane tension (**σ**) and area strain (**α**) were calculated according with equations (2) and (4), respectively, of section 4.1. The area compressibility modulus (K_A) results from a linear regression of equation (5) by plotting **σ** vs **α** at high tension regime ($<$ 0.5 mN/m), where K_A is the slope of the straight line (Figure 18). The standard error (S.E.) was calculated using equation (8) where λ is the standard deviation and N is size of the sample. Also, the propagation of error ($(\delta K_a)/K_a$) in each individual experiment was determined with equation (9). In this equation, numerators (δ) represent the uncertainty of independent variables (D_v= diameter of the vesicle, D_p= diameter of the pipette, ΔL= projection length and P= suction pressure) and denominators are the magnitudes of independent variables used to calculate K_A. Figure 19 summarises the overall results.

$$S.E. = \frac{\lambda}{\sqrt{N}} \quad (8)$$

$$\frac{\delta K_a}{K_a} = \sqrt{\left(\frac{\delta D_v}{D_v}\right)^2 + \left(\frac{\partial D_p}{D_p}\right)^2 + \left(\frac{\delta P}{P}\right)^2 + \left(\frac{\delta \Delta L}{\Delta L}\right)^2} \quad (9)$$

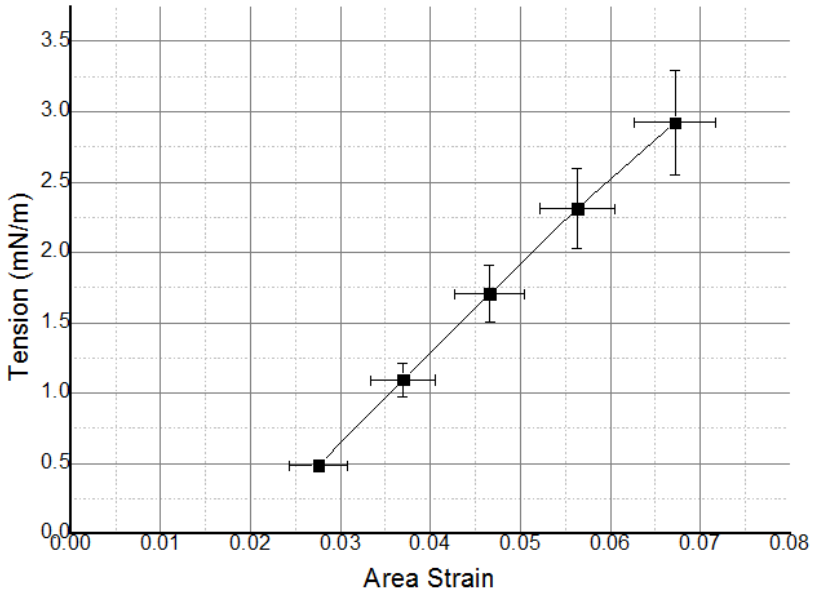

*Figure 18. Graph of tension (**σ**) vs area strain (**α**) at high tension regime for vesicle 1. The error bars were determined by estimating the maximum and minimum uncertainties of each experimental-independent variable of equations (2) and (4) and, then, calculating the corresponding tension and area strain, respectively. K_A is the slope of the straight line.*

According with our observations, the longest percent of errors calculated with equation (9), i.e. vesicles 3 (41.4 %), 5 (33.4 %) and 6 (34.2%) in Figure 19, came from short increments in the projection lengths inside the micropipette and the lack of a fine accuracy in such measurements. This was due to the incapability of obtaining microphotographs with good contrast in vesicle protrusion. Conversely, long increments in the projection length provided low percent of error.

Experiment or Vesicle	K_A (mN/m)	Propagation of Error of K_A (mN/m)
1	28.9	±4.7 (16.4 %)
2	41.8	±5.7 (13.7 %)
3	60.5	±25 (41.4 %)
4	61.6	±16.1 (26.2 %)
5	63.7	±21.3 (33.4 %)
6	112.0	±38.3 (34.2 %)
Mean	61.4 ±23.1	

Figure 19. Table of results of the stretching elasticity modulus of poly(ethylene oxide)$_{16}$-poly(butylene oxide)$_{22}$ ($E_{16}B_{22}$) giant vesicles and the propagation of error in both magnitude and percentage for each individual vesicle experiment. The average value of all experiments is 61.4 mN/m and the two times standard error is ±23.1 mN/m.

The average stretching modulus in our experiments was 61.4 ±23.1 mN/m which is relatively lower than that found for other polymersomes systems, e.g. PEO-PBD with a K_A= 102 mN/m[31]. It should first be mentioned that thermal fluctuations need to be taken into account in order to obtain a more accurate value for the stretching modulus in experiments, since these persist at high tensions, as described at the end of section 4.1. Basically, this correction is applied to the bending modulus (k_c), which in turn is strongly dependent of the hydrophobic membrane thickness "d"[15]. The adjustments to K_A for polymersomes[15] with "d" between 8-15 nm are less than 5 % whereas for liposomes[16] with d= 3.4-4.4 nm they can be up to about 25 %. Since $E_{16}B_{22}$ polymersomes have a membrane thickness of 2.4 ±0.26 nm[32], i.e. a lipid-like membrane which is significantly more flexible than common polymersomes, a relatively large correction e.g. 25-30 % is expected. Using a simple estimation of the correction to K_A of 30 % based on membrane thickness, the uncertainty in values for K_A will be ±18.4 mN/m. However, this correction is already within the overall range of uncertainty in experiments, i.e. 23.1 mN/m, and therefore the estimated standard experimental error is unaffected.

The stretching modulus is related to the interfacial tension (γ) which, in turn, is related to the chemical composition of the bilayer, and can be approximated with the equation: $K_A \approx 4\gamma$[31]. For instance, the interfacial tension for poly(ethylene oxide)-poly(butadiene) (PEO_{29}-PBD_{46}) is ~32 mN/m[33] which would correspond to a K_A of 128 mM/m. The above equation has been shown to provide good agreement with experimental values of K_A via MPA. For example, the stretching modulus of PEO-PBD polymersomes has been found to be between 107 (±14mN/m)[34] (PEO_{26}-PBD_{46}) and 120 (±20mN/m)[35](PEO_{40}-PBD_{37}). Similarly, in the case of poly(ethylene oxide)-poly(butylene oxide) (PEO-PBO) vesicles, the interfacial tension is 22.8 mN/m[32] which leads to a calculated value of K_A= 91.2 mN/m. However, our experiments yield a stretching modulus of 61.4 ±23.1 mN/m which seems to be a little lower than the expected value.

Polymersomes with values lower than 100 mN/m are not commonly found. Though, vesicles made with rod-coil block copolymers (i.e. a hydrophobic part with a $T_g > T_{room}$) can have a stretching modulus as low as 30 ±15[36], more similar to our system. A possible explanation of the low value of K_A in $E_{16}B_{22}$ polymersomes can be as follows: PEO-PBO systems have been extensively studied by SAXS and microphase separation has been observed under supercooling conditions. However, only two samples were in the correct range of molecular weight to show this phenomenon and as such this was not investigated further or published. The temperatures at which this happens suggests a "nematic liquid crystal like phase" in these PEO-PBO systems at low molecular weights. This is further supported by the published work by Booth et al[37] which shows that a "crystal/liquid crystal"

model better describes the data at room temperature. Thus, the low value of K_A seems to be because of similarities with liquid-like crystals.

Also, small differences in protocols, more specifically the waiting time before taking measurements of the projection length, can affect the magnitude of K_A since some protocols advise to take measurements after a short period of time, e.g. about 3 seconds[1], while others propose a delay of 90-120 seconds[38]. This can cause small variations in the value of K_A for the same system. For example, K_A for a block copolymer of a similar molecular weight but measured by different research groups was 88 (±10)[36] and 109[15] mN/m. In liquid crystalline polymersomes, it seems that longer times (120s) favour the system to reach equilibrium[36]. Therefore, possibly, lower values of K_A could have been due to a relatively long waiting time of at least 90 seconds.

A second approach to data analysis can be made considering the formation of multilamellar vesicles since the stretching modulus is associated to the number of bilayers and these values can be found in almost integral multiples[39]. In Figure 19, K_A increases in multiples of about 30. The most accurate results for K_A were conducted for vesicle one and two which were unilamellar. It is possible that within the range of values in Figure 19, if the propagation error is taken into account, there could be two types of vesicles: unilamellars and dilamellars with approximate modulus of 30 and 60 mN/m. According to these results, $E_{16}B_{22}$ polymersomes are extremely fragile. This probably explains the difficulties in measuring K_A in experiments since, for relative big vesicles of about 40 µm, most polymersomes seems to burst at low vacuum pressures of 4-8 cm of water. However, the experimentally obtained value of K_A, 61.4 (±23.1) mN/m, is acceptable since measurements of the stretching modulus are usually wide distributions[35,36,39] . Also, according to the method that we used for vesicle production[40], it is feasible that most of the polymersomes were unilamellar.

References

1. M. L. Longo and V. L. Hung, in *Methods in Membrane Lipids*, ed. A. M. Dopico, Humana Press Inc, Totowa, NJ, 2007, pp. 421–437.

2. R. Dimova, U. Seifert, and B. Pouligny, *Eurupean Phys. J. E*, 2002, **7**, 241–250.

3. J.-Y. Shao, G. Xu, and P. Guo, *Front. Biosci.*, 2004, **9**, 2183–2191.

4. R. Waugh and E. A. Evans, *Biophys. J.*, 1979, **26**, 115–131.

5. E. Evans and A. Yeung, *Chem. Phys. Lipids*, 1994, **73**, 39–56.

6. S. a Soltesz and D. a Hammer, *Biophys. J.*, 1995, **68**, 315–325.

7. Y. Okumura, T. Ohmiya, and T. Yamazaki, *Membranes (Basel).*, 2011, **1**, 265–274.

8. J.-Y. Shao and J. Xu, *J. Biomech. Eng.*, 2002, **124**, 388–396.

9. R. Wick, M. I. Angelova, P. Walde, and P. L. Luisi, *Chem. Biol.*, 1996, **3**, 105–111.

10. C. R. Jacobs, H. Huang, and R. Y. Kwon, in *Introduction to Cell Mechanics and Mechanobiology*, Garland Science, 1th edn., 2012, p. 350.

11. *http://hyperphysics.phy-astr.gsu.edu/hbase/surten2.html#c2*, Retrieved on April 28th, 2013.

12. W. Rawicz, K. C. Olbrich, T. McIntosh, D. Needham, and E. Evans, *Biophys. J.*, 2000, **79**, 328–339.

13. H. V Ly and M. L. Longo, *Biophys. J.*, 2004, **87**, 1013–1033.

14. E. Evans and D. Needham, *J. Phys. Chem.*, 1987, **91**, 4219–4228.

15. H. Bermúdez, D. A. Hammer, and D. E. Discher, *Langmuir*, 2004, **20**, 540–543.

16. W. Rawicz, K. C. Olbrich, T. McIntosh, D. Needham, and E. Evans, *Biophys. J.*, 2000, **79**, 328–339.

17. W. Mueller, K. Koynov, K. Fischer, S. Hartmann, S. Pierrat, T. Basche, and M. Maskos, *Polym. Prepr.*, 2009, **50**, 262–263.

18. 2008, 1–3.

19. S. D. Fowler and P. Greenspan, *J. Histochem. Cytochem.*, 1985, **33**, 833–836.

20. E. A. Evans, R. Waugh, and L. Melnik, *Biophys. J.*, 1976, **16**, 585–595.

21. A. Tian, C. Johnson, W. Wang, and T. Baumgart, *Phys. Rev. Lett.*, 2007, **98**, 208102–(1)–208102–(4).

22. *www.microscopemaster.com*, Retrieved on April 28th, 2013.

23. K. Kita-Tokarczyk, J. Grumelard, T. Haefele, and W. Meier, *Polymer (Guildf).*, 2005, **46**, 3540–3563.

24. R. Bagnell, in *Phatology 464 Class Notes. PDF format.*, 2012, pp. 1–9.

25. *http://en.wikipedia.org/wiki/Phase_contrast_microscopy*, Retrieved on April 30th, 2013.

26. R. Dimova, S. Aranda, N. Bezlyepkina, V. Nikolov, K. a Riske, and R. Lipowsky, *J. Phys. Condens. matter*, 2006, **18**, S1151–S1176.

27. *http://www.microscopemaster.com/differential-interference-contrast.html*, Retrieved on April 30th, 2013.

28. *http://loci.wisc.edu/optical-sectioning/differential-interference-contrast-nomarski-imaging*, Retrieved on April 30th, 2013.

29. V. Heinrich and W. Rawicz, *Langmuir*, 2005, **21**, 1962–1971.

30. *http://www.bioresearchonline.com/doc/polychrome-iv-0001*, Retrieved on April 30th, 2013.

31. H. Bermudez, A. K. Brannan, D. A. Hammer, F. S. Bates, and D. E. Discher, *Macromolecules*, 2002, **35**, 8203–8208.

32. G. Battaglia and A. J. Ryan, *J. Am. Chem. Soc.*, 2005, **127**, 8757–8764.

33. R. Rodríguez-García, M. Mell, I. López-Montero, J. Netzel, T. Hellweg, and F. Monroy, *Soft Matter*, 2011, **7**, 1532–1542.

34. J. C.-M. Lee, H. Bermudez, B. M. Discher, M. A. Sheehan, Y.-Y. Won, F. S. Bates, and D. E. Discher, *Biotechnol. Bioeng.*, 2001, **73**, 135–145.

35. B. M. Discher, Y.-Y. Won, D. S. Ege, J. C.-M. Lee, F. S. Bates, D. E. Discher, and D. A. Hammer, *Science (80-.).*, 1999, **284**, 1143–1146.

36. E. Mabrouk, D. Cuvelier, L.-L. Pontani, B. Xu, D. Lévy, P. Keller, F. Brochard-Wyart, P. Nassoy, and M.-H. Li, *Soft Matter*, 2009, **5**, 1870–1878.

37. S. Mai, J. P. A. Fairclough, K. Viras, P. A. Gorry, I. W. Hamley, A. J. Ryan, and C. Booth, *Macromolecules*, 1997, **30**, 8392–8400.

38. *Introductory Biomechanics-Micropipette Aspiration Lab (Manual)*, 2010.

39. R. Kwok and E. Evans, *Biophys. J.*, 1981, **35**, 637–652.

40. K. Tsumoto, H. Matsuo, M. Tomita, and T. Yoshimura, *Colloids Surf. B. Biointerfaces*, 2009, **68**, 98–105.

Chapter 5: Conclusions and future work

The salting-out of small unilamellar vesicles (SUVs) and giant unilamellar vesicles (GUV) was studied using: dynamic light scattering (DLS) and transmission electron microscopy (TEM), in order to characterised SUVs, and optical light microscope, in order to characterise GUVs. In the case of GUVs, aggregation was observed when 0.2 M K_2SO_4 was added to the vesicle solution. However, it was determined that the salt did not induce this behaviour but the hydration forces created when salt was added to the solution. In the case of SUVs, addition of low (0.3 M NaI and NaH_2PO_4) and relative high salt concentrations (~ 1 M NaI, NaH_2PO_4 and $NaSO_4$) to a $E_{16}B_{22}$ aqueous solution did not provoke nanovesicles agglomeration. SUVs aggregated only at high concentrations with the present of 3 M NaH_2PO_4 observed as an increase in the hydrodynamic radius measured by DLS. The agglomerations were large enough, i.e. microsizes, as observed with a light microscope. Similar high concentrations of NaBr and NaI did not have an impact in the colloidal behaviour of the polymer solution. The analysis of samples with TEM provided evidence of nanovesicles formation with diameters between 20-60 nm as well as the existence of other type of morphologies, such as worm and pear-shape vesicles. In the case of the salting effect, a polymer solution with Na_2SO_4 (0.1 M) revealed some vesicle aggregates with sizes between ~100 nm to ~1 µm. However, this result could be an artefact of sample preparation of TEM.

A new method to prepare vesicles was discussed in chapter 3 using the inkjet printer technology which consists on depositing polymer microdrops over a glass surface. Then, the addition of water causes bilayers to swell and form vesicles. Firstly, how hydrophobic surfaces affected vesicle formation were studied by modifying this property on glass microscope slides. Apparently, hydrophobic surfaces did not have a great impact in vesicle hydration since most samples had incomplete vesicle formations, i.e. hemispherical, and polymersome separation from the polymer substrate was not observed. Addition of sugars (sucrose and glucose) and salt (NaH_2PO_4) aqueous solutions did not improve vesicle growth since bilayer membranes were still embedded into the polymer dots. However, when glucose or a salt (NaI or NaH_2PO_4) was dispersed within the bilayers, spherical polymersomes with diameters between 10-45 µm were seen. In order to obtain complete formation of vesicles, the additive needs to be in a molar ratio of at least 1:10 (polymer/additive). The best results were achieved using glucose in a ratio of 1:20.

Also, the ability of the inkjet technique to form polymersomes in a salt environment was tested. Samples containing glucose (1:20) and then hydrated with a salt solution at either high (0.1 M NaH_2PO_4 or NaBr or NaI) or low (0.01 M NaH_2PO_4 or NaI) concentrations were not successful in

forming vesicles since salts deflated the polymersomes. However, when polymer dots themselves contained glucose were hydrated with water and, after some hours, were re-hydrated with a salt solution, some spherical vesicles were observed in the solution which were not collapsed. So, polymersome formation is possible at low salt concentrations, i.e. 0.01 M, just after water hydration.

The new methodology for vesicle preparation was used in MPA experiments in order to measure the area expansion modulus (K_A) of $E_{16}B_{22}$ polymersomes. According with the results, a modulus of 61.4 ±23.1 mN/m was calculated which indicates fragile vesicles. This value of K_A is little lower than common stretching modulus of other polymer vesicles, i.e. ~102 mN/m. The low magnitude is attributable to the liquid-crystal like behaviour of low molecular weights EB systems since rod-coil block copolymers vesicles also have low magnitudes of K_A, close to the value obtained in this work. Another possible explanation about this result is the discrepancy in experimental protocols for measuring K_A, i.e. relative long waiting times for the projection length to reach equilibrium can modified the stretching modulus.

5.1 Further work

Future experiments using the block copolymer $E_{16}B_{22}$ will involve the study of the fusion event in synthetic vesicles. Fusion is of paramount importance because it is related to vital biological process such as the intake of food and the export of waste, endocytosis and exocytosis, fertilization, protein trafficking, signalling in nerve cells, virus infection, amongst others[1]. Furthermore, membrane fusion is essential for the formation of many complex organs, such as muscles, bones, and it is one of the key events in the origin of life[2]. Hence, a better understanding of this phenomenon is important in order to improve and optimize fusion dependent applications such as gene transfer, drug delivery and bioengineering.

The fusion event in biological organism is extremely fast, of the order of milliseconds, well control and involves a wide range of fusogenic proteins. As was described in chapter 1, synthetic vesicles have been used to mimic this phenomenon. In fact, most of the hypotheses of the molecular mechanism of fusion come from the study of phospholipid vesicles[3]. However, the advantage of using giant polymersomes over liposomes is that the fusion event occurs on the order of minutes[2] while liposomes on the order of seconds[4]. The fusion event in giant vesicles combined with the micropipette aspiration technique provides the tools to examine this phenomenon. Vesicle fusion can be induced by making defects or fluctuations in a membrane by physical or chemical means[5]. Taking as a base experiments in literature[6,7,8,9,10], different fusion experiments can be carried out under various conditions using the MPA technique and fluoresce phase contrast microscopy. For

example, a simple experiment would be to bring two vesicles together, reducing the intermembrane distance, and monitoring fusion[6] or making a pore in an adjacent vesicle with an electroporation equipment[7] or injecting a small concentration of solutes such as salts[8,9,10] sufficiently close to the vesicles.

In this last case, some reports[8,11] mentioned that the presence of salts affect membrane morphology, and as a result the bending elasticity. So, bending modulus can be related to the propensity of the membrane to fuse. This modulus can be measured using MPA or flickering spectroscopy. This last technique consists of analysing the vesicle contour and calculating the membrane fluctuations via a mathematical model. Other possible experiments are related with studying the variation of the bending modulus when adding salts to the vesicle solution.

References

1. L. Chernomordik, M. M. Kozlov, and J. Zimmerberg, *J. Membr. Biol.*, 1995, **146**, 1–14.

2. Y. Zhou and D. Yan, *J. Am. Chem. Soc.*, 2005, **127**, 10468–10469.

3. K. Arnold, in *Handbook of Biological Physics*, eds. R. Lipowsky and E. Sackmann, Elsevier Science B.V., 1995, vol. 1, pp. 903–957.

4. G. Battaglia, C. LoPresti, H. Lomas, M. Massignani, and T. Smart, *J. Mater. Chem.*, 2009, **19**, 3576–3590.

5. G. Cevc and H. Richardsen, *Adv. Drug Deliv. Rev.*, 1999, **38**, 207–232.

6. J. Heuvingh, F. Pincet, and S. Cribier, *Eur. Phys. J. E. Soft Matter*, 2004, **14**, 269–276.

7. J. Lehn, R. Lipowsky, C. K. Haluska, K. A. Riske, and R. Dimova, *Proc. Natl. Acad. Sci. U. S. A.*, 2006, **103**, 15841–15846.

8. F. M. Menger and S. J. Lee, *Langmuir*, 1995, **11**, 3685–3689.

9. T. Tanaka and M. Yamazaki, *Langmuir*, 2004, **20**, 5160–5164.

10. S. Mondal Roy and M. Sarkar, *J. Lipids*, 2011, **2011**, 528784.

11. I. M. Henderson and W. F. Paxton, *Angew. Chem. Int. Ed. Engl.*, 2014, **53**, 3372–3376.